INVESTIGATION OF STRUCTURAL, ELECTRICAL AND OPTICAL PROPERTIES OF $CU_{1-X}AG_XINSE_2$ THIN FILMS AS A FUNCTION OF X CONTENT

A THESIS SUBMITTED TO
THE GRADUATE SCHOOL OF NATURAL AND APPLIED SCIENCES
OF
MIDDLE EAST TECHNICAL UNIVERSITY

BY

HASAN HÜSEYİN GÜLLÜ

IN PARTIAL FULFILLMENT OF THE REQUIREMENTS
FOR
THE DEGREE OF MASTER OF SCIENCE
IN
PHYSICS

SEPTEMBER 2010

Approval of the thesis:

INVESTIGATION OF STRUCTURAL, ELECTRICAL AND OPTICAL PROPERTIES OF $CU_{1-X}AG_{X}INSE_{2}$ THIN FILMS AS A FUNCTION OF X CONTENT

submitted by **HASAN HÜSEYİN GÜLLÜ** in partial fulfillment of the requirements for the degree of **Master of Science in Physics Department, Middle East Technical University** by,

Prof. Dr. Canan Özgen
Dean, Graduate School of **Natural and Applied Sciences** ______________________

Prof. Dr. Sinan Bilikmen
Head of Department, **Physics** ______________________

Prof. Dr. Mehmet Parlak
Supervisor, **Physics Dept., METU** ______________________

Examining Committee Members:

Prof. Dr. İbrahim Günal
Physics Dept., METU ______________________

Prof. Dr. Mehmet Parlak
Physics Dept., METU ______________________

Prof. Dr. Bülent Akınoğlu
Physics Dept., METU ______________________

Prof. Dr. Nizami Hasanli
Physics Dept., METU ______________________

Assoc. Prof. Dr. Caner Durucan
Metallurgical and Materials Engineering Dept., METU ______________________

Date: September 15th, 2010

I hereby declare that all information in this document has been obtained and presented in accordance with academic rules and ethical conduct. I also declare that, as required by these rules and conduct, I have fully cited and referenced all material and results that are not original to this work.

Name, Last name: Hasan Hüseyin Güllü

Signature:

ABSTRACT

INVESTIGATION OF STRUCTURAL, ELECTRICAL AND OPTICAL PROPERTIES OF $CU_{1-X}AG_XINSE_2$ THIN FILMS AS A FUNCTION OF X CONTENT

Güllü, Hasan Hüseyin
M.Sc., Department of Physics
Supervisor: Prof. Dr. Mehmet Parlak
September 2010, 106 pages

In this work, we will focus on the quaternary system $Cu_{1-x}Ag_xInSe_2$ (CAIS) to investigate the effects of silver (Ag) contribution and exchange with copper (Cu) in $CuInSe_2$. This system is located between the ternary semiconducting chalcopyrite compounds $CuInSe_2$ and $AgInSe_2$. These are two most popular materials applied in photovoltaic cells because of their high optical absorption coefficient, which is an important factor for the manufacture of devices, direct energy gap with values E_g ~1.05 and 1.24 eV, respectively, and excellent thermal stabilities in air. As being a quaternary alloy, we expect that $Cu_{1-x}Ag_xInSe_2$ will show the advantage of a large degree of variation of their properties as a function of the composition, which allows adjusting of the band gap and other properties. We will analyze the behavior of Ag in the structure depending on the annealing and the effects of the Ag exchange to the Cu vacancies in this crystal structure by changing x (Ag content).

The crystals will be characterized structurally by X-ray diffraction (XRD). It will be used to prove crystallinity, determine perfection and lattice parameters depending on composition. Surface morphology and stoichiometry will be examined using scanning electron microscope (SEM) equipped with EDXA. Moreover, electrical properties including the temperature dependent electrical conductivity, and carrier concentrations and mobility extracted from Hall effect measurements, and, optical properties including absorption coefficient, photoconductivity, spectral transmission, and optical band gap have been determined to characterize $Cu_{1-x}Ag_xInSe_2$ thin films deposited using e-beam evaporation technique.

Keywords: $Cu_{1-x}Ag_xInSe_2$, quaternary alloy, chalcopyrite, e-beam evaporation, thin film

ÖZ

$CU_{1-X}AG_XINSE_2$ İNCE FİLMLERİNİN YAPISAL, ELEKTRİKSEL VE OPTİKSEL ÖZELLİKLERİNİN X İÇERİĞİNİN BİR FONKSİYONU OLARAK İNCELENMESİ

Güllü, Hasan Hüseyin
Yüksek Lisans, Fizik Bölümü
Tez Yöneticis: Prof. Dr. Mehmet Parlak
Eylül 2010, 106 sayfa

Bu çalışmada, $CuInSe_2$ bileşiğinde gümüş (Ag) katkısının ve bu elementin bakır (Cu) ile yer değişimi etkilerinin incelenmesi için $Cu_{1-x}Ag_xInSe_2$ dört elementli bileşiği üzerine yoğunlaşılacaktır. Bu bileşik, yapı olarak üç elementli yarıiletken kalkopirit $CuInSe_2$ ve $AgInSe_2$ bileşiklerinin arasında yer almaktadır. Bu bileşikler aygıt üretiminde önemli bir faktör olan yüksek soğurma katsayıları, sırasıyla ~1.05 ve ~1.24 eV olan doğrudan bant aralıkları ve havadaki mükemmel termal kararlılıkları sayesinde fotovoltaik hücrelerde en yaygın kullanılan malzemelerdendirler. Dört elementli bileşik olmasıyla $Cu_{1-x}Ag_xInSe_2$, komposizyonuna bağlı olarak yasak enerji aralığı gibi özelliklerinde büyük çeşitlilik göstereceği ve bu özelliklerinin kullanım için uygun hale getirilebilineceği beklenmektedir. Ayrıca $Cu_{1-x}Ag_xInSe_2$ kristal yapısında, x değerinin (Ag içeriği) değişimi ile tavlamaya bağlı olarak yapıdaki Ag davranışı ve Cu boşluklarına Ag geçişinin etkileri analiz edilecektir.

Kristal, yapısal olarak X-ışını kırınımı ile karakterize edilecektir. Bu yöntem, kristallik yapısını tanımlamak, kristal kusursuzluğunun ve bileşime bağlı olarak kafes (lattice) parametrelerinin belirlenmesi için kullanılacaktır. EDXA'lı taramalı elektron mikroskobu kullanılarak filmlerin yüzey özellikleri ve içeriği incelenecektir. Sıcaklık bağımlı elektriksel iletkenlik ve Hall etkisi ölçümleri ile elde edilen taşıyıcı konsantrasyonları ve mobilitesini içeren elektriksel özellikler, soğurma katsayısı, fotoiletkenlik, tayfsal geçirgenlik ve yasak enerji aralığını içeren optiksel özellikler belirlenerek elektron demeti buharlaştırma tekniği ile büyütülmüş $Cu_{1-x}Ag_xInSe_2$ ince filmleri karakterize edilecektir.

Anahtar Kelimeler: $Cu_{1-x}Ag_xInSe_2$, dört elementli bileşik, kalkopirit, electron demeti ile buharlaştırma, ince filim

To my grandfather

ACKNOWLEDGMENTS

I would like to express my deep gratitude and thanks to my supervisor Prof. Dr. Mehmet Parlak for his endless patience, understanding, cooperation and support throughout this study.

I appreciate to Hakan Karaağaç for his invaluable help with the experiments, suggestions, comments and friendship during thesis study. I would also like to present my sincere thanks to Mustafa Kulakçı for his precious help with the experiments, fruitful discussions and valuable friendship. I also appreciate to Dr. Tahir Çolakoğlu for his stimulating guidance and discussions. I will always be grateful to my lab colleagues Dr. Murat Kaleli and İdris Candan. The technical assistance and cooperation I received from Yücel Eke is gratefully acknowledged.

I am indebted to Assist. Prof. Erman Bengü and his group members; Gökçe Küçükayan and Kuldeep Rana for their scientific contributions to this study.

I wish also to thank my friends Fırat Es, Ruslan Hummatov, and my roommate M. Meliz Metbulut for sharing of knowledge and kind friendship.

I am also grateful to all academic and administrative staff of the Department of Physics, especially Gülşen Özdemir Parlak and Zeynep Eke.

Special thanks go to all of my family for their continuous support and love at the each stage of my educational life. Very special thanks go to Seda Kayra whose love, steadfast confidence and constant encouragement. Without them this work would never have come into existence.

I also thank The Scientific and Technological Research Council of Turkey (TÜBİTAK) for the financial support I received for this study.

TABLE OF CONTENTS

LIST OF TABLES

TABLES

LIST OF FIGURES

FIGURES

CHAPTER 1

INTRODUCTION

The study of solid material thin films has an old history as a standard technique, but in recent years thin film technology has developed around the world into a major research area and also this subject is a major component of works in today’s solid state physics [1, 2]. Interest in thin films arises because of the variety of uses and applications that they offer. The work area of this field process on the films with thicknesses varying at a few microns, and properties of systems classified in intermediate-size which are evaluated between atoms/molecules and bulk materials, where phenomena length scales becomes comparable to the size of the structure [3]. At this time, the developments in microelectronics and nanotechnology lead the improvement related to the thin film science [4]. In present, the increase in demand for thin film materials and devices are the main reason for the development of new processes, materials and technologies with creating new opportunities. As an example, the importance of coatings and the synthesis of new materials for industry have resulted in a significant increase of forward-looking thin film science.

When thin film is mentioned, a film is a simply layer of material, and the term thin is generally used to describe a layer of thickness less than 1 μm [5]. Thin film has all the properties of the grown material and a capability to tailor its characteristics. Since thin films are so thin, they are also very fragile and they have to be formed on and are supported by a substrate. Therefore, it becomes one of the vital areas of the thin film works. The crystallographic form of films and many of their properties depend on substrate conditions. Moreover, in order to compare bulk material and thin film properties, deposited thin film must ensure stoichiometric ratio as in the bulk material and also uniformity [5].

Thin film technology has improved with various kinds of methods that are used to produce many products. Applications of thin films include minimization of dimensions and weight of electronic systems in very large scale integrated circuits, for electronic packaging, sensors, transistors and devices; optical films and devices for the use of protective and decorative coatings, filters and photovoltaic device [6].

One of the major research areas on thin film technology is applications on the photovoltaic device. Photovoltaic effect is the process of direct conversion of sunlight into electrical energy and with the result of this; this type of energy generation is the most promising one as a future energy technology. Since the thin film technology provides fewer material use, and simpler processing steps as compared to a traditional wafer based crystalline solar cells; it leads to an interest in this area. For this purpose, recently, the study of thin film growth methods and characterization has become popular [7]. The chalcopyrite semiconductors, especially, ternary and quaternary forms, which are in the family of I, III, and VI group of elements have great attraction because of their high optical and electrical characteristics [8].

Polycrystalline thin film solar cells based on $CuInSe_2$ (CIS) and $AgInSe_2$ (AIS) ternary chalcopyrite semiconductor compounds belong to a group of I-III-VI_2 compounds are popular in solar cell applications [9] and non-linear optical devices due to being stable and efficient absorber material [10]. Family of these ternary chalcogenides is isoelectronic with the zinc-blende II-VI group of semiconductors. By substituting two cations instead of one in a regular zinc-blende type lattice, alternate series of bonds can be obtained which results in differences with respect to the structural, electrical and optical properties. These chalcopyrite semiconductors within the same family have direct band gap, and high absorption coefficients and as a result of this, they are popular in the photovoltaic applications [11].

Most of the works related to the $Cu_xAg_{1-x}InSe_2$ and similarly $Cu_{1-x}Ag_xInSe_2$ films, which are the quaternary alloy of CIS and AIS materials, carries the properties of these ternary chalcopyrite compounds. Therefore, they are focused on the applications of being an absorber material for hetero-junction solar cells are a subject of interest since quaternary alloys can provide opportunity to a large degree of variation of their properties as a function of x component in the composition, and as a result of this, it provides to adjust the properties of these materials. Therefore, this quaternary alloy can give facility to adjust the characteristics, such as optical band gap, absorption properties and lattice parameters, of the material for the requirements on usage. Because the composition of this compound is defined as a function of some elements' contributions, substituting one element in place of other, as in our case, copper instead of silver, the optical band gap can be arranged between 1.05 [12] and 1.24 eV [13].

In the literature, there is very little work on the CAIS thin films [12-20]. Generally, they were deposited from crystals grown by using vertical furnace operated as Bridgman-Stockbarger crystal growth technique or direct fusion of the constituent elements. For deposition of the films, there are also some distinct methods due to very little researches on it; they are pulsed laser deposition, flash evaporation and solid solutions. Most of the works are related to structural [12, 18, 19], electrical [12, 15] and optical properties [13, 14, 15, 16, 19], and also device characteristics [17, 20] of this thin film, but there is no complete work about these characteristics, the research are concentrated on some distinct works, such as, for structural analysis, effects of surface temperature on crystallinity of the thin films; for optical properties, dielectric constant.

Gremenok et al. [21] reported the studies on $Cu_xAg_{1-x}InSe_2$ (x=0, 0.3, 0.5, 0.7 and 1.0) thin films deposited on the glass substrates by pulsed laser deposition and their characterization as a function of x content. The films were deposited at the substrate temperature range 450-480 °C with having single phase and in polycrystalline form. Their work is on refractive index and absorption coefficient of the films with transmittance and reflectance measurements. Among these chalcopyrite semiconductor compounds, many of the investigations were about $Cu_{0.5}Ag_{0.5}InSe_2$. Venkata et al. [12, 13, 19, 20] worked on $Cu_{0.5}Ag_{0.5}InSe_2$ thin films deposited by the flash evaporation technique at the substrate temperatures between 363 and 803 K at a pressure of 2×10^{-6} Torr. Structural studies are related to deposition substrate temperature, and as a result of this, the elemental weight percentages in the composition, grain structures and sizes, and also crystallinity of the films were analyzed. Consequently, according to the effects of substrate temperature on the atomic ratio of the constituent elements; structure and surface morphology of these films, the $Cu_{0.5}Ag_{0.5}InSe_2$ films deposited at a substrate temperature of 693 K, were found in single phase, polycrystalline with a strong (112) preferred orientation and the mean grain size of single phase films were around 500 nm [12, 19]. Moreover, the lattice parameters were calculated as a = 0.5937 nm, c = 1.1633 nm, with (c / a) = 1.959. The other results they found as an outcome of the works on the $Cu_{0.5}Ag_{0.5}InSe_2$ films were about electrical and optical analysis. The films were p-type from the Hall effect measurements, in addition to this, electrical resistivity of the films were found in the range 30-300 (Ω.cm), and the thermo-electric power in 10-50 (cm^2 / (V.s)) [12]. From the optical transmission measurements, the optical band gap energies, spin–orbit and crystal-field parameters were investigated and the absorption properties depending on transitions from the valence sub-bands to the conduction band were analyzed. The optical absorption spectra analysis of $Cu_{0.5}Ag_{0.5}InSe_2$ films under varying film thicknesses (most of the analysis were concentrated on for three film thickness; 500, 1000 and 1500 nm) revealed band gaps for these thin films as in the range of 1.14 to 1.45 eV which were indicated as the fundamental, band splitting by crystal-field and spin-orbit effects [13].

Furthermore, optical transmittance spectra of $Cu_{0.5}Ag_{0.5}InSe_2$ films deposited under the experimental condition of substrate temperatures were investigated. With the substrate temperatures of 623, 693 and 723 K, the fundamental optical band gaps of the thin films were found as 1.12, 1.14 and 1.15 eV, respectively [19]. The other works related to the structure, electrical and optical properties of the films were on the comparison of these characteristics of the ternary $AgInSe_2$, $CuInSe_2$ and quaternary $Cu_xAg_{1-x}InSe_2$ compounds. Changing lattice constants with x parameter, values of positional parameter and bond lengths were calculated for $CuInSe_2$, $AgInSe_2$, ternary compounds and $Cu_{1-x}Ag_xInSe_2$ solid solutions synthesized by one temperature method [18] and pulsed laser evaporation [14]. By the transmission and reflection spectra near the edge of natural absorption, the refractive index and coefficient of optical absorption were measured and as it was done for $Cu_{0.5}Ag_{0.5}InSe_2$, the energies of inter-band transitions and the crystalline and spin-orbit splitting were determined for the film solid solutions obtained by pulsed laser evaporation [14]. Additionally, the dielectric function $\varepsilon(w)$ of the quaternary chalcopyrite semiconductors $Ag_{1-x}Cu_xInSe_2$, which have polycrystalline bulk structure, were determined at room temperature [15] and spectral dependences of the refractive index n [14, 15] and extinction coefficients k for the investigated materials were analyzed [15] with changing x content between 0 and 1 with 0.2 increment. The nonlinear dependence of the energy gap E_g on x = 0, 0.5 and 1.0 of the solid solutions $Cu_xAg_{1-x}InSe_2$ were investigated both theoretically and experimentally [16]. Moreover, there are some works about the device characteristics of this type of quaternary chalcopyrite alloys. For this purpose, the capacity for measuring current–voltage curves for the p-type $Cu_xAg_{1-x}InSe_2$ crystals; x having values 0.95 and 0.72, samples were done [17] and also the current-voltage, capacitance-voltage and photo-response were investigated for a Al/p-$Cu_{0.5}Ag_{0.5}InSe_2$/Au Schottky diode at 303 K. Under the works on Schottky diode characteristics, the Schottky barrier height, the semiconductor work function and the electron affinity of the semiconductor, the results of these measurements were obtained as 0.55, 4.72 and 3.75 eV, respectively. The effective charge carrier concentration and the built-in potential found by using the capacitance-voltage measurements were 4.5×10^{15} cm^{-3} and 0.38 V, respectively [20].

In this work, we focused on the quaternary system $Cu_{1-x}Ag_xInSe_2$ (CAIS) to investigate the effects of silver (Ag) contribution and exchange with copper (Cu) in $CuInSe_2$. The grown single crystal and deposited thin films were characterized structurally by XRD, and using SEM equipped with EDXA. In addition to this, electrical properties including the temperature dependent electrical conductivity, and carrier concentrations and mobility extracted from Hall effect measurements, and optical properties including spectral transmission and reflection, optical band-gap, absorption coefficient, photoconductivity, and photoresponse were tried to determine in order to characterize CAIS thin films deposited e-beam evaporation technique.

Furthermore, systematic annealing process was applied on the thin film samples in order to understand the effect of post annealing on the properties of them.

CHAPTER 2

THEORETICAL CONSIDERATIONS

2.1 Introduction

In this chapter, initially, basic material information about the polycrystalline and chalcopyrite structures will be given, and then the crystal growth and thin film deposition techniques will be discussed. Finally, the structural, electrical, and optical characterization techniques will be described. For this purpose, XRD, SEM, absorption, photoconductivity and photoresponse characteristics for semiconductors will be introduced in detail.

2.2 Material Properties

2.2.1 Properties of Polycrystalline Thin Films

Solid materials show different characteristics with respect to their structures. Every solid material has its own characteristics and they are classified in terms of the atoms that are arranged within them. Materials in which atoms are placed randomly are called amorphous; if they are placed in a high ordered structure are called crystalline. Crystal structures can be in single crystal or polycrystalline form. Single crystalline materials have the continuous crystal lattice structure which is unbroken to the edges of the sample, with no or very few grain boundaries; and polycrystalline materials have a high degree of short-range order, but no long-range order as in the structure of the single crystals. They consist of small crystalline regions with random orientation, grains, which are separated by grain boundaries.

Materials may be divided into two main classes with respect to their electrical conductivity characteristics; that are insulators and conductors. Insulators have very large resistance to the flow of electric current, on the other hand, in a conductor; electric current can flow freely without any obstruction. In addition to these materials, as a third class, semiconductors can be classified as a thermally excited insulator. The main difference between an insulator and a semiconductor comes from the value of the energy gap. At 0 K, the valence band of these materials is full of electrons, and in this case, their conduction band has no charge carriers. At any temperature higher than 0 K, there exist a huge number of free charge carriers in the conduction band of the semiconductor, but these carriers are not more than the case in the metals. Therefore, it is the distinct point for the semiconductors from the insulators and the conductors. Semiconductors have conductivities between insulators and conductors which have very low and high conductivities respectively. In addition to the sensitivity to temperature, the conductivity of a semiconductor can be changed with illumination, magnetic field and impurity contribution [24]. The study of these materials and device characteristics are shaped on the basic properties of current mechanisms that are the concept of mobile charges carriers and transport mechanism of these mobile carriers through the semiconductor.

2.2.1.1 Energy Band of a Semiconducting Material

To understand the semiconductor materials, it is first necessary to look at the atomic structure of intrinsic semiconductors to complete the knowledge of their characteristics. In the case of being a single crystal, the semiconductor materials have a periodic arrangement of atoms. Ideal crystal structure can be defined as in infinite dimension where atoms are completely immobile and there is no vibration in the lattice. However, in real case, due to the vibrations, phonons, in the lattice structure, it causes a defect analysis over the ideal case [25]. For an intrinsic semiconductor, the conduction band is completely empty at absolute zero and is separated by a forbidden region called energy gap from the filled valence band (Fig.2.1).

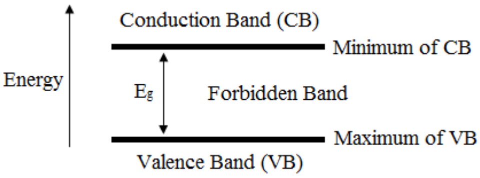

Figure-2.1: Band diagram of an intrinsic semiconductor

Semiconductors are characterized by an energy band structure where the conduction band and the valence band are separated from one another by an energy gap that is typically less than about 3 eV [26]. The pure semiconductor has its Fermi energy in the middle of the energy gap that assures that the valence band is full and the conduction band is empty of electrons at 0 K. The small energy gap in semiconductors compared to insulators permits free carrier generation by three mechanisms. The semiconductor can absorb incident photons if their energy is greater than the energy gap, so that the electrons are transferred from the valence to the conduction band; transition of an electron from the valence band to conduction band creating a free electron in the conduction band and an empty energy level in the valence band can be triggered by thermal energy change in a semiconductor; impurities intentionally put in the semiconductor occupy energy levels within the energy gap. If these energy levels, donor or acceptor levels, are sufficiently close to the valence band or conduction band, thermal energy can facilitate the transfer of electrons from the valence band to the acceptor impurity energy level creating a vacancy in the valence band, or promote an electron to the conduction band from the donor energy level of the impurity creating a conduction electron [27].

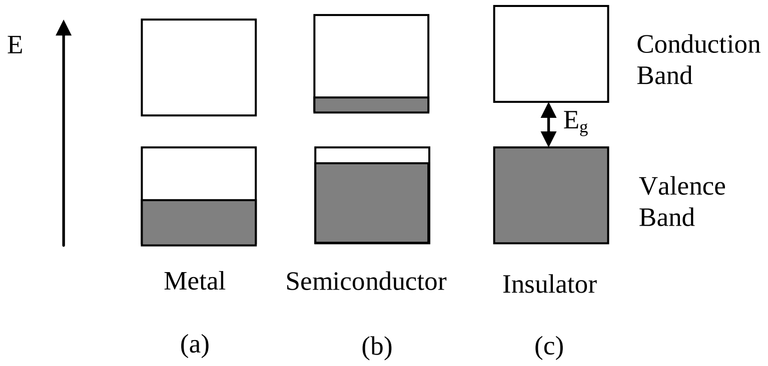

Figure-2.2: Possible band structures of metal, semiconductor and insulator a) a half-full band, b) nearly full band with a small band gap energy separation from an almost empty band and c) a full band and an empty band with a large band gap energy difference

The best values of the band energy can be obtained by optical absorption. There are two types of absorption processes due to transition between the conduction and valence bands. In the direct energy gap structure of the semiconductor case, an electron makes a transition from the valence band to the conduction band at the same $\vec{k}$-value ($k = 0$). On the other hand, in indirect case, since the valence band maximum and the conduction band minimum are at the different $\vec{k}$-value, direct electron transition cannot satisfy the requirement of conservation of energy and momentum, therefore, it is done with the additional phonon creation in the system (Fig.2.3) [28].

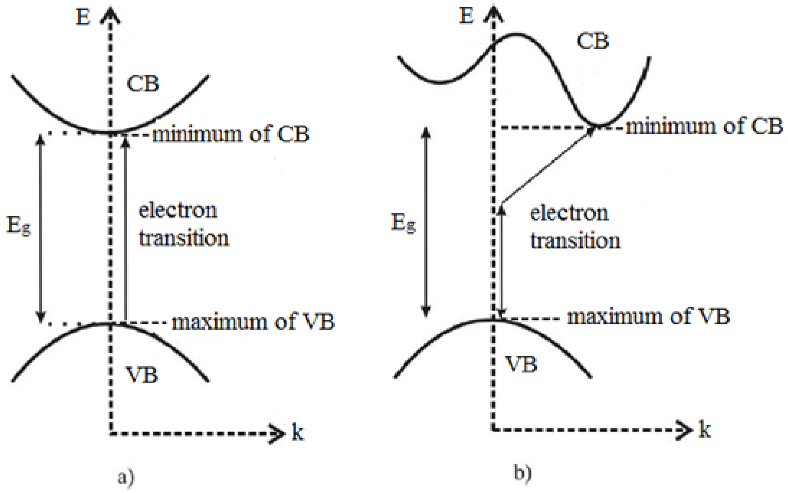

Figure-2.3: Direct (a) and indirect (b) electron transitions in semiconductor

2.3 Structural, Electrical and Optical Properties of CAIS Single Crystals

2.3.1 Structural Properties

2.3.1.1 Chalcopyrite Structures

Chalcopyrite means the copper containing pyrite as it is commonly known. It is the most abundant copper-bearing mineral containing nearly equal parts of copper, iron and sulfur. It is in a chemical composition as $CuFeS_2$ and it has a tetragonal structure with nearly equal to 2 for *c/a* ratio where *c* = 525 nm and *a* = 1032 nm [31]. The structure of chalcopyrite materials is almost similar to well-known zinc-blende, ZnS, structure (Fig.2.4). It has nearly the same organization of anions; but, the ordered distribution of the cations is different in these structures where the arrangements of the cations forms the unit cell as tetragonal with *c*-axis about twice the *a*-axis of the zinc-blende type unit cell. It is found for many compounds of composition I-III-IV_2, and II-IV-V_2 (ABC_2) [32]. There are many compounds known with a general formula A (Cu, Ag), B (Al, Ga, In, Tl, Fe), C (S, Se, Te)$_2$. Generally, the chalcopyrite structure is known as a low temperature phase of ternary I-III-IV$_2$ semiconductor compounds [33] since their structures are close to chalcopyrite form [34]. The bonding type is primarily covalent with sp^3 hybrid bonds. The chalcopyrite structure can be constructed with the well-known disordered zinc-blende structure by organizing the A and B atoms which belong to non-symmetric space group $I\bar{4}2d$ [33, 35]. In this structure, each A and B atoms, which have cation characteristics, are tetrahedrally coordinated to four C atoms, which are in anion characteristics. Moreover, each C atom is tetrahedrally coordinated to two A and two B atoms in an ordered format [36].

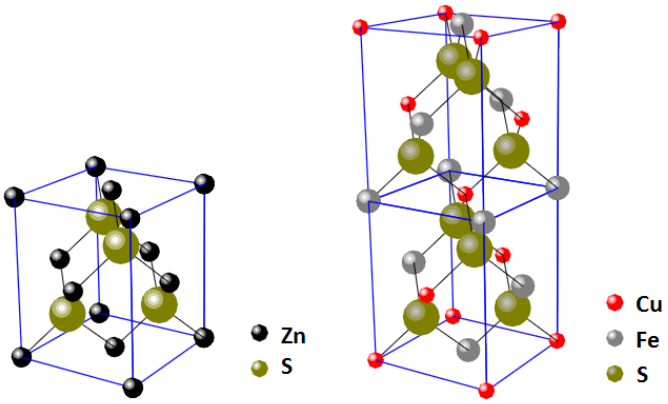

Figure-2.4: Crystal structure of (a) zinc-blende and (b) ternary chalcopyrite lattice

As mentioned before, our works are based on CIS and AIS materials since the alloy CAIS is the quaternary compound of them. These materials belong to the semiconducting I-III-VI$_2$ group of elements and crystallize in the tetragonal chalcopyrite structure. As an example, the structure of CIS is obtained from the cubic zinc-blende structure of II-VI family of elements, such as ZnSe, by occupying the Zn sites alternatively with I (Cu) and III (In) atoms. Each I or III atom constructs four bonds with the VI (Se) atoms. On the other side, each Se atom forms two bonds with both Cu and In atoms. Because the strengths of the I-VI and III-VI bonds are in general different from each other, the ratio of the lattice constants c/a is not exactly 2. Instead, the quantity (2 - *c/a*) (which is -0.01 in CIS and 0.077 in AIS) [34] is a measure of the tetragonal distortion in chalcopyrite materials. In the case of CAIS material, replacing Cu atom with Ag, it is also possible to have a distortion from the tetragonal structure. In addition to this, the difference between the characteristics of the Cu and Ag atoms can cause some difference from the case in ternary chalcopyrite lattice structure.

2.3.1.2 Crystal Growth

One of the important factors in production of thin film materials is the availability of convenient material for the deposition of thin films and consequently, for fabrication electronic and optoelectronic devices [27]. The first step in the fabrication of thin film is the growth of a single crystal of a semiconductor whether the direct fusion of the constituent elements is not a choice.

It is not easy to produce high quality crystals, they require special conditions for their formations. Especially, crystal growth is involved with the control of a phase change. Thus, it may be defined as three categories of crystal growth process, solid, melt and vapor growth. Solid growth is a method to grow the crystal using solid to solid phase transitions, similarly, melt growth involves liquid to solid phase transitions and vapor growth involves gas to solid phase transitions in the process of crystal growth [37].

Although the determination of the most appropriate method for the production of single crystals of a particular substance depends on the nature of the substances, the intended application, desired quality and laboratory conditions are also taken into consideration. As a result of this, the most popular single crystal growth techniques are Czochralski (CZ), Bridgman and floating zone methods [25].

The Bridgman-Stockbarger crystal growth method is a method of growing single crystal ingots with directional solidification. It is a popular method of producing certain semiconductor crystals, such as gallium arsenide, II-V Crystals (ZnSe, CdS, CdTe) where the Czochralski process is more difficult [38]. The advantages of this method are; providing to produce crystals with good dimensional tolerances quickly; having relatively simple technology; and requiring neither control system nor many hours of supervision [39].

The main process of this growth method is slowly cooling the melt polycrystalline material from the bottom of the container where it is placed in. The length of the container is the most effective part that characterizes the form of the single crystal. In the applications of this method, horizontal or vertical geometry can be preferred for this process.

In this method, the crystal growth is obtained with moving the melt material in a furnace to a temperature below its melting point. It is done by slowly lowering a crucible containing this melt from a high temperature zone into a low temperature zone. In this process, the crucible is usually placed as its tip pointed bottom that enters the freezing zone first to avoid not more than one nucleation. As the crucible is lowered nucleation is occurred at the tip of the crucible and crystallization proceeds vertically as gradually cooling the sample by the slow movement of the ampoule through the furnace from its hot, upper zone down to its cold, lower zone which satisfies cooling from the temperature up to melting point to down below the solid-solid phase transition temperatures [40, 41]. In the growth process, sample is placed into a crucible which is lowered through a furnace so that freezing start at the lowest point in the crucible and the solidification face moves slowly up to crucible. Therefore, precise temperature gradient is required for the successive growth.

2.3.1.3 Thin Film Deposition Techniques

The thin film deposition technique is one of the crucial factors in semiconductor device technology in the material formation processes. Furthermore, the deposition science is the major key to the fabrication of electronic devices because microelectronic solid-state devices, which are mainly produced as a thin solid film from a variety of materials by deposition from gas, vapor, liquid or solid phase, are all based on material structures formed by thin film deposition [43]. Although the deposition method should be convenient for the material used, economical factors and feasibility on the control systems of measuring film deposition parameters are vital for thin film deposition. For the thin film deposition process, as thin is a relative term, but most deposition techniques should control layer thickness within a few tens of nanometers up to micrometer range. In deposition techniques, vacuum system is also important factor to deliver evaporant uniformity to substrate, deposit uniform films, optimize flow for maximum deposition rate, and prevent impurity contribution.

Thin films are ordinarily prepared by condensation of atoms or molecules from gas phase on the surface of a solid called substrate. These atoms from gas phase striking the substrate surface, some of them become bound to it by either dipolar or quadrapolar, van der Waals, forces. This binding on the surface is called adsorption. After atoms starts to place on the substrate, which are called adsorbed atoms, the following ones affect and cause some of them to move from their initial places on the surface. This mobile species is called adatom [47].

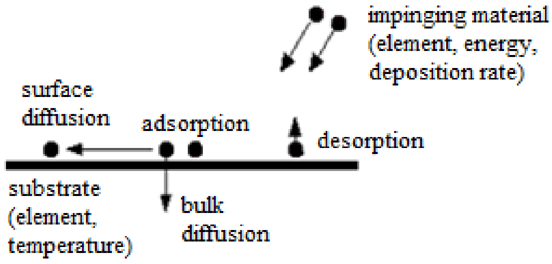

Figure-2.5: Basic thin film deposition process

When the evaporated material reaches to the substrate surface, it condenses on the substrate in a complex sequence of events that are the factors affect the most of the physical properties of the deposited thin film. The growth process of thin film is generally evaluated as into steps; nucleation and growth. In nucleation step, the surface absorbs the loss thermal energy due the motion of the mobile atoms and molecules towards the surface of the substrate. This motion of adatoms continues until they lose the thermal energy required to move about the surface of the substrate. With this event, the nuclei continue to form, and as a result of this, the film makes a continuous sheet on the substrate. Chemical interactions between the adatoms and the surface determine the strength of the bond between the film and substrate. After evaporant atoms start to form a mono-layer on the substrate surface, the film deposition continues as if the entire substrate were made of the material being deposited [47].

Mainly, the adsorption process is classified into 2 branches; physisorption and chemisorption. Physisorption is defined with weakly bounds and in this case the atoms bind by van der Waals forces where there is no exchange of electrons and binding energy is around the fraction of eV. On the other hand, chemisorption provides strong bounds having binding energy ~5-10 eV because chemical bounds are formed with the exchange of electrons.

Methods of deposition play fundamental roles in the properties of these films. They can be classified due to their techniques used. Basically, the thin film growth methods may be grouped into two main classes; substrate is active where the active species react with the substrate atoms, and substrate is passive where the active species do not react with the substrate atoms. Then, under these classes, there are a vast number of thin film deposition techniques for material formation, such as, vapor deposition, epitaxy, oxidation, ion implantation, spin on, spray pyrolysis, solid solutions [48]. Generally, thin film deposition techniques are classified as either purely physical, like evaporation method, or purely chemical, like gas- and liquid-phase chemical processes. In a different manner, the techniques that give opportunity to both physical and chemical reactions as in low discharges and reactive sputtering methods have a variety of usage for formation of thin films; and these coinciding processes can be classified as physical-chemical methods.

Vapor deposition (VD) is divided into two subgroups; physical vapor deposition (PVD) (no chemical reaction) and chemical vapor deposition (CVD) (there is a chemical reaction). In PVD, momentum transfer between the source atoms and evaporation of source atoms are the main mechanisms of deposition. However, in CVD purely chemical reactions occur during the deposition.

Chemical vapor deposition (CVD) is chemical reactions which transforms gas molecules, called precursor, into a solid material, in the form of thin film or powder, on the surface of a substrate. Instead of the physical transfer of atoms from a condensed evaporation source or sputtering target to the substrate, chemical vapor deposition primarily relies on gas phase and gas-solid chemical reactions to produce thin films. Because they are subject to thermodynamic and kinetic limitations and constrained by the flow of gaseous reactants and products, CVD processes are generally more complex than those involving PVD [49].

Generally, physical vacuum deposition (PVD) process consists of three main steps: creation of an evaporant using the source material, transportation of this evaporant from the source material to the substrate, and condensation of the evaporant onto the substrate surface to form the thin film deposit gas molecules. Besides, during the transportation of the evaporant from source to substrate and growth of the dense films, the net deposition rate would be arranged significantly, and uniformity on the film surface would be provided.

Physical vapor deposition (PVD) is concentrated on the physical treatment during the film deposition process and it has also sub-techniques; most commons are evaporation and sputtering. The popular evaporation techniques are thermal evaporation, electron beam evaporation and flash evaporation.

Evaporation of a material and its subsequent condensation on a substrate is one of the simplest processes for thin film deposition [50]. In this method, the material to be deposited is in the form of a solid or a liquid phase and requires thermal energy for transformation into the vapor phase. Thus, evaporation includes sublimation when a solid directly transforms into vapor and vaporization when the liquid transforms into vapor on thermal treatment. The vapor, by its own nature, expands into an evacuated chamber that contains the substrate. The evaporation process is performed in low pressure, under high vacuum because the melting point of materials decreases as pressure decreases. The vapor condenses on the cold surfaces that are kept at a lower temperature than the evaporation source [50]. There are two popular evaporation techniques for source heating processes; e-beam and thermal evaporation methods.

2.3.1.3.1 Thermal Evaporation

Among the thin film deposition techniques, the oldest and basic one is thermal evaporation or vacuum evaporation. However, this method is the more preferred deposition process for depositing metal and metal alloys [51]. The main step in thermal evaporation process is heating a boat, where the source materials are placed, electrically with a high current to make the material evaporate.

It is cost effective and suitable for useful compounds only. Disadvantages of resistively heated evaporation sources include contamination by crucibles, heaters, and support materials and the limitation of relatively low input power levels [49].

2.3.1.3.2 E-Beam Evaporation

In e-beam evaporation, the main process is local heating and evaporation with aiming electron beams into the source materials. For this purpose, in order to heat source materials to high temperatures, thermal emission of electrons from a filament source (usually tungsten) is used. Basically, electron beams are preferred when temperature to evaporate the source materials for deposition process are too high to obtain in thermal evaporation method. A typical electron gun system consists of a cathode and an anode. The electrons from the cathode are accelerated across the potential difference maintained between the cathode and the anode. Then, magnetic fields are used to steer the electron beam into source [52]. This is done to allow shielding of tungsten filament and prevent contamination. The use of electron beam heating in evaporation under high vacuum has several advantages over resistance and induction heating, in particular, higher temperature and better controllability. It is substantially easier to limit contamination of the evaporation source by self containing it and also by cooling systems, water-cooled crucible [53]. Generally, this evaporation method gives many opportunities; basically, relatively high deposition rates, dense coatings, high controllability variations in the structure and composition of condensed materials, columnar and polycrystalline microstructure, low contamination, and high thermal efficiency [55]. Therefore, it is on interest in order to control an evaporation process and deposition rate very closely, to deposit films of high melting point materials and to have films of high purity. It also provides an advantage for multiple source deposition that is the films can be deposited with using more than one crucible having different sources.

2.3.1.3.3 Flash Evaporation / Pulsed Laser

Pulsed laser deposition (PLD) has become popular with having advantages on the easy usage and accurate deposition for complex stoichiometry in the composition of films, [56]. A short pulse of high-density optical radiation generated by a laser gives a sudden thermal rise on the irradiated surface of the solid which causes that all of its components can be evaporated similarly [52]. The main advantage of PLD is that it is based on a photon interaction to create an ejected vapor of material from any target. In order to collect this vapor on a substrate surface of the film, the distance between the target and the film is arranged as shorter relative to the other methods. Although, for evaporation, the actual physical processes of material removal from the surface of the target are quite complex, the ejection of material occurs due to rapid explosion of the source surface with superheating. When considering thermal evaporation technique, the composition of the deposited films depends on various parameters, such as the melting points or the vapor pressures of elements in the target material. On the other hand, compositional transition from the source material to the thin film is not dependent on such factors. Thus, it is easy to obtain the desired film stoichiometry for multi-element materials using PLD than with other deposition technologies. Generally, PLD has become popular application for deposition of high-temperature superconductors and has been widely begun to use in thin film deposition for semiconductors, dielectrics, organo-metallics and chalcogenides materials [57].

2.3.1.3.4 Epitaxy

Epitaxy deposition technique is mainly used to produce thin oriented layers on a substrate with similar crystal structure. As a one type of epitaxy technique, molecular beam epitaxy (MBE) is one of the popular methods of depositing thin films. Actually, it can be defined as a modern application of thermal evaporation. This technique helps to the formation of semiconductor materials with required crystallographic orientations between the layers of different materials with high purity. It is also an evaporation method to grow crystalline thin films in ultrahigh vacuum with precise thickness, composition and morphology controllability, at very low deposition rates but at relatively low substrate temperatures [58]. Knudsen cell is the special thermal evaporation source in an MBE vacuum system during the evaporation process [48]. In practice, however, the requirement of ultrahigh vacuum makes the hardware of the system complex and expensive to operate. The basic process in this method is the formation of the films on single crystal substrates by slowly evaporating the elemental or molecular constituents of the film from the source. In fact, the main idea for this method is producing thin film structure onto previously deposited materials. This is done by creating a molecular beam of a material which impinges on to the substrate. The basic technique is the process continues building on the substrate with the same crystallographic orientation with the substrate acting as a seed for the deposition. In other words, if amorphous/polycrystalline substrate surface is used, the film will also be in amorphous/polycrystalline structure. This method is mostly preferable in the deposition of epitaxial layers of III-V semiconductor compounds. In addition, with the help of this method, silicon, metals, silicides, and insulators can also be deposited as single crystal form [46].

2.3.1.3.5 Spin-on

The application area for the spin-on techniques is mainly concentrated on organic polymeric materials or organo-metallic-based glass-forming solutions. The first step for the production is putting a coating material in the center of the substrate. Then, a liquid puddle is accelerated on a rotating substrate for deposition. With rotating the puddle, the source material can be deposited on the surface of the substrate. The idea behind this method is a balance between two main forces; centrifugal forces controlled by spin speed and viscous forces determined by solvent viscosity. The spin-on deposition technique is most widely used in preparing compositionally uniform films over large areas and tolerating relatively large thickness variations [59].

2.3.1.3.6 Sputtering

Sputtering is a method where deposition process in the source material is at much lower temperature than evaporation. It is referred as an alternative technique instead of depositing thin films with source material in vapor phase by the physical interaction of particles impacting, physically removes portions of the source material often called as the target and deposits a thin, firmly bonded film onto a substrate surface. Basically, as in the other deposition process, it also involves the transport of material from the target to the substrate surface. In this method, atom releasing is done with using gaseous ions bombardment to the surface of the source material under high voltage acceleration. With the collision between these ions and the target surface, there occurs a momentum transfer between incident ions and the target. Therefore, atoms or maybe entire molecules of the target material are ejected from a target material due to bombarding the target by energetic ions, where they have a very tight bond. The resulting accumulation of these atoms or molecules on the substrate surface exists by mechanical forces, despite of the fact that, in some cases, and alloy or chemical bond may be the factor for it. For the sputtering process, there are various ways that the primary particles can be obtained. As an example, plasma, ion source, and accelerator or by a radioactive material emitting alpha particles can be used [60]. In addition, there are many sputtering techniques such as RF, ion beam, diode, and magnetron sputtering. This deposition process is generally utilized for thin-film deposition, etching and surface treatment. On the other hand, this technique is expensive due to its technological requirements compared to the evaporation methods; however, it may be useful for alloy deposition having different melting points [48].

2.3.1.4 Structural Analysis of Polycrystalline Thin Films

The measurements of the structural characterization of the grown crystal and the deposited thin films were conducted for the purpose of investigation of the arrangement of the atoms in the solid. There are three methods that were used in this characterization; XRD technique, SEM and EDXA.

We used XRD technique to specify the structural parameters, the existed phases, and the orientation of the grown crystal and the polycrystalline thin films, and as a first sense about analysis for the elemental composition of them. Additionally, the SEM was used to obtain images the sample surfaces and surface analysis; and also EDXA to get elemental analysis on the chemical characterization of the samples [31].

2.3.2 Electrical Properties of Polycrystalline Thin Films

2.3.2.1 Resistivity

Resistivity (or its inverse, conductivity) is one of the most important electrical parameter of semiconductors. Because of the charge carrier and phonon interactions, carriers lose their energies which are expressed as resistivity of the material and it is an intrinsic electrical property related to carrier drift in materials. Therefore, it is a measure of how strongly a material opposes the flow of electric current. Resistivity and its temperature dependence are often used to categorize materials into metals, semiconductors and insulators. However, due to the possibility to obtain the same resistivity from the different semiconductor materials, and also the possibility to measure different resistivity values from one semiconductor material, resistivity is not evaluated as a fundamental material property. In the case of homogeneous semiconductor material, it is defined as the proportionality constant between the applied electric field, E, and the drift current density, J,

$$E = \rho J \tag{2.1}$$

Its reciprocal value is defined as the conductivity;

$$\sigma = {}^{1}\!/_{\rho} \tag{2.2}$$

and, therefore,

$$J = \sigma E \tag{2.3}$$

The current density flowing in the sample depends on the velocity of the mobile carriers, and it can be written as the sum of the product of the charge of each carriers times its velocity;

$$J = nqV_d \tag{2.4}$$

where n is the number of the charge carriers in unit volume, and V_d is the drift velocity due to the applied electric field.

Using the $\overrightarrow{\mathrm{V_d}} = \mathrm{\mu}\vec{\mathrm{E}}$, we have,

$$J = qn\mu E \tag{2.5}$$

which can be rewritten for electrons as

$$J_e = qn\mu_e E \tag{2.6}$$

and for holes

$$J_h = qp\mu_h E \tag{2.7}$$

where n and p are the concentration of electrons and holes respectively and μ_e and μ_h are their mobilities.

If an electric field applied to a semiconductor material, electrons in the conduction band and holes in the valence band drift in opposite directions and both contribute current flow in this sample with respect to their opposite charges. As a result of this, the total current flow is the sum of electron and hole current components,

$$J = J_e + J_h = (qn\mu_e + qp\mu_h)E \tag{2.8}$$

where the quantity in parenthesis is the total conductivity with the contribution of electrons and holes in the sample.

In the case of a semiconductor from

$$n = p = n_i \tag{2.9}$$

and

$$n_i = \sqrt{N_C N_V} e^{-(E_C - E_v)/_{2kT}} \tag{2.10}$$

for the effective densities of states for the conduction and valence band, we can write

$$n = p = constant \times T^{3/2} e^{-(E_g/2kT)} \tag{2.11}$$

Rapidly changing number of free charge carriers over temperature interval is the main affect on the electrical conductivity in different ambient temperature. Therefore, due to the dependence on the carrier concentration, the electrical conductivity is

$$\sigma = constant \times q(\mu_e + \mu_h) T^{3/2} e^{-(E_g/2kT)} \tag{2.12}$$

and also it can be rewritten as

$$\sigma = \sigma_0 e^{-(E_g/2kT)} \tag{2.13}$$

Thus, by plotting *ln(σ)* as a function of *1/T*, the energy gap can be obtained from the slope. In this case the $T^{3/2}$ variation and the temperature dependence of E_g are neglected when it is compared with the exponential temperature variation term.

2.3.3 Optical Properties of Polycrystalline Thin Films

There are three main situations occurred when a light beam interacts with the semiconductor material, it can be scattered, absorbed, or transmitted.

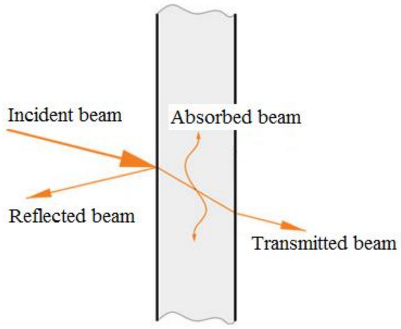

Figure-2.6: Schematic diagram for reflection, absorption and transmission of an electromagnetic wave when it interacts with a material

Transmitted light is the component of the light beam which passes through the material with effecting due to the properties of the materials. This transmitted light propagates in the same direction as the incident light. The some parts of the incident beam emerge in a different direction from the incident light when it hits to the atoms inside the material. The absorption is the case of the incident energy of the light beam is taken up by matter when it interacts with carriers and atoms. Optical absorption can be described with the absorption coefficient, which is the capability of the matter to absorb the light. The probability that the light is removed from the incident beam is related to the cross section which is an effective area of the atom or molecule. In the simplest case where reflection or interference effect is neglected, the Beer-Lambert law [73] gives a description to the fundamental absorption which is the band to band transition, the electron excitation from the valence band to the conduction band.

$$I = I_0 e^{-\sigma N x} \tag{2.14}$$

where σ is a cross-section area, N is the number of effective cross-section areas, I_0 is the initial photon intensity, and I is the transmitted photon intensity. The relation σN gives the absorption coefficient of the sample; therefore, the Eq.2.14 can be rewritten as

$$I = I_0 e^{-\alpha x} \tag{2.15}$$

where α is the characteristic absorption coefficient of a material. There are two types of optical transition that shows the absorption characteristics of the sample; they are direct and indirect depending on the material's band gap energy profile. These two different types of absorption were mentioned in the case of direct and indirect energy gaps.

In addition to the main illumination effects on the semiconductor material, there occurs change in the number of charge carriers and as a result of this, in the conductivity of the sample changes due to incident radiation. Photoconductivity is the generation and recombination process with absorption of radiation of proper energy and charge carrier transport to the electrodes.

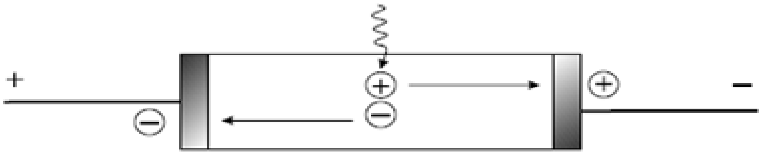

Figure-2.7: Photoconductivity process under the applied external electric field

Out of the zero temperature, there are some free charge carriers in the conduction and valence bands of the semiconductor. Without any external effect, the conductivity of the semiconductor is the addition of these carriers' conductivities which is expressed by

$$\sigma_{dark} = qn_{dark}\mu_{e,dark} + qp_{dark}\mu_{h,dark} \tag{2.16}$$

where the mobilities and carrier concentrations of the mobile charges and the conductivity of the material are labeled as dark in order to underline that there is no irradiance effect. However, under the illumination, the conductivity of the material changes due to the external effect of it. If the excess carriers arise from optical excitation, the resulting increase in conductivity is called photoconductivity. In general, the conductivity increases with the photoconductivity effect when the radiation is incident on the sample [37, 52] and the conductivity in the new situation, σ_{light}, is

$$\sigma_{light} = \sigma_{dark} + \Delta\sigma \tag{2.17}$$

where $\Delta\sigma$ is the photoconductivity contribution to the intrinsic conductivity of the sample. For the case of one-type mobile carrier in the semiconductor, the conductivity with the photo-excitation is given by

$$\sigma_{dark} + \Delta\sigma = q(n_{dark} + \Delta n)(\mu_{dark} + \Delta\mu) \tag{2.18}$$

where Δn and $\Delta\mu$ express the change concentration and mobility of the material respectively. Then, the photoconductivity can be written as

$$\Delta\sigma = q\Delta n\mu_{dark} + q(n_{dark} + \Delta n)\Delta\mu \tag{2.19}$$

Since the change in the concentration is related to the direct generation (recombination) rate and lifetime of the charge carriers, Eq.2.19 can be rewritten as

$$\Delta\sigma = qG\tau_n\mu_{dark} + qn_{dark}\Delta\mu \tag{2.20}$$

where G is the number of excess electron in unit volume in unit time interval and $\tau_n$is the electron lifetime.

If the lifetime τ_n is a function of G, the change in conduction of the material can show different characteristics under different G-dependence. If the lifetime is not affected by the generation rate, the change is in the form

$$\Delta\sigma = qG\tau_n\mu_{dark} \qquad (2.21)$$

However, if the proportionality between the carrier concentration and the generation rate is linear, then the conductivity change is given by

$$\Delta\sigma = qG\tau_n(G)\mu_{dark} \qquad (2.22)$$

This relation shows that the change in the conductivity varies with the photo-excitation rate in some order greater than one. If τ_n in the form of $G^{\Upsilon-1}$, $\Delta\sigma$ changes with G^{Υ} where Υ is an integer. In this case, if it is less than one, the lifetime decreases with increasing the generation rate, the behavior of the semiconductor is called sublinear photoconductivity; if it is greater than one, the lifetime increases with increasing the generation rate, the material becomes more photosensitive with increasing photo-excitation intensities, and this behavior is called as supralinear photoconductivity [74, 75].

CHAPTER 3

EXPERIMENTAL TECHNIQUES

3.1 Introduction

In this chapter, experimental techniques of single crystal growth procedure, CAIS thin film deposition procedure, post-depositional heat treatment and structural, electrical, and optical characterization techniques will be presented.

This chapter starts with the explanation of preparation of CAIS single crystals and the Bridgman-Stockbarger growth method with which these crystals were produced. Then, the preparation of CAIS thin films will be presented. In this subsection, as the deposition technique of the CAIS thin films, the electron beam physical evaporation technique will be summarized. Finally, the experimental techniques that were used to analyze the characteristics of these as-grown films and also annealed films will be given in remaining sections. Structural characterizations of these samples were carried out by XRD and EDXA measurements. For electrical characterization, thin films were coated with indium by using appropriate mask geometries by the thermal evaporation technique. The temperature dependent conductivity and Hall effect measurements were carried out in between 100-450 K in order to obtain the electrical characteristics of the thin films. Their optical properties were determined by the absorption measurements in wavelength range of 325-900 nm, reflection measurements in the range of 200-1100 nm, the temperature dependent photoconductivity measurements under different illumination intensities in the temperature range of 100-450 K, and the wavelength dependent photoresponse measurements in the range of 200-1350 nm under different bias voltages.

3.2 Preparation of CAIS single crystals

The most common crystal growth techniques were mentioned in the previous chapter, and the Bridgman-Stockbarger method was used to prepare the single crystal source for the thin film deposition. In this method, before crystal growth, the starting point is determining a suitable growth ampoule, called crucible, since it is the point where grown material and growth system have a contact. Therefore, this choice affects the quality of crystal and its all properties including impurity contamination. In this case, initially, choosing convenient crucible needs an important concern.

The first property that should be cared about is the melting point of the crucible. Because of being in contact with the grown material, the chosen crucible must have considerably higher melting point than the grown material inside it, and it prevents the probability that the crucible surface reacts with the grown crystal during the crystal growth process. Moreover, it is better to have a crucible having smaller thermal expansion coefficient compared to that of the grown crystal, and it helps to avoid breaking when increasing and decreasing the thermal application on the crucible. It is also desirable that the crucible should have smaller thermal conductivity than the material inside in order to have suitable shape of the solid-liquid interface isotherm to grow high quality crystals. As a result of these required properties, quartz is appropriate for crucible to use for growing our crystal [39]. In addition to these properties, the size and shape of a crucible influences on growth crystal. In fact, the bottom of the crucible has an important effect on nucleation and propagation of a single crystal, so that the crystal orientation depends on the bottom of the crucible.

Considering all of these conditions, we used the crucible having 16 mm diameter, 100 mm overall length and 1.5 mm wall thickness. After determining the most preferable crucible for the crystal growth, it must be cleaned in order to reduce the level of contamination on the growth crystal since the surface of the crucible is directly in contact with the grown material. The purpose of cleaning step is to remove surface particles as well as organic and inorganic contaminants, and prepare a clean surface prior to the growth process step. The first step in the cleaning operation is brushing the crucibles with detergent and boiling water to remove the grease and dusts, which are possibly stacked to the surface of crucible. Then, we applied chemical cleaning procedure as we kept it in a 40% HNO_3 bath for 4 hours to remove metallic impurities on the surface and to clean of the surface of the crucible from the chemical we used; it was rinsed with distilled water in an ultrasonic bath for 15 minutes. In order to get rid of the remaining impurities inside the crucible, the crucible was kept in hot soapy water for 12 hours, and also rinsed with distilled water in ultrasonic cleaner and for 1.5 hour put in isopropyl alcohol. At the final step, heat treatment was applied to the crucible as it was placed into furnace under the inert argon gas atmosphere. After all steps were done, the crucibles were cleaned with distilled water and leaved to dry [39].

3.2.1 Crystal Growth Techniques

According to the aim of this thesis, the crystal was grown in the $Cu_{0.5}Ag_{0.5}InSe_2$ form. In order to have a crystal in this structure, it was synthesized by mixing stoichiometric amount of Cu, Ag, In and Se elements, at the weights 1.77, 3.01, 6.41, and 8.81 gr., respectively. Then, they were loaded in the crucible which was cleaned with using the cleaning procedure mentioned in the previous section. Before sealing this quartz ampoule, it was connected to a vacuum pump for 2 hours to reach a vacuum value approximately 1×10^{-5} Torr.

Because our Bridgman-Stockbarger crystal grown system has not any unit that can provide rotation to the crucible during the grown process, in order to satisfy homogeneity and also to start initial the chemical reaction in the prepared mixture, the sealed quartz tube was heated at 1050 °C which is close to the highest melting point between the elements using for crystal growth, for 4 days and by shaking frequently at this temperature. This temperature point was reached with increments of 100 °C up to 400 °C, 50 °C between 400 °C and 750 °C and again 100 °C up to final temperature at 30-minute time intervals. The heating process was carefully carried out to avoid the explosion of the loaded ampoule because Se is in the gas phase at this temperature and its vapor pressure could damage the crucible. After synthesis, the furnace was slowly cooled to the room temperature with decreasing 10 °C at 10-minute time intervals.

Table-3.1: Melting and boiling points of the elements composed CAIS crystal

Element	Melting Point (˚C)	Boling Point (˚C)
Cu	1085	2562
Ag	962	2162
In	157	2072
Se	221	685

For this work, CAIS polycrystalline structure was grown with using the Crystalox MSD-4000 model three-zone vertical Bridgman–Stockbarger system in our Crystal Growth Laboratory of Physics Department. Its schematic diagram is shown in Fig.3.1. This system involves heating polycrystalline material in a container above its melting point and slowly cooling it from one end which is the bottom of the crucible.

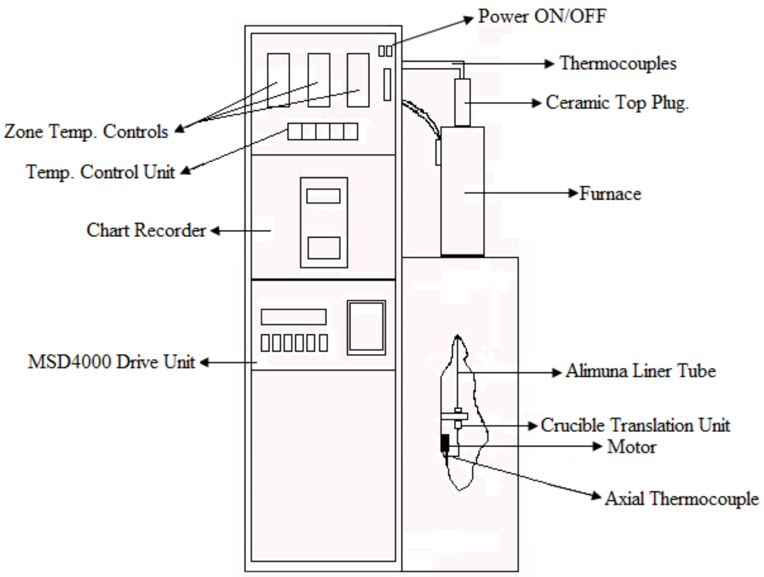

Figure-3.1: Schematic diagram of Bridgman-Stockbarger system

This Bridgman-Stockbarger technique employs a vertical furnace includes three independent heating zones, and each of them has 150 mm long. The furnace was arranged so that the upper temperature zone is maintained about 1150 °C which is over the melting point of the material to be grown, while the middle zone is kept about 950 °C and the lower zone about 850 °C. The temperature gradient for the grown CAIS crystal is given in the Fig.3.3. Thus, a temperature gradient is maintained between the upper and lower portions of the furnace, with the melting point of the material to be grown approximately midway along the gradient. The crucible was placed in the upper part of the furnace with caring about the thermocouple tip of it. Then, the crucible was lowered slowly down the furnace. The translation of the crucible was performed with 1.0 mm/h. After the crucible reached to the cold zone, its temperature gradually lowered to the room temperature. Therefore, the crystal grown process in the Bridgman-Stockbarger system was took approximately 6 days.

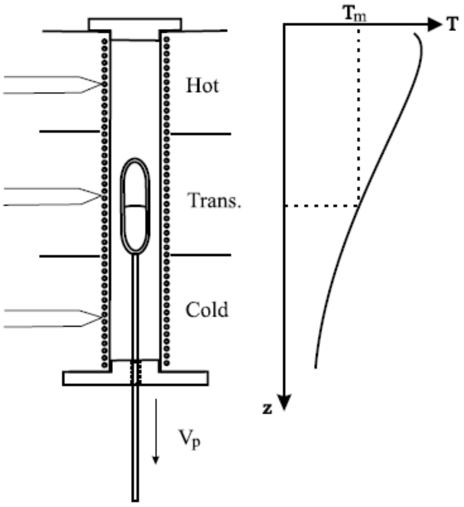

Figure-3.2: Furnace unit of the Bridgman-Stockbarger growth system and the ideal temperature distribution along the axis of a crucible

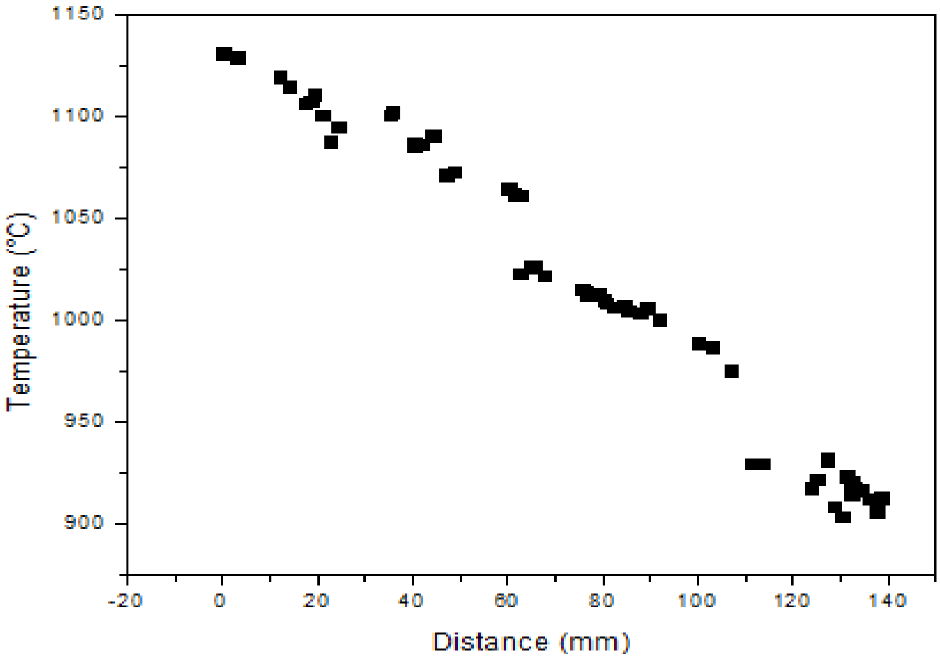

Figure-3.3: Temperature gradient profile of grown CAIS crystal

At the end of the whole process for the crystal growth, the crucible was broken. The grown CAIS crystal is shown in the Fig.3.4. We divided it into three parts, and each of them analyzed with EDXA and XRD powder method in order to get information about its structural characteristics.

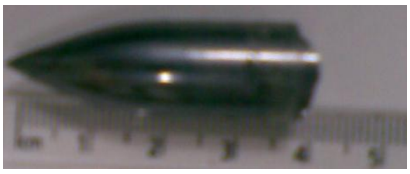

Figure-3.4: CAIS crystal ingot grown using Bridgman-Stockbarger system

3.3 Preparation of CAIS Thin Films

3.3.1 Substrate and Sample Preparation

The optically flat soda lime glass and indium tin oxide (ITO) coated glass substrates were used as substrate material for the deposition of CAIS thin films. The glass slides were commercial microscope lamellas, and they were prepared in different dimensions as squares with 6 mm; and as rectangles with 6 mm and 12 mm edge lengths by using a diamond cutter tool. These dimensions were determined with caring of the substrate holder and masks having suitable geometries for characterization processes. For preparation of high-quality thin films, before depositing films, substrates must be cleaned in order to remove the contaminants on the substrate surface. The cleaning procedure was performed with using four different pot. One of them were filled with acetone, the other with a solution of 50% H_2O_2 and 50% distilled water, and the other two with distilled water. The pots having distilled water and hydrogen peroxide solution were boiled using hot plate. The first step was shaking the glass slides in the acetone, and then they were rinsed in the boiling distilled water. Then, they were boiled in the H_2O_2 solution with 5 minutes, and this pot having peroxide solution were shaken in the ultrasonic cleaner with 10 minutes. This process provides removing organic contaminants on the substrate surface. After this process, each slide was shaken in the other distilled water using a tweezers in order to get rid of the possible residues attained during the cleaning procedure. The substrates, after the cleaning process, were kept in methanol. This was done to keep substrates clean until the deposition and before using for the deposition they were dried by blowing hot air or pure nitrogen. In addition to these slides, ITO coated glass slides were used as a substrate, however, they were taken as prepared and cleaned before. The only operation done for them is shaking them in about 10 minutes using ultrasonic bath in order to remove possible contaminants on the surface of them.

In electrical and optical characterizations, the main measurement technique was van der Pauw method and therefore some of the substrates were masked with a specific geometry, Maltese-Cross, in order to take successful measurement. The shape of this mask is shown in the Fig.3.5.

Figure-3.5: Maltese-Cross geometry

The van der Pauw method is a standard technique for investigating the electrical resistivity (or conductivity) characterization of thin film materials using four point contacts formed on the circumference of the sample arbitrarily. This method is widely used since it decreases the measurement errors which arise in classic characterization techniques due to the possibility of contact resistance and also it gives opportunity to apply it for samples of any shape [81].

There are some main cases which should be taken into account when carrying out resistivity and also Hall effect measurements. Primary aspects are ohmic contact quality and its size, uniformity of the sample and accurate thickness determination, thermo-magnetic effects because of non-uniform temperature, and photoconductive and photovoltaic effects which can be eliminated by carrying out the measurements in a dark environment. Moreover, the sample lateral dimensions should be large compared to the size of the contacts and the sample thickness. In addition to this, the factors that can affect the accuracy of the measurements, for instance, sample temperature, electrical current, and voltage; and for the Hall effect measurements magnetic field intensity, should be taken in control [71].

In order to have accurate results, semiconductor thin film materials can be deposited on the substrates with masking and adopting a suitable geometry, as illustrated in the Fig.3.6. Because relative errors caused by non-zero values of D are of the order of D/L [83], for the preferable geometry, the average diameters D of the contacts, and sample thickness d should be much smaller than the distance between the contacts L.

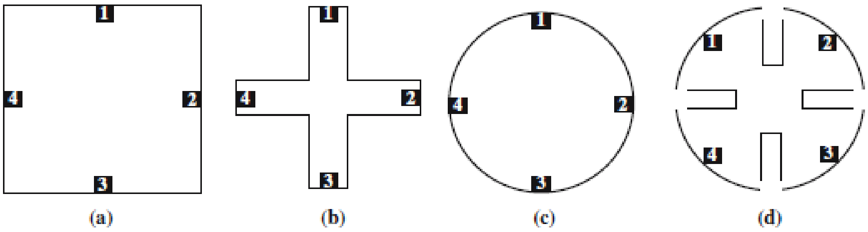

Figure-3.6: Symmetrical van der Pauw structures: (a) square, (b) Greek cross, (c) circle and (d) cloverleaf

3.3.2 Growth Process of CAIS Thin Films

In this thesis, the CAIS thin films were deposited on soda lime and ITO glass substrates with using e-beam evaporator in the Department of Physics at METU.

Figure-3.7: The picture of the e-beam evaporation system

It is the thin film deposition system giving opportunity for thermal and e-beam evaporation, for these cases it has two different units. In order to use e-beam deposition, the system has an electron beam source consists of a 3-kW electron gun, and an electromagnet to deflect the produced electron beam into the source material. Moreover, there is a water-cooled cavity for placing graphite crucible containing source material to eliminate the effects due to heating this container. The system is surrounded with a stainless steel vacuum chamber which is in the dimensions of 50 cm diameter and 75 cm height. Besides, the vacuum chamber is sealed the stainless steel base plate with a rubber o-ring. There are two systems in order to attain necessary vacuum value; starting vacuum system helps to reach a vacuum value for a turbo-molecular pump which is the main vacuum system in this evaporator. The picture and schematic diagram of the electron beam evaporation system are shown in the Fig.3.7 and Fig.3.8.

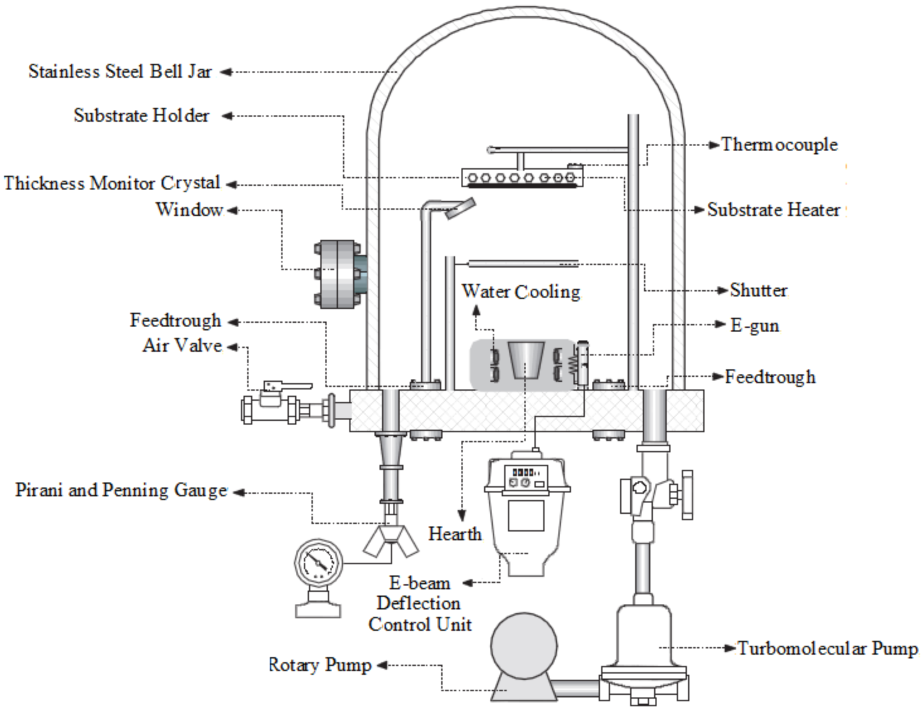

Figure-3.8: The Schematic diagram of the e-beam evaporation system

The crystal powder grown by Bridgman-Stockbarger technique was used in the deposition of CAIS thin films. Before starting to thin film deposition process, from this crystal, approximately 6 gr. powder (it was not constant parameter for all thin film deposition runs) was prepared as a source material. As it is mentioned, the grown crystal was separated into three parts, the part having most appropriate for the required stoichiometry was chosen in order to be a source material. Then, it is put in the 2 cm diameter graphite crucible and placed in the water-cooled cavity in the system. Besides, before producing thin films, with the copper masks, the glass substrates were placed on the aluminum substrate holder containing nine rectangular holes. In order to fix the substrates and to maintain a uniform substrate heating, copper sheets were placed on the back side of the substrates. Then, the substrate holder was closed with the part that can be attached to the e-beam system. This part has resistive heating unit having chrome-nickel heating wires covered with insulating quartz tubes. It is required to control the substrate temperature which is the important factor on the composition, structure and morphology of the film by affecting film adhesion, grain structure, the surface roughness and the rate of any chemical reaction occurring on the substrate. After placing glass substrates in the substrate holder unit, the height of it was arranged approximately 15 cm above the source. A Pt/Pt-13%Rh thermocouples were attached to the substrate holder unit to measure substrate temperature. Fluke digital thermometer was used to measure the temperature at the substrates during the deposition. Stainless steel shutter was mounted between the source and the substrate holder and then the chamber was closed to start the vacuum process. The vacuum was taken up to 10^{-2} Torr with the help of Varian 3117 vacuum system, and then Laybold turbo-molecular pump system was operated in order to reach the vacuum value necessary to start the deposition process. After system vacuum reached approximately to 6×10^{-6} Torr, 60 V_{rms} AC potential was applied to substrate heater to obtain starting substrate temperature about 190°C. Power supply of e-beam source was opened after the substrates were reached to the required temperature. Giving voltage to the current carrying filament, electrons generated by thermionic emission were accelerated and electron beam was focused on the source by the help of the electromagnets. With using the intensity controller unit, intensity beam of electrons was adjusted and the shutter was opened to start the thin film production. When the electrons were deflected to a small localized area on the source material, these energetic electrons melt of material and rapid evaporation from source. Therefore, these evaporants condensed onto substrate surface to form thin film layer. During this process, deposition vacuum was about 8×10^{-6} Torr, deposition substrate temperature was about 200 °C and beam intensity was controlled to obtain 10 Å/sec deposition rates which was measured by Inficon XTM/2 Deposition monitor connected to the quartz thickness crystal inside the vacuum chamber. After obtaining expected film thickness, the shutter was closed and the beam intensity was switched off. Then, the substrate heater was slowly closed, and after waiting a few minutes, the turbo vacuum system was closed. In order to prevent possible oxidation of the films, system was allowed to cool down to room temperature. After reaching the room temperature, the initial vacuum system was turned off, and the deposited thin films were taken out from the system.

3.3.3 Annealing

The thin films were characterized firstly in as-grown form, and then the post-growth heat treatment was applied to some of the samples to deduce the effects of annealing on the structural, electrical and optical properties of the deposited thin films. This annealing treatment was done with using annealing furnace and also the thin films were heated under the nitrogen environment. The temperature range of this annealing that was studied on were 300-500 °C with 30-minute time interval. For this purpose, firstly, the furnace was heated to the desired temperature and during this procedure the nitrogen gas was given to the glass tube in the furnace in order to prevent any contaminant from the interior surface of the glass tube. After reaching the temperature, thin films were placed at the centered of the glass tube. Then, the films were kept inside at 30 minutes under the nitrogen gas flow, and after 30 minutes furnace was turned down. However, the films were slowly gone out the tube and they were taken when the system was cooled down to the room temperature. The nitrogen gas atmosphere was applied until the furnace temperature decreased to the room temperature in order to prevent oxidation on the surface of the films. This process was applied to the films one by one, since each thin film was annealed at different temperature.

3.3.4 Electrical Contacts

For electrical and optical characterizations, electrical contacts were needed. They were deposited on the surface of the thin film using the suitable copper mask as shown in the Fig.3.9. In was used as a contact element and it was deposited on the thin film by thermal evaporation method. The schematic diagram of the thermal evaporation system is shown in the Fig.3.10.

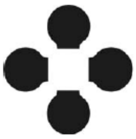

Figure-3.9: Indium contact geometry

This contact formation was used to obtain an ohmic contact which provides a region of the current-voltage curve of the device is linear and symmetric. The fundamental steps in contact fabrication are masking the thin film, contact metal deposition, and annealing. These ohmic contacts were costed on the thin films, having suitable mask geometry, from the pure indium source with using thermal evaporation technique.

Before the deposition of the contacts, the thin films were prepared that its surfaces were wrapped with the copper masks which are suitable in order to make contact at the edges of the film surfaces. Then, the films were placed into the substrate holder and attached to the evaporation system. Moreover, the indium source was put into the system using the tungsten boat. The vacuum chamber was placed to the system the water cooling system was opened and then the vacuum process was started. The evaporation system has two vacuum systems; rotary pump and a diffusion pump. Firstly, the rotary pump, and simultaneously the heater of the diffusion oil were turned on. After approximately 15 minutes, liquid nitrogen was added to the system and the vacuum was waited to reach at least 1 x 10^{-6} mbar. To do this, after rough pumping, a diffusion pump was operated. At the necessary vacuum pressure, the contact deposition was started with heating the tungsten boat slowly giving AC voltage. At 90 volt, the shutter was opened for nearly 3 minutes to deposit indium on the surfaces of the thin films. Then, the voltage source was turned off with slowly decreasing the voltage given and also the heater was closed. When the surface temperature of the diffusion pump reached to the room temperature, the vacuum system was switched off and the system was opened.

After completing the deposition of the indium contacts, in order to provide contact diffusion, thin films were annealed at 100 °C under the nitrogen atmosphere. The post-annealing system is shown in the Fig.3.11.

At the end of the contact deposition and annealing, the copper wires were attached on the contact surface using silver paste to complete the sample preparation process for characterization.

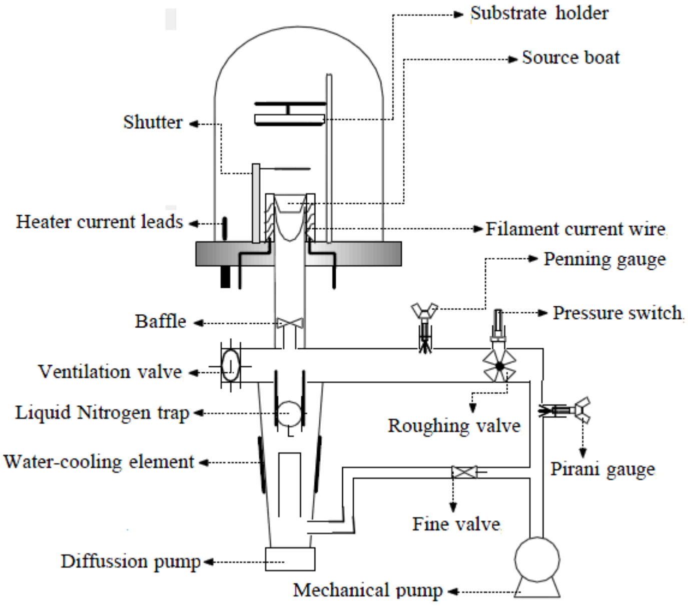

Figure-3.10: Thermal evaporation system for contact formation

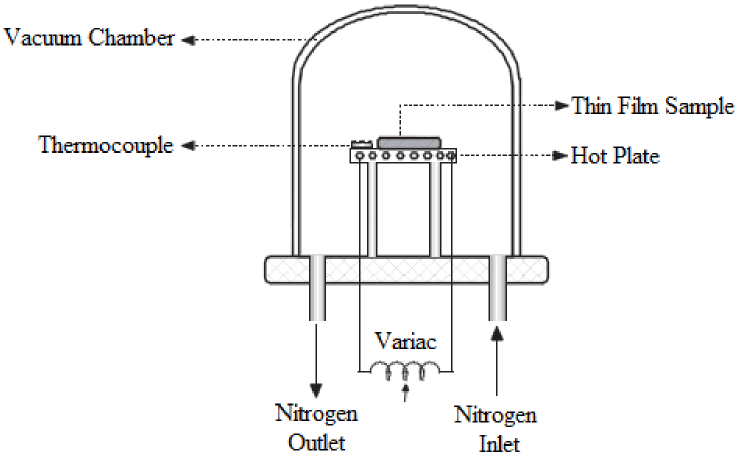

Figure-3.11: Post-annealing system after contact deposition

3.4 Structural Characterization

Structural properties of the deposited CAIS thin films were examined through thickness measurement, XRD and EDXA. They were also used to optimize the deposition parameters for the next thin film productions.

3.4.1 XRD Technique

XRD technique was used to study the structural properties and to find the structural parameters of the deposited CAIS thin films. The XRD measurements were performed by using a Rigaku Miniflex XRD system equipped with CuKα radiation of average wavelength 1.54059 Å. All X-ray measurements were taken with the same parameters, such as, 2θ is in between 10° and 90° and scan speed of 2 degree/min. In addition to these, the peak matching analysis was made by using the computer software and ICDD database where specifically ICDD database was used to match the measured peak with the known structures.

In addition to this, after growing the CAIS crystal, its XRD measurement was done by the powder method. We used the powder of the crystal which was made during the cutting procedure and also was crushed some part of it into fine particles. Then, they were placed into to sample holder and analyzed by XRD machine. Thin films were analyzed with sticking them on the sample holder without any operation on them.

3.4.2 EDXA

The elemental atomic composition of the samples was accomplished with an EDXA attached to the SEM. We used two SEMs with EDXA, one of it is JSM-6400 in the Central Laboratory at METU and another one is Evo-40 from the Department of Chemistry at Bilkent University. The compositional characterization of the materials was investigated at two different energy values because the range of electron penetration depends on the incident electron-beam energy. In order to carry out surface or near the surface analysis, an electron beam with relatively low energy, 6 kV, and for the deeper layer analysis a more energetic electron beam, 30 kV, were used to determine the atomic ratio of the constituent elements in grown single crystal and deposited CAIS thin films. In some cases, in order to get average information for the composition, we used electron beam energy at 20 kV. In most applications, data were collected over a selected area of the surface of the sample.

3.5 Electrical Measurements

The measurements of resistance, temperature dependence of the dark conductivity, mobility and carrier concentration and type of CAIS thin films were carried out on the van der Pauw samples.

3.5.1 Resistance Measurements

Although careful controlling during crystal growth, and also during the deposition of the thin film processes, there might be high resistive samples. Therefore, before the electrical and optical measurements, in order to have an opinion for initial applied voltage to the samples, we measured the resistance of the thin films at room temperature.

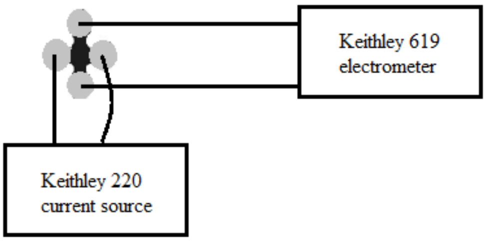

Figure-3.12: Schematic diagram of the resistance measurement

3.5.2 Hot Probe Technique

Hot probe (or thermoelectric probe) method is the simplest technique to determine the type of the semiconductors. The idea used in this method is that the carriers move within the semiconductor from the hot probe to the cold probe. For this experiment, a multimeter is used and the region of the material, where the positive terminal of the meter is pointed, was heated while the cold probe is connected to the negative terminal. With this arrangement, when applying the probes to n-type material, it gives a positive voltage reading on the meter, while p-type material yields a negative voltage.

3.5.3 Hall Effect Measurements

For wide range electrical characterization, Hall effect measurements of deposited CAIS thin films were analyzed by using the conventional four-point dc van der Pauw technique. As it is mentioned before, the thin films were produced in appropriate with van der Pauw geometry, and also electrical contacts were obtained by evaporation of indium. Van der Pauw method provides elimination of two important experimental errors; imperfect alignment and thermoelectric voltage generated by the thermal gradient between probes. In general, the applicability of this method is taken into consideration when the sample resistance is the range of 10^3-10^9 ohms [6]. For less resistive materials, it can be taken with the current-voltage measurement from the parallel contacts as shown in Fig.3.13. However, if the semiconductor is high resistive material, it is more appropriate to measure across different pairs of contacts (Fig.3.14) for conductivity and Hall effect analysis.

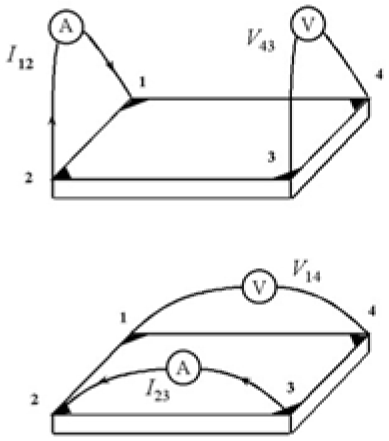

Figure-3.13: Schema of a van der Pauw configuration used in the electrical characteristics of less resistive materials

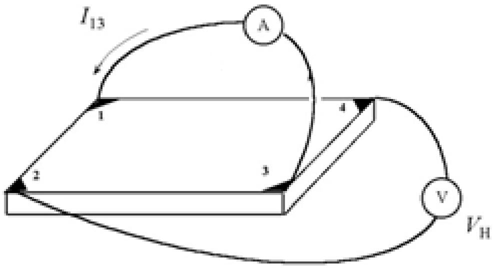

Figure-3.14: Schema of a van der Pauw configuration used in the electrical characteristics of high resistive materials

The temperature dependent dark conductivity and Hall effect measurements were carried out in the temperature range of 100-400 K by means of a Janis Liquid Nitrogen VPF Series Cryostat, as shown in Fig.3.15. The temperature of the samples inside the cryostat was measured with a GaAlAs diode sensor and controlled by a LakeShore-331 temperature controller. Measurements were done under nearly 1.3 x 10^{-2} Pa vacuum inside the cryostat by the help of Ulvac Rotary pump. Cooling of the system was performed by adding liquid nitrogen to the trap through the fill port. After the addition of the liquid nitrogen, the temperature of the sample cools down to 100 K and then was gradually increased by 10 K steps to perform the required measurements. The current was supplied by a Keithley 220 programmable current source, and the voltage was measured by Keithley 619 multimeter. Walker Magnion Model FFD-4D electromagnet was used for producing the magnetic field. Strength of applied magnetic field was kept constant (about 0.90 T) in all measurements. Whole measurements for electrical characterization was completed without using any computer program, they were done by hand.

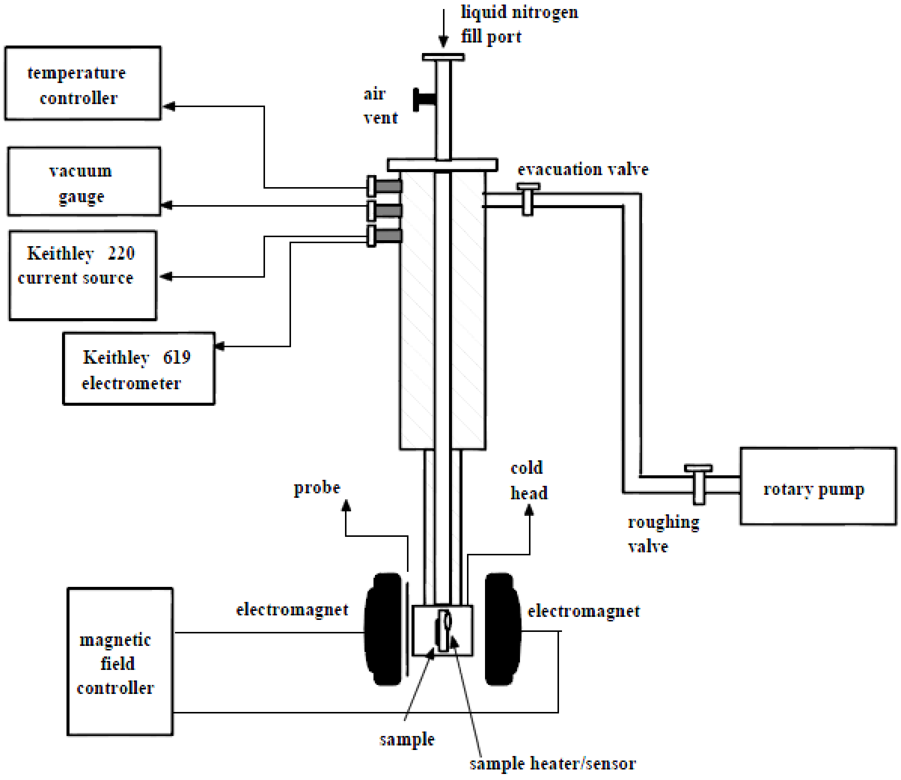

Figure-3.15: Hall effect measurement set-up

Single measurement was done to find the all parameters related to electrical properties of the thin film. In this experiment, the current-voltage values were measured with and without magnetic field effect. Twelve measurements were taken to determine them in each temperature step. Initially, four measurements were completed under no magnetic field effect, and they were used for dark conductivity calculations. In addition to this, for Hall effect characterization, the two sets of measurements having four current-voltage measurements were done with various combinations of the magnetic field directions (given in the Table-3.2).

Table-3.2: Combination of the measured potential differences with respect to the applied current directions

Magnetic Field	Applied Current (Keithley 220)	Measured Potential Difference (Keithley 619)
B=0	I_{13}	V_{24}
B=0	I_{31}	V_{42}
B=0	I_{24}	V_{13}
B=0	I_{42}	V_{31}
+B	I_{13}	V_{24}
+B	I_{31}	V_{42}
+B	I_{24}	V_{13}
+B	I_{42}	V_{31}
-B	I_{13}	V_{24}
-B	I_{31}	V_{42}
-B	I_{24}	V_{13}
-B	I_{42}	V_{31}

The resistivity was found from the relation

$$\rho = f\,\frac{\pi d}{4\ln(2)}\left(R_{13,24\,(B=0)} + R_{31,42\,(B=0)} + R_{24,13\,(B=0)} + R_{42,31\,(B=0)}\right) \qquad (3.1)$$

where f is a function of the potential difference measured, and it is called as a correction factor. In other words, it is a geometrical factor based on the symmetry and also related to the resistance values measured from the contact points of the material. When the material has perfect symmetry, this value can be approximated as 1. Therefore, with our resistance measurements, the measured potential differences with respect to the applied current direction, contact points, gave approximately same values with their symmetry. According to having symmetrical contacts, f was taken as 1 [90] and the resistance values were called with the contact numbers which were used for current and voltage; for example,

$$R_{13,24\,(B=0)} = {}^{V_{24}}\!/_{I_{13}} \tag{3.2}$$

As a result of this, dark conductivity was found from the reciprocal of the resistivity value. For Hall effect measurements, the resistivity values were found for each current-voltage data, and then the calculated resistance values with or without magnetic field were subtracted from each other. Therefore, two resistance values, due to the direction of the applied magnetic field, were found;

$$\Delta R_{+} = R_{+B} - R_{B=0} \quad \text{and} \quad \Delta R_{-} = R_{-B} - R_{B=0} \tag{3.3}$$

Thus, with using these values, we calculated the Hall coefficient R_H as

$$R_H = \frac{10^8 \times d \times (\Delta R_{+} + \Delta R_{-})}{8 \times B} \tag{3.4}$$

where 10^8 comes from the unit transformations, and the division constant, 8, from having 8 different measurements, d is the thickness of the sample. One of the characteristic of R_H is that it the sign of it gives the type of the material, and so we determined the types of the samples for each deposition. Moreover, from this coefficient, the carrier concentration was calculated using the relation

$$n = \frac{r}{qR_H} \tag{3.5}$$

where r is the Hall factor and it was taken as 1 [91], n represents the electron concentration, but if the sample is p-type it is changed to p symbol, and q is the electron charge. As a final step, mobility was found with using the relation

$$\mu = \frac{\sigma}{nq} \tag{3.6}$$

These temperature dependent mobility, carrier concentration and conductivity measurements were then analyzed with plotting logarithm of these results versus 1/temperature.

3.6 Optical Measurements

Optical measurements are attractive because most of them can be done non-contacting measurement and with minimal sample preparation. The instrumentation for many optical techniques is commercially available and they can be operated automatically. Besides, the measurements with automatic from the instrument or computer assisted measurements give very high sensitivity results.

3.6.1 Transmission, Reflectance and Absorption

The optical transmittance measurements were done using Pharmacia LKB Ultrospec III UVVIS spectrometer for 325-900 nm regions and also Bruker Equinox 55 FT-IR-NIR spectrometer in 600-1150 nm regions. On the other hand, the reflectance measurements were done in the range of 200-1100 nm by the help of Unico UV-Vis Sepctrophotometer. All of the measurements were referenced to the glass because they were deposited on the glass substrates.

The results of the transmittance and reflectance measurements were used to have information about the interaction with electromagnetic radiation, illumination with respect to the wavelength. Furthermore, the absorption characteristics of the samples were found from the relation

$$\alpha = \frac{1}{d}\ln\left(\frac{T}{(1-R)^2}\right) \text{ or } \alpha = \frac{1}{d}\ln\left(\frac{I}{I_0}\right) \tag{3.7}$$

The absorption coefficient of a direct transition is related to the energy band gap as

$$\alpha = {(h\nu - E_g)^{1/2}} \Big/ {h\nu} \tag{3.8}$$

Therefore, with the help of the relation between $(\alpha h\nu)^2$ and $h\nu$, the optical band gap energy of the samples can be calculated from using the intercept of the linear portion of the curve on the photon energy $(h\nu)$ axes.

3.6.2 Photoconductivity

The temperature dependent photoconductivity measurements between the temperature ranges of 100-450 K were performed inside the Janis cryostat equipped with a cooling system by means of liquid nitrogen. The samples were placed in the cryostat, however, for this measurement 12-Watt halogen lamp were arranged as being on the thin film surface at a suitable height to provide a homogenous illumination on the whole surface. The photoconductivity characterization of the samples was carried out with measuring the photocurrent under different illumination intensities at 10 °C temperature steps with constant bias voltage. For this measurement, lamp current was supplied by Keithley 220 programmable current source and the illumination intensity of the lamp was arranged by changing the current passing through the lamp in the range of 50-90 mA with 10 mA steps. As a conclusion, with changing the current passing through the halogen lamp (50, 60, 70, 80 and 90 mA), we obtained different illumination intensities (17, 34, 55, 81 and 113 mW/cm^2). Using by Keithley 2400 sourcemeter, bias voltage was applied to the sample and resultant current was measured. The schematic diagram for the photoconductivity measurement set-up is shown in the Fig.3.16. For the determination of the illumination intensities IL Ford 1700 Radiometer was used. In addition to this, this optical measurement was assisted by computer using a LabVIEW program. In this experiment, for each temperature step, initial data was taken under no illumination, and then the others at five different light intensities.

Experimentally, we obtained intensity values corresponding to different temperatures and illumination conditions. Having obtained light intensity dependent photocurrent values, the photocurrent versus inverse temperature was plotted for different light intensities and they were analyzed to determine the conductivity of the sample under illumination. As an example for this analysis, the dark resistance R_{dark} for one temperature value was found from the relation

$$R_{dark} = \frac{V}{I_{dark}} \tag{3.9}$$

where I_{dark} is the measured intensity and V is the given bias voltage value. The resistivity value was calculated using the equation

$$\rho_{dark} = \frac{\pi d}{\ln 2} R_{dark} \tag{3.10}$$

where d is the thickness of the sample. Then, the conductivity of the sample was the reciprocal of the resistivity value,

$$\sigma_{dark} = {}^{1}/_{\rho_{dark}} \tag{3.11}$$

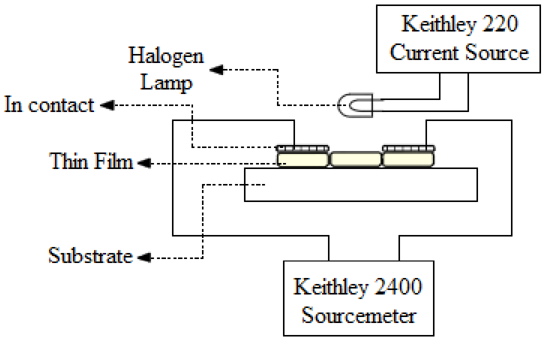

Figure-3.16: Photoconductivity set-up

Besides, to determine if the sample have supralinear or sublinear characteristics, we plotted logarithm of the relative illumination intensity versus logarithm of the illumination intensity that were applied by halogen lamp. For specific temperature values, they were plotted, and the linearity of them provided required information about the samples.

3.6.3 Photoresponse

Photoresponsivity spectra for the illumination at different wavelengths were measured at room temperature giving initial bias voltage to the sample. In this experiment, current passing through the sample was measured at each wavelength in the range 325-1350 nm. The light with different wavelengths was produced and also focused on the sample using a Newport Oriel Apex Monochromator Illuminator which has a 1200 lines/mm diffraction grading. To take the data under dark and illumination, a shutter placed between the lamp and the monochromator was used. Keithley 2400 sourcemeter supplied the bias voltage and also it was used to measure the photocurrent values. All of the measurements were controlled by computer using a LabVIEW program. The schematic diagram of this set-up for the photo-response measurement is shown in the Fig.3.17. The obtained photoresponse spectra measurements were corrected for the spectral distribution of the illumination light. The power spectrum of the light radiated by halogen lamp used for this correction is shown in Fig.3.18. The experimental data were used to plot photocurrent versus wavelength graphs, and from the peaks in this graph, activation energies of the sample were calculated as

$$E_a = {}^{1240}\!/_{\lambda\ (nm)} \tag{3.12}$$

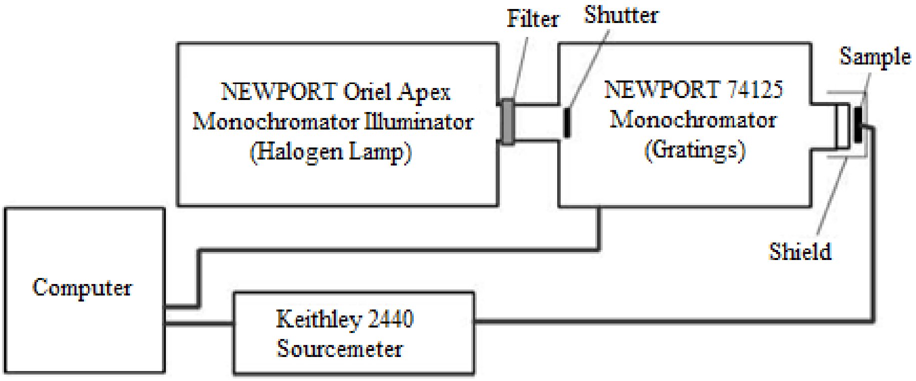

Figure-3.17: Schematic diagram of the photoresponse system

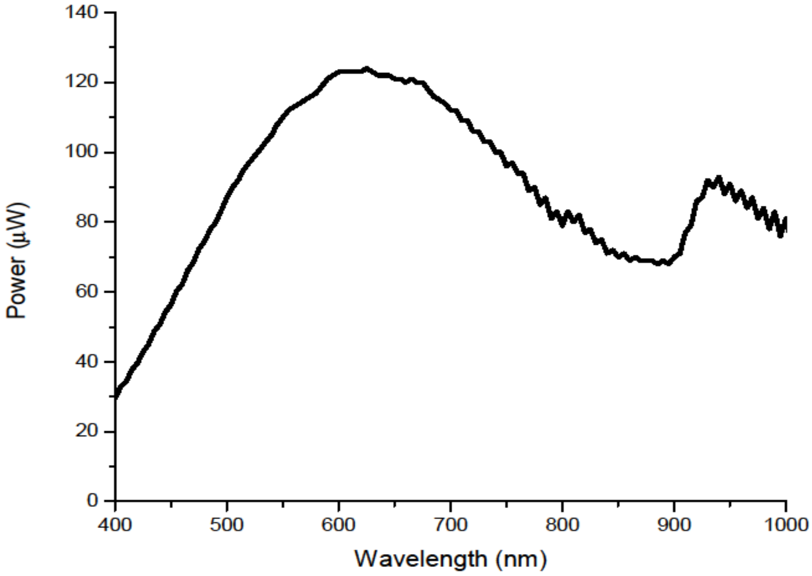

Figure-3.18: Spectral correction curve of the radiated power for the light outgoing through monochromator

CHAPTER 4

RESULTS AND DISCUSSIONS

4.1 Introduction

In this chapter, the results of structural, optical and electrical measurements of CAIS thin films in the form of as-grown and annealed at different temperatures will be presented. Firstly, the structural and compositional analyses of the samples will be given, and then the results of temperature dependent dark conductivity and Hall effect will be discussed in the temperature range of 100-450 K. In the last section, the results of the optical characterizations will be presented. In general, the characterizations of the CAIS thin films will be discussed with respect to the different atomic ratio of the constituent elements.

During this study, effects of the substrate temperature and most of the deposition parameters were kept to be the same for all depositions; however, the weight of the CAIS powder source were changed in each run in order to obtain expected thin film structures having the required atomic ratios of the elements. In R2 and R3 productions, only CAIS powder was used as a single source for the thin film deposition. However, for R5 deposition, instead of single CAIS layer, we also used Cu and Se sources having layer by layer deposited thin films in order to achieve the required elemental ratios in the composition (see Table-4.1).

Table-4.1: Summary of deposition parameters of samples

Sample Name	Sources	Deposition Property	Substrate Temperature (°C)	Thickness (nm)
R2	CAIS powder	Single CAIS layer	188	600 – 620
R3	CAIS powder	Single CAIS layer	194	760 – 820
R5	CAIS powder & Excess Cu and Se sources	Layer by layer (CAIS-Cu-CAIS-Se) CAIS (~250 nm) Cu (~25 nm) CAIS (~240 nm) Se (~10 nm)	203	580 – 600

4.2 Structural and Compositional Characterization

As mentioned in the third chapter, for the structural and compositional characterization, EDXA, SEM, and XRD were used in order to investigate the influence of deposition parameters, atomic ratios of the elements in the composition and post-annealing conditions on the structural, morphological and compositional properties of CAIS thin films.

4.2.1 EDXA and SEM Results

The compositions of the films were determined by EDXA in order to study the stoichiometric compositions of the deposited thin films and also investigate the Cu/(Cu+Ag) ratios in these films. The atomic ratios of the elements in the powder and deposited thin films are tabulated in Table-4.2 – 4.4 with respect to the annealing temperatures.

Table-4.2: EDXA results of CAIS powder in percentage

Sample	kV	Cu	Ag	In	Se
Single Crystal (middle)	20	8.85	14.02	24.19	52.94
Single Crystal (top)	6	10.53	18.20	27.71	43.57
Single Crystal (top)	30	11.02	9.72	18.47	60.79
Single Crystal (bottom)	6	11.76	8.56	31.75	47.93
Single Crystal (bottom)	30	12.38	10.32	28.99	48.31

Table-4.3: EDXA results of CAIS R2 thin films in percentage

Sample	kV	Cu	Ag	In	Se
As-grown	6	1.38	37.58	26.69	34.34
300 °C Annealing	6	0.00	25.26	52.14	22.60
400 °C Annealing	6	3.33	28.36	41.14	27.17
500 °C Annealing	6	0.70	19.09	46.61	33.61
As-grown	30	1.48	13.71	42.04	42.77
300 °C Annealing	30	0.00	13.24	44.69	42.06
400 °C Annealing	30	1.95	11.95	43.22	42.87
500 °C Annealing	30	1.60	12.14	42.15	44.12

Table-4.4: EDXA results of CAIS R3 thin films in percentage

Sample	kV	Cu	Ag	In	Se
As-grown	20	3.49	16.43	36.56	43.52
300 °C Annealing	20	3.46	21.34	39.98	35.22
400 °C Annealing	20	2.61	21.47	39.37	36.54
500 °C Annealing	20	2.93	19.04	37.52	40.50

Table-4.5: EDXA results of CAIS R5 thin films in percentage

Sample	kV	Cu	Ag	In	Se
As-grown	20	11.73	3.65	37.14	47.47
300 °C Annealing	20	10.06	4.30	38.42	47.22
400 °C Annealing	20	11.91	3.69	40.74	43.66
500 °C Annealing	20	12.45	3.54	37.85	46.17

Due to the mechanical problems about the SEM machine, and also having more samples to analyze in a limited time, we used two different SEM machine for EDXA characterization, some EDXA analyses were carried out in different energy values.

As it is given in the tables, there are significant distinctions in the atomic ratios of the elements for three different depositions and the CAIS powder. There is no systematic decrease or increase of the ratio of the constituent elements. The composition analyzes of the CAIS crystal shows that it is approximately in the form of $Cu_{0.5}Ag_{0.5}InSe_2$. However, this stoichiometric ratio changes in the powders which were obtained from the different regions of the CAIS single crystal. In the thin film depositions, we used the powder obtained from the bottom region of the crystal as a powder source due to having the most consistent $Cu_{0.5}Ag_{0.5}InSe_2$ composition. Actually, it is apparent from Table-4.2, 4.3 and 4.4 that homogeneous synthesis was not attained from the starting atomic composition Cu:Ag:In:Se = 0.5:0.5:1.0:2.0. CAIS powder does not melt congruently since its constituent elements have different melting points, and as a result of this, in the previous researches about this quaternary alloy, rapid decomposition methods, such as flash evaporation [12, 13, 19], were used to produce this type of films. Therefore, it may be the reason in the differences of the EDXA results between the source and deposited thin films. In other words, the different vapor pressures of the constituent elements ($P_{Se} > P_{In} > P_{Ag} > P_{Cu}$) may be responsible for obtaining the off-stoichiometric CAIS thin films form the atomic ratios of the powder [93]. Moreover, since the EDXA results give the atomic ratios of the constituent elements, if the weight of some elements decreases in the composition, the ratio of the others increases to satisfy the total hundred percentages. On the other hand, there is a systematic relation in the three thin film decompositions, R2, R3 and R5, of the Cu/(Cu+Ag) ratios; that are, 0.10, 0.18 and 0.76 in as-grown forms; 0.11, 0.14 and 0.77 in annealed 400 °C forms; and 0.12, 0.13, and 0.78 in annealed 500 °C forms, respectively.

Moreover, it was found that there was a considerable fluctuation in the contribution of the elements to the composition of the thin films with applying the post-depositional annealing process. The change in the weight of the elements in the annealed thin films shows that there is a notable decrease in the Se and an increase in the In content with annealing. With increasing the annealing temperature, the possible re-evaporation of selenium atoms from thin film surface, which is because of having high vapor pressure, before making the bond to construct the crystalline structure, may be the reason for the decrease in the atomic percentage of selenium [94]. On the other hand, averagely, there is very slight change in the atomic percentage of copper and silver contents with increase in the annealing temperature.

The film surface topology and morphology, including grain size, were studied using SEM. The SEM of CAIS films, in terms of decomposition and annealing temperatures are shown in Fig.4.1 - 4.3.

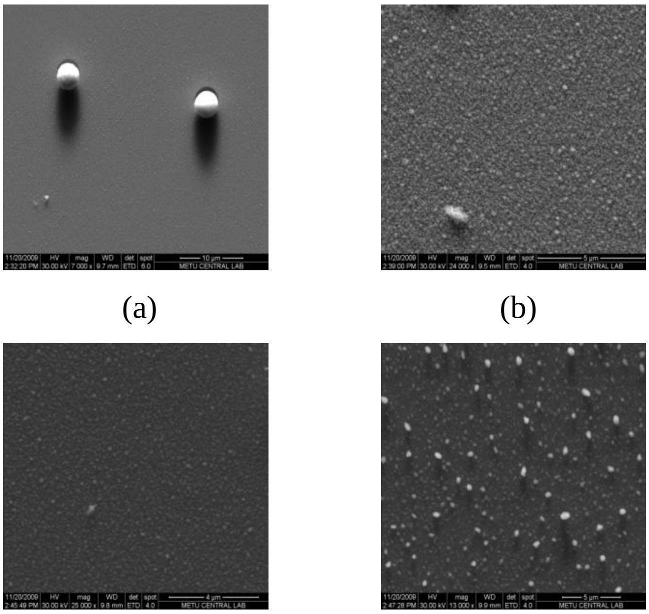

(a) (b)

(c) (d)

Figure-4.1: SEM micrographs for R2 a) as-grown b) annealed at 300 °C, c) 400 °C and d) 500 °C

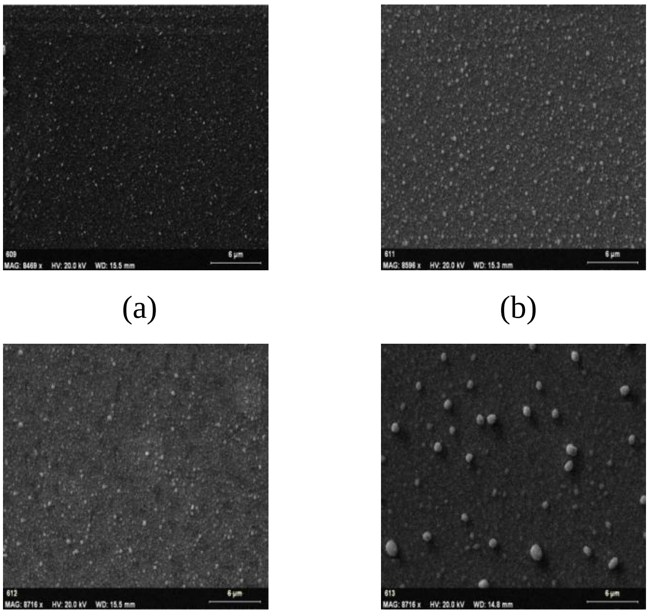

(a) (b)

(c) (d)

Figure-4.2: SEM micrographs for R3 a) as-grown b) annealed at 300 °C, c) 400 °C and d) 500 °C

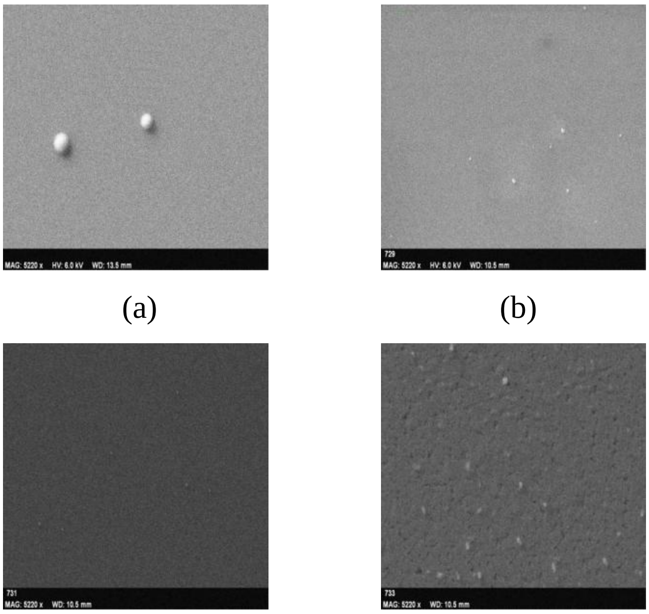

(a) (b)

(c) (d)

Figure-4.3: SEM micrographs for R5 a) as-grown b) annealed at 300 °C, c) 400 °C and d) 500 °C

As seen from figures, the film surfaces show the clusters of small grains with the average size in the range of 50-2000 nm. Therefore, according to the results of the SEM analysis, it can be said that the surfaces of the thin films are smooth and the grain sizes are very small. Because of their high resistivity and discharging effect, it is very hard to resolve and observe them from the SEM patterns as seen in the SEM figures of them. The bright grains are Se crystallites according to EDXA analysis. After annealing process under the nitrogen atmosphere, these Se spots disappear. This may indicate that Se atoms may diffuse to the film structure. In addition to this, according to the EDXA results, the other reason may be re-evaporation of these elements from the surface of the films.

4.2.2 XRD Measurements

As it is mentioned that XRD measurement was used to determine the XRD patterns and as a result of this, phases and orientations of the deposited polycrystalline thin films. Besides, this analysis helps to observe the possible changes in the film structures depend on the compositional differences and annealing temperatures. To do this, characteristic 2θ values and intensity values of the diffraction peaks corresponding to as-grown and annealed thin films for each run were compared with each other with the appropriate XRD data sets from ICDD data base. The XRD analyses of the thin films are given in Fig.4.4 – 4.8.

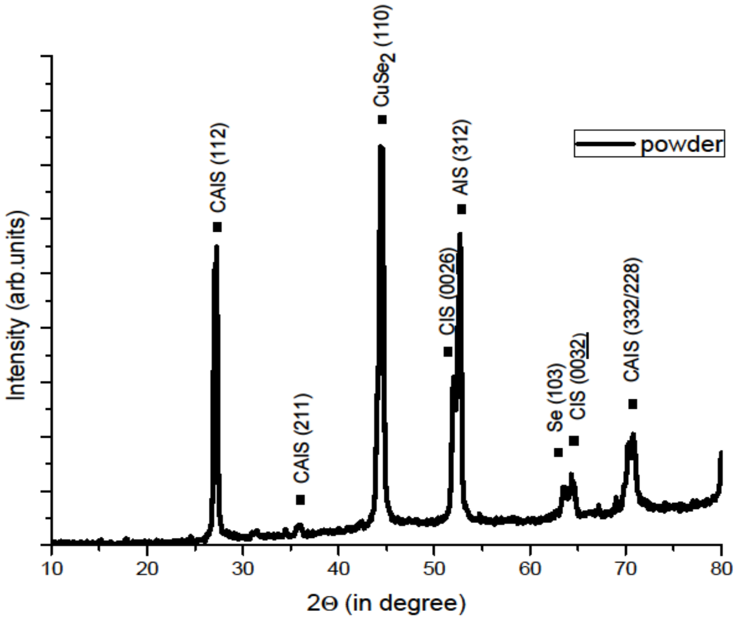

Figure-4.4: XRD patterns for the synthesized powder

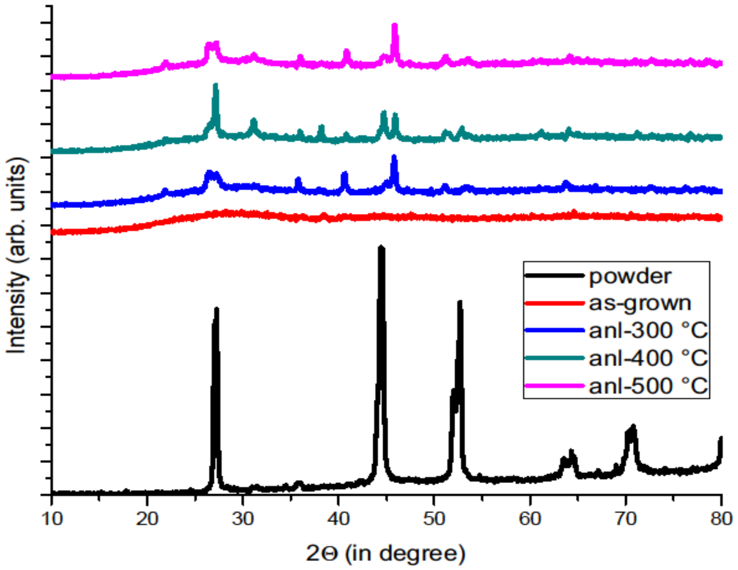

Figure-4.5: XRD patterns for R2_CAIS thin films at different annealing temperatures

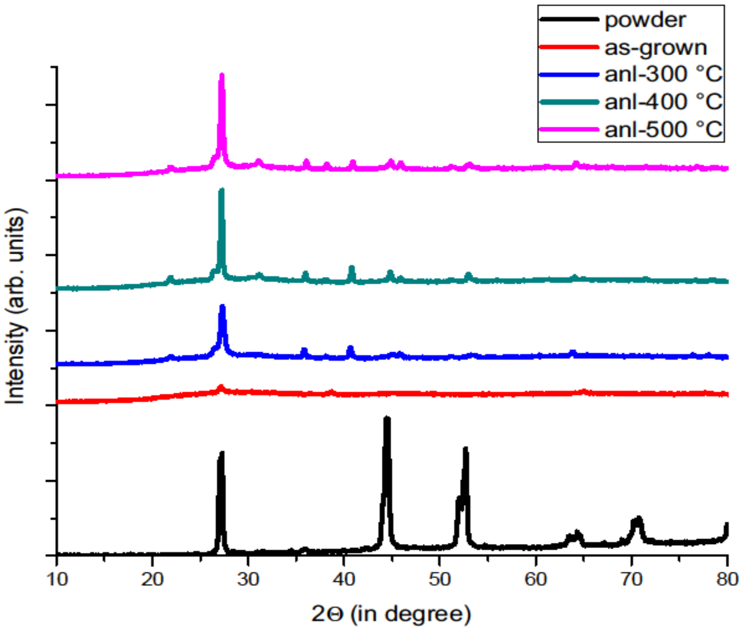

Figure-4.6: XRD patterns for R3_CAIS thin films at different annealing temperatures

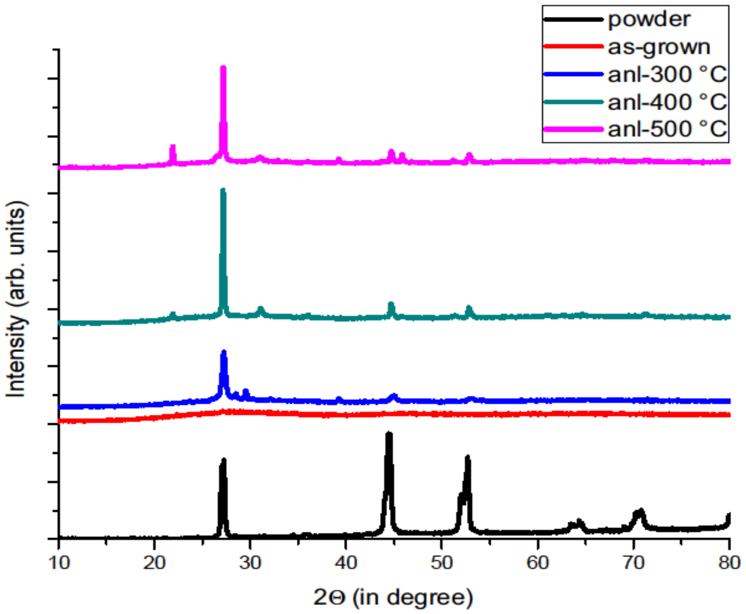

Figure-4.7: XRD patterns for R5_CAIS thin films at different annealing temperatures

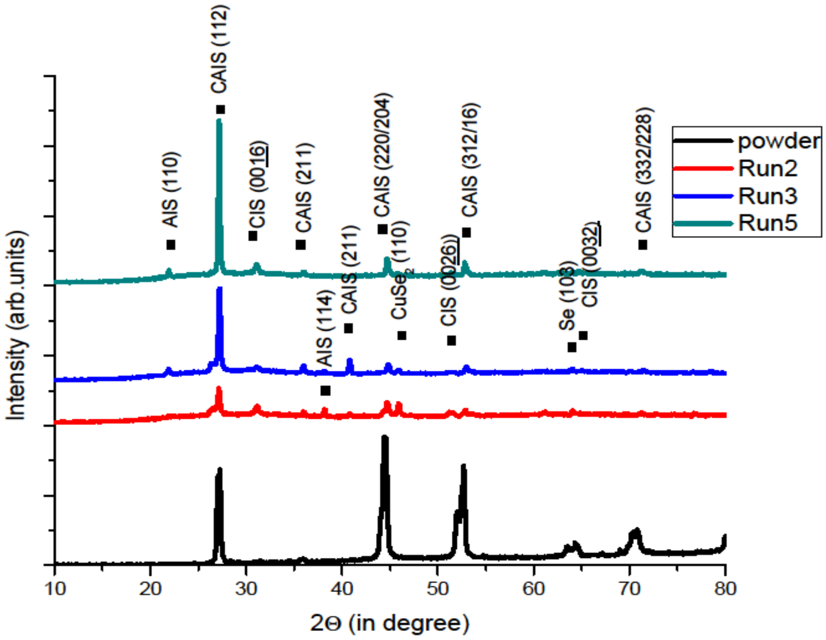

Figure-4.8: XRD patterns of R2, R3, and R5 films annealed at 400 °C

Initially, as seen in the figures above, the analysis of XRD data show that synthesized CAIS powder has a polycrystalline nature. In addition to the expected quaternary crystalline structure, it is understood from the XRD patterns of the thin films that they consist of a mixture of crystalline phases (ternary, binary and single) of constituent atoms of powder source; Cu, Ag, In, Se. It may be because of the characteristic of the CAIS powder and the additional elemental sources.

In the investigated XRD pattern of the CAIS thin films, the crystalline phases could not be precluded because their diffraction peaks may coincide with some of the others peaks. Therefore, the presence of small amounts from other crystalline phases were hardly detected and analyzed. Although there are some experimental works on structural properties of $Cu_{0.5}Ag_{0.5}InSe_2$ quaternary chalcopyrite materials [12, 19, 21], there are no complete set of XRD data for $Cu_{1-x}Ag_xInSe_2$ depending on x content. Therefore, the XRD analyses of the CAIS material was done according to XRD profile of $Cu_{0.5}Ag_{0.5}InSe_2$ thin film reported in the literature [12].

As it is shown in the figures above, XRD patterns for the as-grown films have low intensity diffraction peaks, and for each run, although there is no change in peak positions of samples annealed at different temperatures, there is an increase in intensity at specific annealing temperatures and a decrease in other annealing temperatures. With the increase in annealing temperature, it is observed that the peak intensity along the preferred direction increases and the other directions corresponding to different chemical formations decrease. According to the EDXA results, with increase in the annealing temperature, Se ratio decreases in the composition of the films, and they may contribute to the CAIS structure formation. Therefore, the minor peak intensities of the binary, also single, crystalline phases decrease, and the peak intensities of the CAIS structure increase. However, at 400 °C annealing temperature, the peak intensity of the preferred orientation direction reaches the highest value. At this annealing temperature, the increase in peak intensities may be due to that there is a decrease in structural disorder and an increase in crystallinity with a maximum appropriateness [84].

As observed from the XRD pattern of the deposited thin films with respect to the powder, the preferred orientation is changed, and the structure of the thin films shows CAIS structure with preferred direction along in the (112) plane. The deposition parameters and conditions, and also the sources may cause this change in the preferred orientation. In addition to this, as seen from Fig.4.8, there is a very weak shift change between the XRD peaks on the (112) preferred direction in the R2, R3 and R5. The shift may be related to change in the elemental ratio of elements in the thin film structures. The percentages of the constituent elements were different in the three depositions that may cause the change in the spacing between the planes in the atomic lattice, and as a result of this, 2θ shift in the peak positions.

In the XRD measurements of the thin films, the high intensity reflection was obtained at the major peak $2\theta \cong 27.15°$ which indicates the preferred orientation of CAIS films. It is reported as in the (112) phase orientation and giving tetragonal crystalline structure. The reported structural patterns calculated from this diffraction phase are $a = 0.5937$ nm and $c = 1.1633$ nm. Therefore, the tetragonal distortion for these chalcopyrite materials can be found approximately as 0.040.

Fig.4.8 shows the XRD pattern of the deposited films is quite similar to that of $Cu_{0.5}Ag_{0.5}InSe_2$ thin films [12]. However, there are extra diffraction peaks in the XRD pattern of each thin film. When XRD data were compared with the most appropriate ICDD database, the structures of these diffraction peaks were characterized. There are ternary phases found as ε-$(Cu_2Se)_x(In_2Se_3)_{1-x}$ and $AgIn_5Se_8$ which are indexed in the ICDD card no 38-0957 and 36-1397, respectively. There are also binary structures corresponding to some XRD peaks; that are In_2Se_3 and CuSe with the ICDD reference card numbers 71-0250 and 06-0427, respectively. In addition to this, in XRD pattern of R2, there is a single phase of selenium with card no 83-2438. As shown in the Fig.4.8, all runs have ternary CIS and AIS phases, but R2 and R3 have binary phases, and there is a single crystalline phase in the XRD pattern of the R2. This may happens due to the atomic ratio of the elements, deposition conditions and the bonding capability of the constituent elements in each run. Also, the thin films deposited in R5 have the most appropriate XRD pattern as reported in the literature [95].

The average microcrystalline grain size d was estimated from the XRD pattern using the Scherrer's formula [62, 66, 67] expressed as

$$d = \frac{k\lambda}{\beta cos\theta} \tag{4.1}$$

The grain sizes of R2, R3, and R5 for the as-grown thin films were found to be as 26, 474, and 584 nm; for the films annealed at 400 °C as 580, 828 and 2957 nm, respectively. Moreover, it is found that the grain size of the thin films increase with annealing temperature, but decrease after reaching 400 °C. The increase in grain size is a clear indication of improvement in crystallinity following to the annealing process, and the limit temperature point 400 °C shows that it is the optimum temperature of the post-thermal annealing process for these CAIS thin films. Almost the same values of grain sizes were also obtained from SEM analysis.

4.3 Electrical Characterization

The electrical measurements were carried out on the Maltese-Cross sample geometry (Fig.3.5) by the van der Pauw technique to eliminate possible finite contact effects. For the electrical measurements, indium metallic contacts were deposited by the thermal evaporation of indium through the suitable masks. Before the dark conductivity and Hall effect measurements, the ohmicities of these contacts were checked and the resistance of the samples for the base of the whole electrical measurements were determined.

4.3.1 Conductivity Measurements

The temperature dependent conductivity in CAIS thin films was analyzed in the temperature range of 100-400 K, in order to reveal the existent current transport mechanisms and the general behavior of the conductivity and to obtain the general behavior of conductivity against the ambient temperature, temperature dependent conductivity measurement was carried out for the as-grown and annealed at 400 °C and 500 °C. In all of the CAIS samples, the conductivities show Arrhenius behavior and they increase exponentially with increasing sample temperature as presented in Fig.4.9.

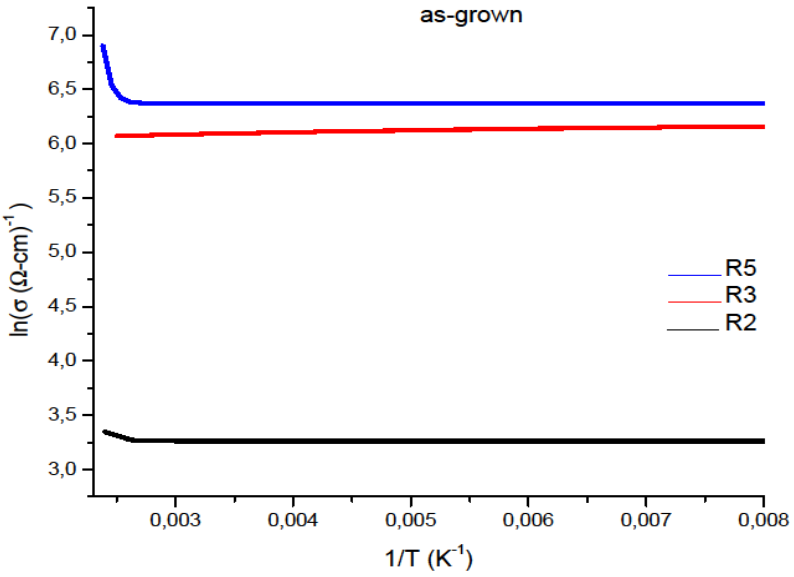

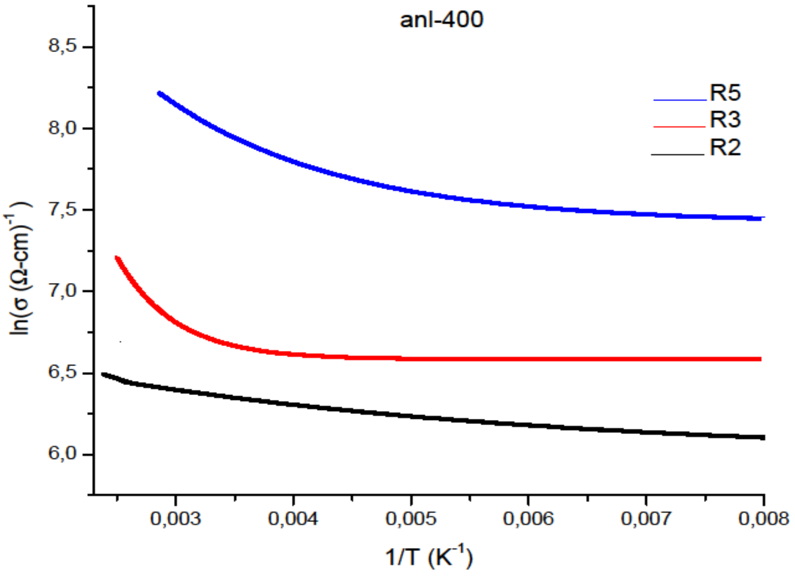

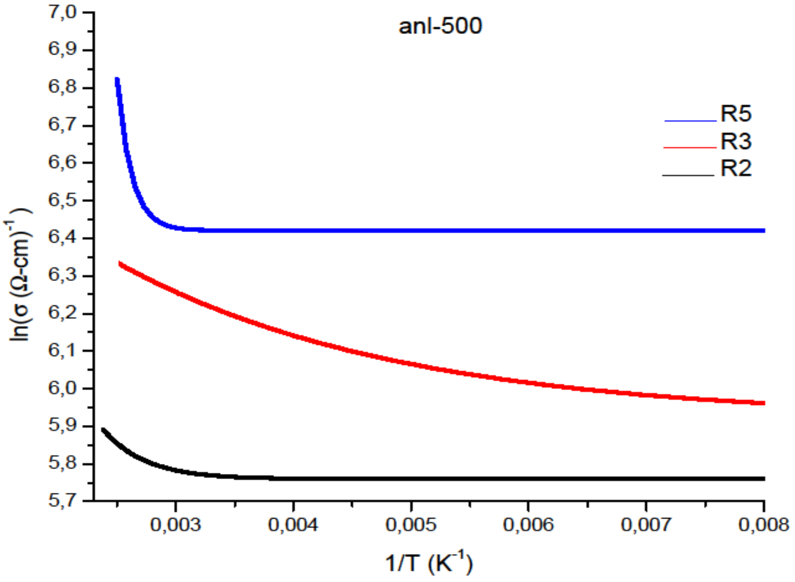

Figure-4.9: The temperature dependent electrical conductivity of the as-grown and thin films annealed at 400 °C and 500 °C

As seen from Fig.4.9, the change in the temperature dependent conductivities indicates an exponential decrease in these values with decreasing sample temperature for the as-grown and annealed thin films. This behavior is a typical exponential variation of conductivity with temperature for polycrystalline semiconductor thin films.

There were no significant variations in the dark conductivity of the samples in the high temperature region. However, between 100 and 300 K temperature range, there was a slight change in the conductivity values of the samples. As a result of conductivity analysis in different temperature range, the room temperature conductivity values obtained for the CAIS thin films lie in the range 25 - 3000 (Ω^{-1}.cm^{-1}) depending on the annealing temperature. The room temperature conductivities were found to be 26.1, 581, and 320.3 (Ω^{-1}.cm^{-1}) for the R2 samples; 475, 828.2, and 496 (Ω^{-1}.cm^{-1}) for the R3 samples; 584.1, 2957.5, and 618.8 (Ω^{-1}.cm^{-1}) for the R5 samples; in as-grown, 400 °C and 500 °C annealing conditions respectively. As it clearly seen from the Fig.4.9, the conductivity values increase with the annealing temperatures, at each constant sample temperature [96].

There is an increasing trend for the values of the conductivity CAIS samples with annealing and Cu/(Cu+Ag) ratios. However, an interesting situation about them arises starting from the annealing case at 400 °C and also in the R5 samples. The increment in the conductivity of the films can be explained by structural transformation from amorphous to polycrystalline structure via annealing. As it is the case for the conduction processes that grain boundaries are very effective in polycrystalline structures, a change in the grain size with heat treatment may be responsible for the changes obtained in the dark conductivity of the thin films. The grain size of the samples increases if they are treated under post-thermal annealing process, and since larger grain means less boundaries responsible for the trap density of free carriers, with annealing process the conductivity of the samples increases [98]. Therefore, it is clearly observed from the conductivity analysis that increasing the annealing temperatures makes the samples low resistive which may be due to modification of crystallization in their structure. In addition to this, the atomic ratio of Cu element is excessive in the R5 samples than the others, so the more contribution of Cu in the structure may cause the increase in the conductivity values.

Besides, as it was similar in the XRD analysis, the results of the conductivity measurements of the films proved that the optimum temperature of the post-thermal annealing process for CAIS thin films is 400 °C in order to reach most convenient conditions for the semiconductor characteristics of the deposited thin films.

Furthermore, the effect of the Cu and Ag ratio, Cu/(Cu+Ag), as well as the heat treatment at different temperatures on the electrical conductivity of the CAIS thin films was studied. With increasing Cu/(Cu+Ag) ratio and Cu content of the film, the conductivity of the samples increases. Variations of electrical conductivities as a result of atomic ratio in the composition could be related to these structural changes. Cu is well known to be a mobile constituent in CIS materials. Therefore, it has pronounced effect in the increasing conductivity values with respect to Cu/(Cu+Ag) ratio. Fig.4.10 shows the room temperature conductivity values with respect to the Cu and Ag ratio.

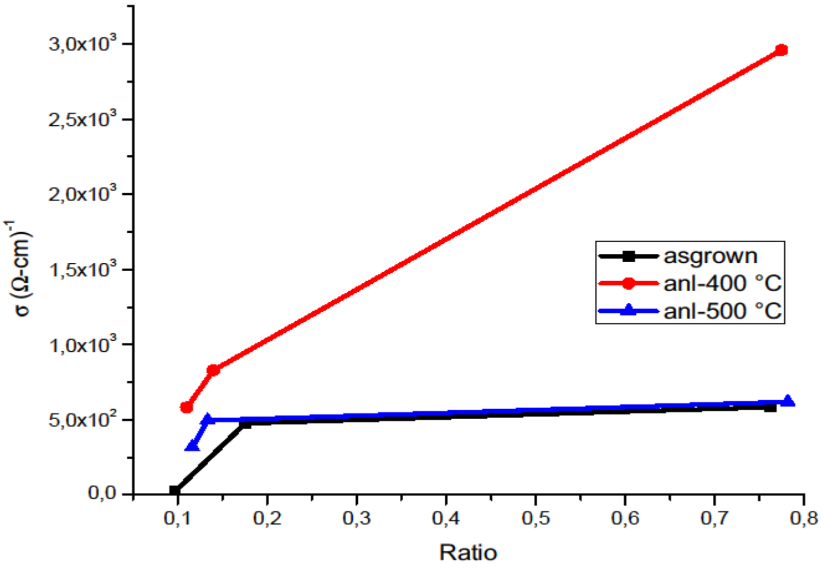

Figure-4.10: The room temperature conductivity depend on the variations on the composition of the CAIS samples

Depending on the annealing temperature, the dark conductivity depending on the temperature changes gives different behaviors and different activation energies in the corresponding temperature regions. In the low temperature region, the variation of conductivity with temperature is very small, almost temperature in sensitive up to 250 K, but in the high temperature region above 300 K, there is a sharp increase of the conductivity and the activation energies E_A, obtained from the slope of the conductivity-temperature relation were 81, 78 and 91 meV for the as-grown; 104, 154 and 85 meV for the 400 °C annealed samples; and 115, 190, and 88 meV for the 500 °C annealed samples with respect to the different Cu/(Cu+Ag) ratios derived from R2, R3 and R5 samples. Activation energies of the samples increased with the annealing process. This increase of activation energy with the annealing temperature is the indication of the improvement in the crystallinity in the samples, annealing decreases the structural defects and clears out some traps exist in the band gap region introduced during the deposition of the films as observed in the XRD analysis. In other words, the activation energies calculated from the electrical conductivity measurements are very small which is due to the presence of impurities and imperfections. However, the difference between the activation energies if Cu/(Cu+Ag) ratio is concerned may be under the effect of measurement errors and having very slight values.

In addition to the conductivity measurements, the conductivity type of each thin film was determined by the hot-probe technique and all CAIS thin showed n-type conduction. Therefore, it can be said that the type nature of CAIS thin films in the as-grown and annealed condition indicates that conduction was due to electrons as charge carriers.

4.3.2 Determination of Carrier Concentration and Mobility

The temperature dependent Hall effect measurements were conducted in order to investigate the charge carrier concentrations and Hall mobilities of the thin films in the temperature range of 100-400 K. Logarithmic plots of carrier concentrations and mobilities of the CAIS samples with the reciprocal absolute temperature are shown in the Fig.4.11 in terms of the ratios of Cu and Ag which are in R2, R3 and R5.

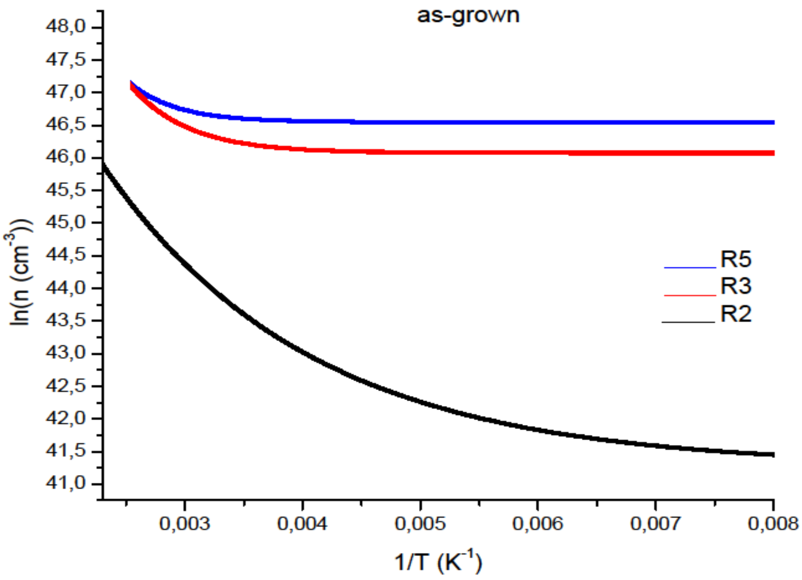

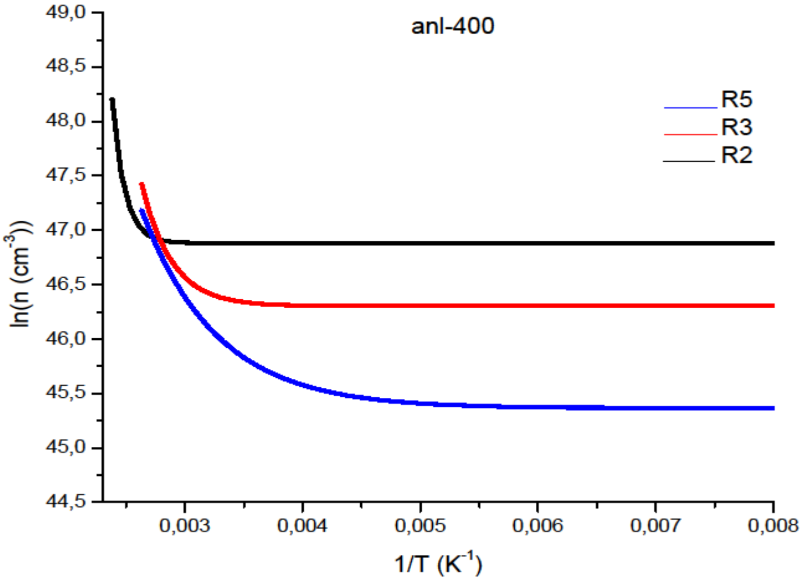

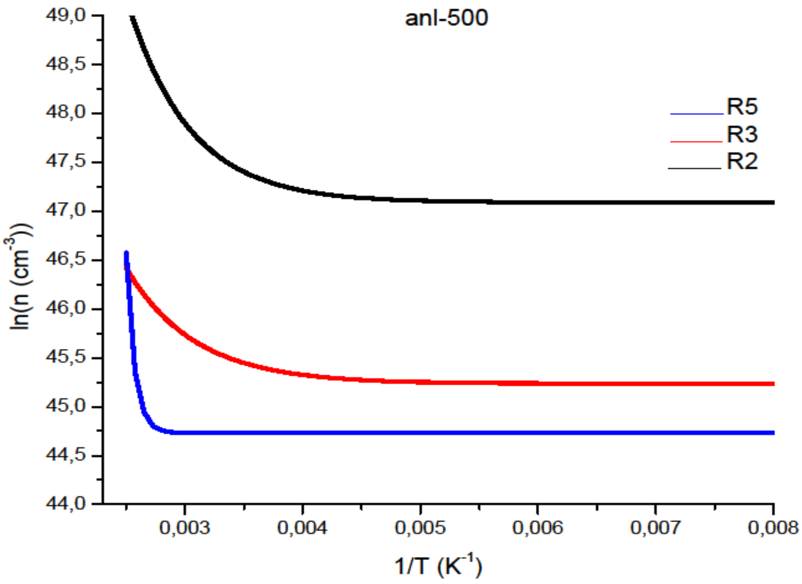

Figure-4.11: Temperature dependent electron concentration of the as-grown, 400 °C and 500 °C annealed CAIS samples with the reciprocal absolute temperature

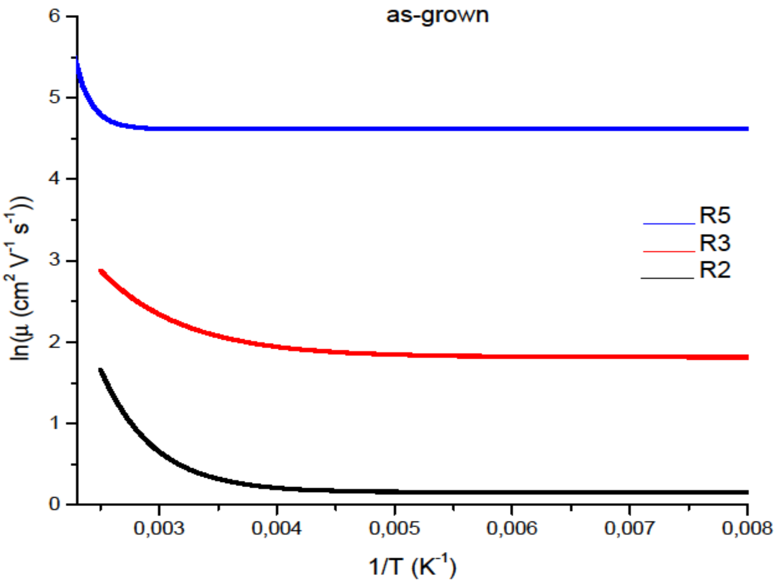

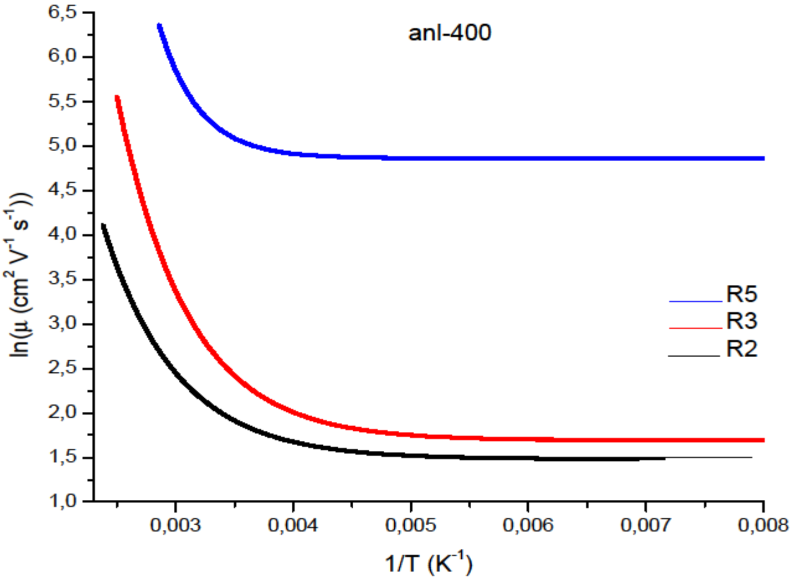

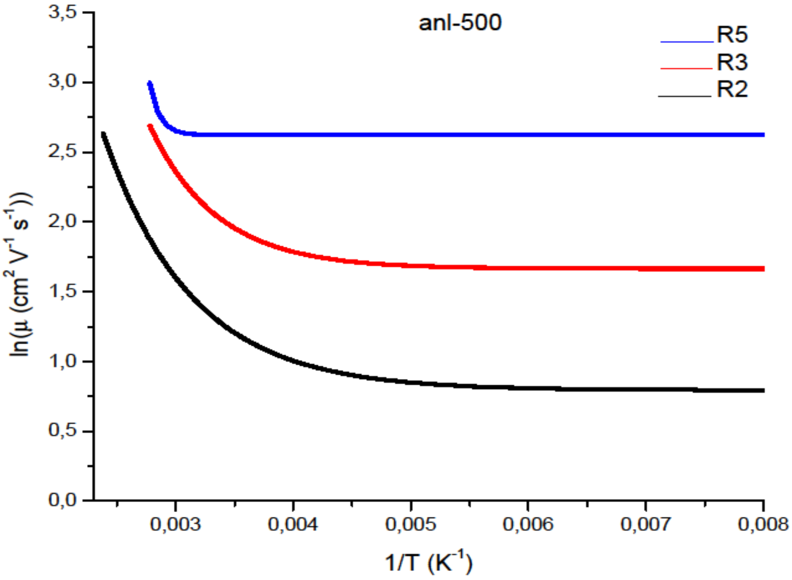

Figure-4.12: Temperature dependent Hall mobility of the as-grown, 400 °C and 500 °C annealed CAIS samples with the reciprocal absolute temperature

It is apparent that the carrier concentrations and mobility of the samples show the same characteristics with the conductivity behaviors. In other words, it is also increasing exponentially with the increase in the ambient temperature. Therefore, as the same reasons with the case in the dark conductivity measurements, the structural improvement might be responsible for this behavior.

The results of the Hall effect measurements show that CAIS is n-type. The origin of the conduction type can be related to the Se and cation (Cu, Ag, In) vacancies. The carrier concentration found at different temperatures varies between 1 x 10^{19} - 2 x 10^{21} cm^{-3} and a mobility of around 5 – 580 (cm^2 / (V.s)). The room temperature electron concentrations were calculated as 1.1 x 10^{19}, 1.8 x 10^{20}, and 1.1 x 10^{20} cm^{-3} for the R2 samples; 9.8 x 10^{19}, 2.3 x 10^{20}, and 1.4 x 10^{20} cm^{-3} for the R3 samples; and 1.8 x 10^{20}, 4.3 x 10^{20}, and 2.3 x 10^{20} cm^{-3} for the R5 samples in as-grown, 400 and 500 °C annealing conditions, respectively. The activation energy obtained from the variations in the carrier concentrations of the samples were calculated as 39, 24 and 51 meV for the as-grown; 113, 29 and 52 meV for the 400 °C annealed samples; and 115, 35, and 55 meV for the 500 °C annealed samples with respect to the different Cu/(Cu+Ag) ratios. In addition to this, the Hall mobilities were found to be 1.5, 158.8, and 12 (cm^2 / (V.s)) for the R2 samples; 7.7, 196.1, and 14.4 (cm^2 / (V.s)) for the R3 samples; and 13, 196.4, and 158 (cm^2 / (V.s)) for the R5 samples in as-grown, 400 °C and 500 °C annealing conditions respectively at the room temperature. From the mobility-temperature relation of the samples, the activation energies were found approximately as 140, 38, and 25 meV for as-grown; 182, 70 and 32 meV for 400 °C annealed; and 190, 95, and 42 for 500 °C annealed samples in the order of Cu and Ag atomic ratios.

Besides, the effect of the ratio of the Cu and Ag, Cu/(Cu+Ag), as well as the thermal treatment at different temperatures on the electrical conductivity of the CAIS thin films was studied. As in the case of the conductivity analyses, with increasing Cu/(Cu+Ag) ratio, the electron concentration and also mobility of the samples increases. The room temperature measurements about the ratio of the Cu and Ag are shown in the Fig.4.13.

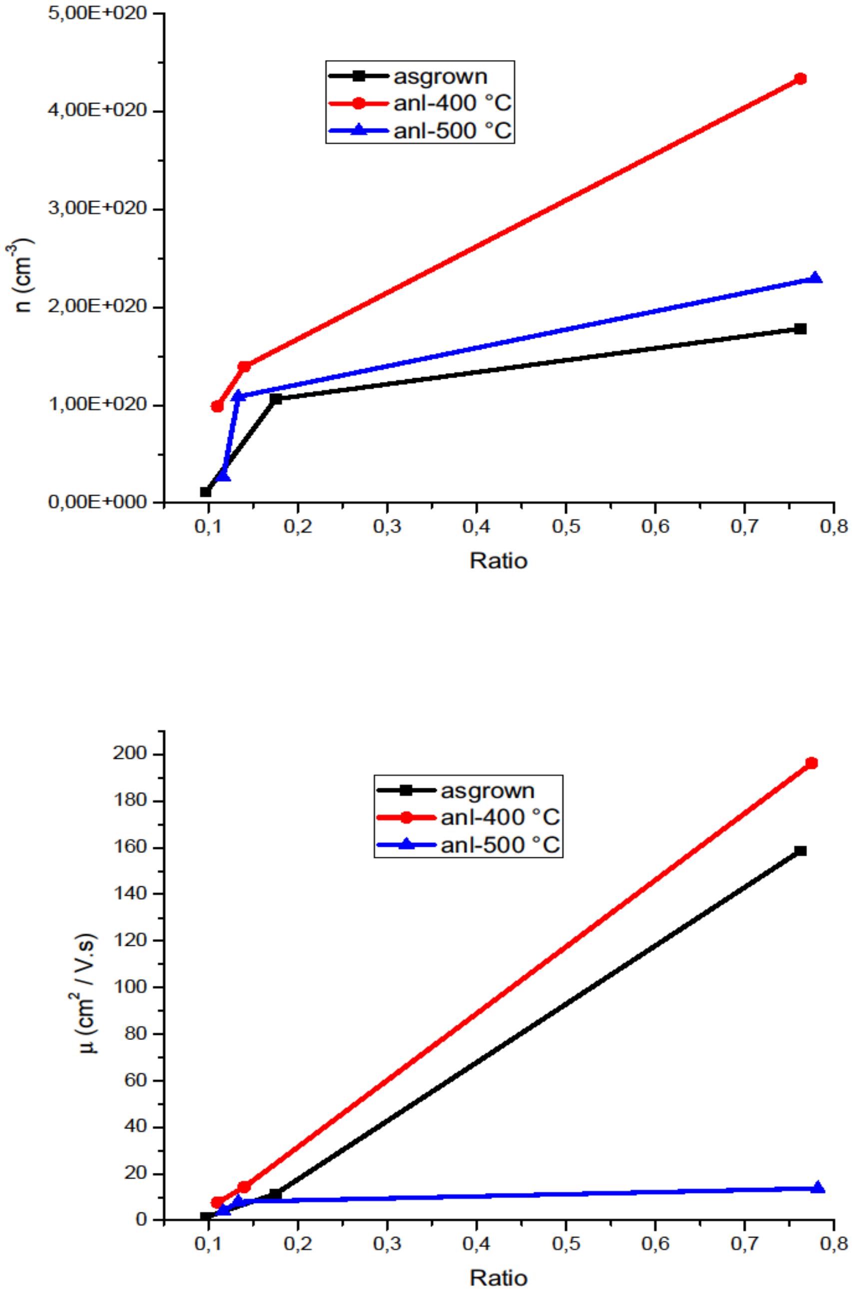

Figure-4.13: The room temperature carrier concentration and mobility depend on the variations on the composition of the CAIS samples

The analysis of the temperature dependent mobility of the samples was performed according to the existent scattering mechanisms. The logarithm plots of mobility with temperature were shown in Fig.4.14. The plot of this relation gives a linear behavior with the slope of 0.7, 0.8 and 0.6 for as-grown samples; 1.9, 2.1 and 0.9 for samples annealed at 400 °C; and 0.7, 0.8 and 0.5, for samples annealed at 500 °C, that gives a relation $\mu \alpha T^n$ and positive values of n implies that the ionizes impurity scattering is dominant scattering mechanism in these samples [27].

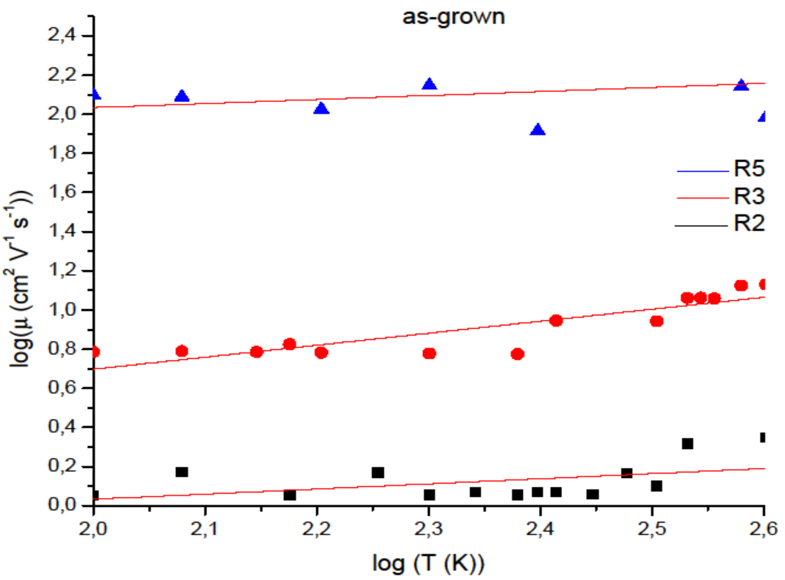

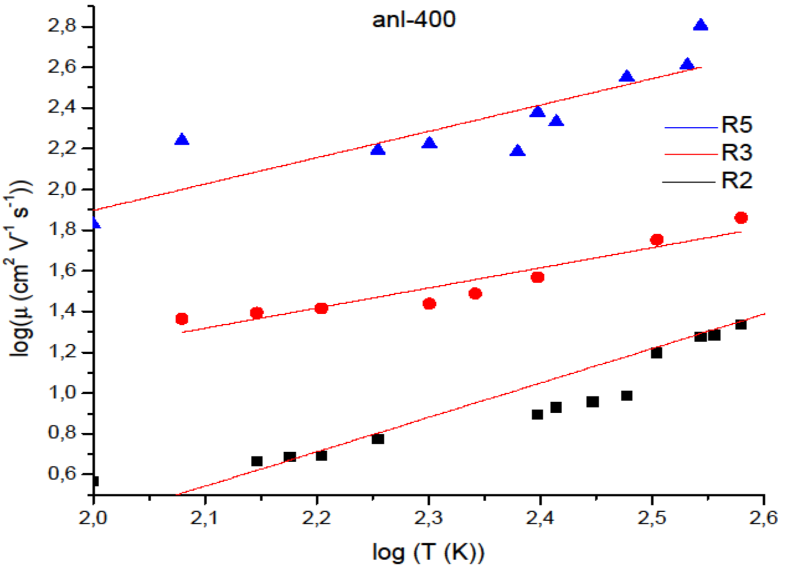

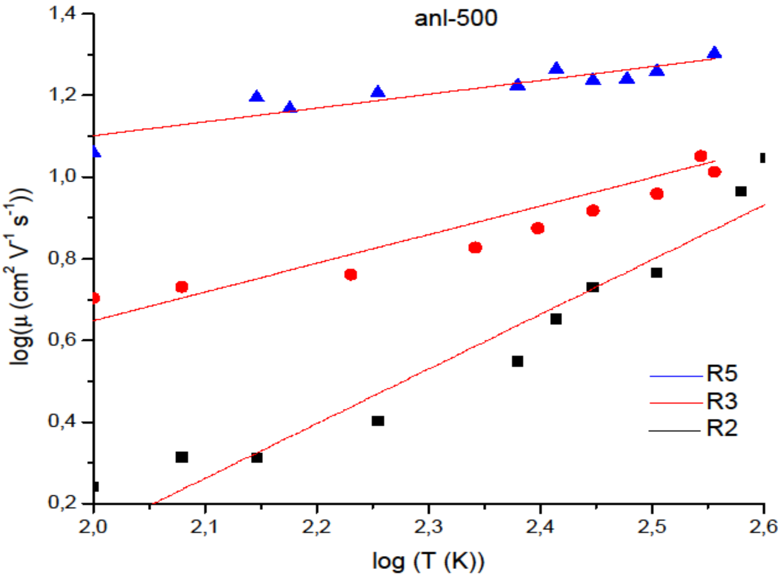

Figure-4.14: Determination of scattering mechanism of CAIS samples

4.4 Optical Characterization

The initial measurements about the optical characterization of the films are transmission, reflection and absorption analysis. All of these measurements were done on both as-deposited and annealed samples at room temperature. $\%T$ (transmission) versus λ (wavelength) and $\%R$ (reflection) versus λ (wavelength) curves of all the samples are shown in Fig.4.15 and 4.16.

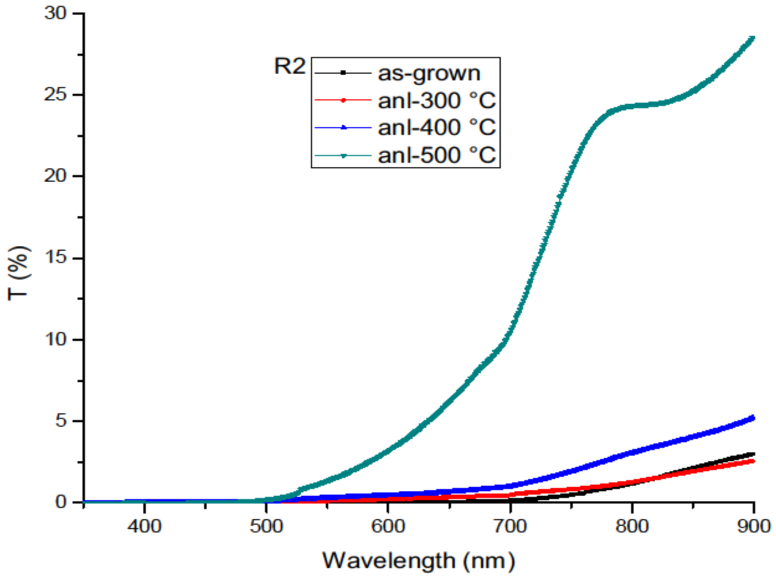
R2
as-grown
anl-300 °C
anl-400 °C
anl-500 °C
T (%)
0
5
10
15
20
25
30
400
500
600
700
800
900
Wavelength (nm)

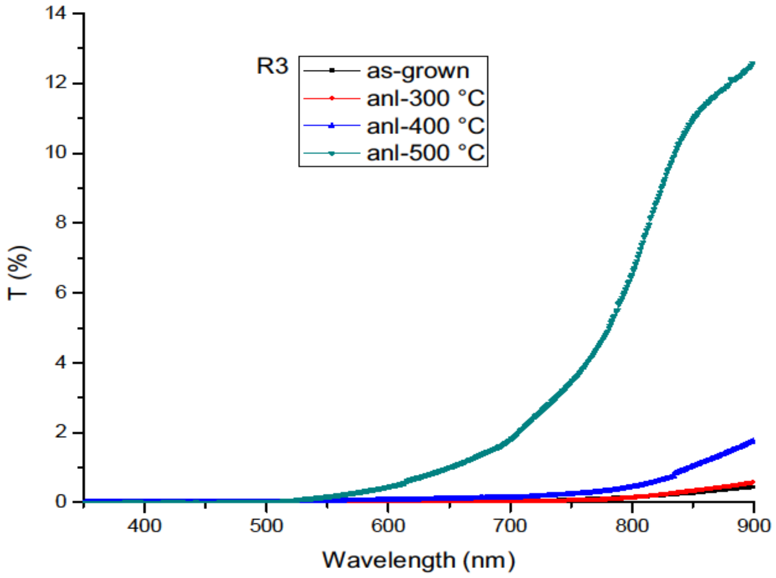
R3
as-grown
anl-300 °C
anl-400 °C
anl-500 °C
T (%)
0
2
4
6
8
10
12
14
400
500
600
700
800
900
Wavelength (nm)

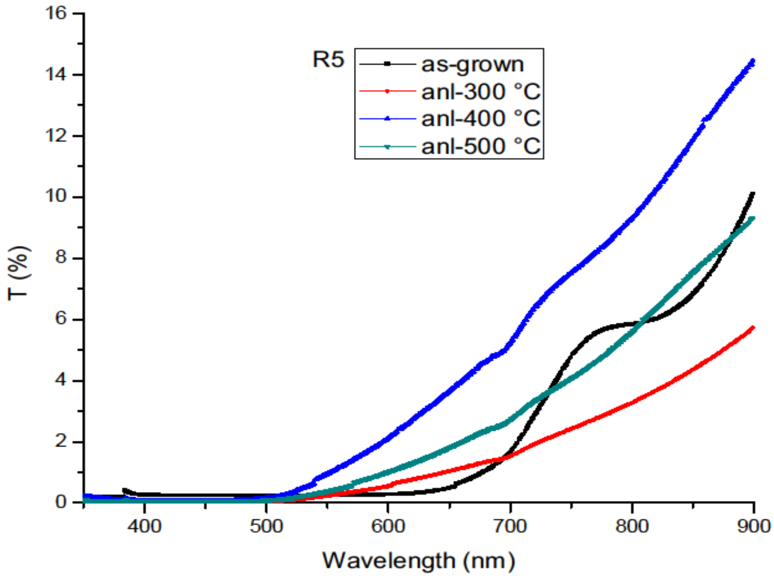

Figure-4.15: The transmission spectra for R2_CAIS, R3_CAIS and R5_CAIS thin films

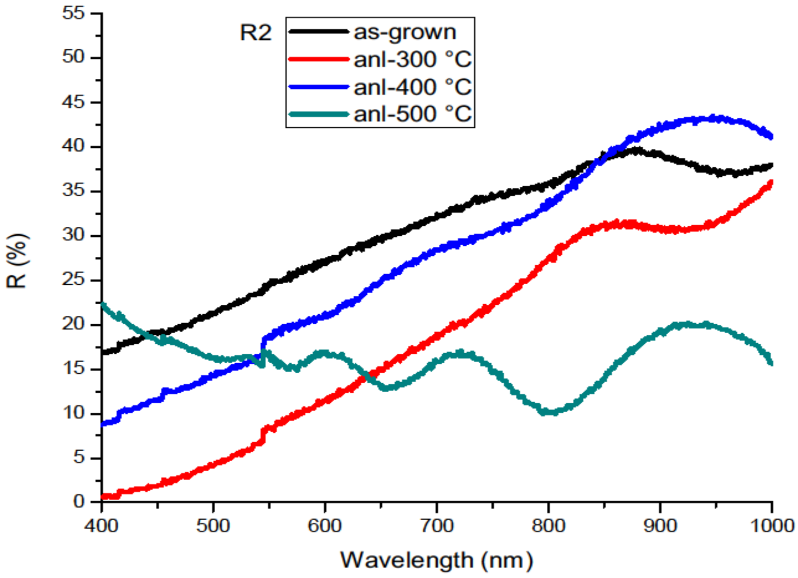

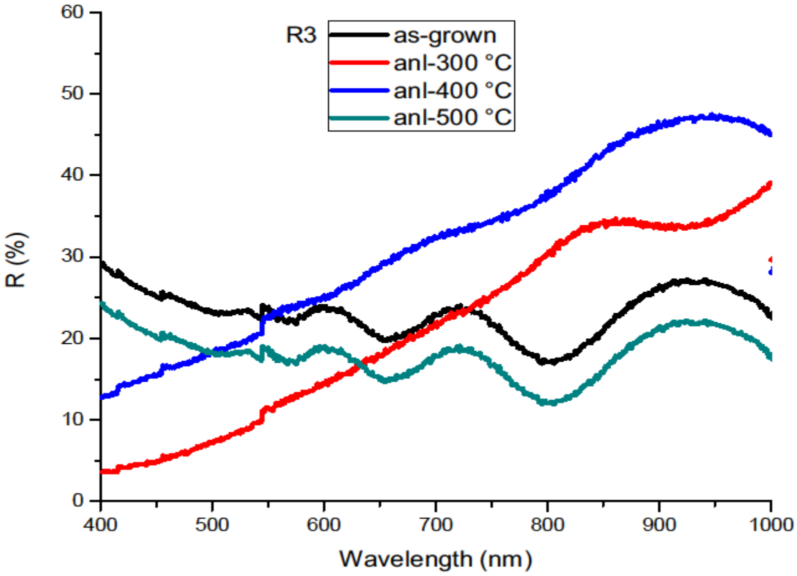

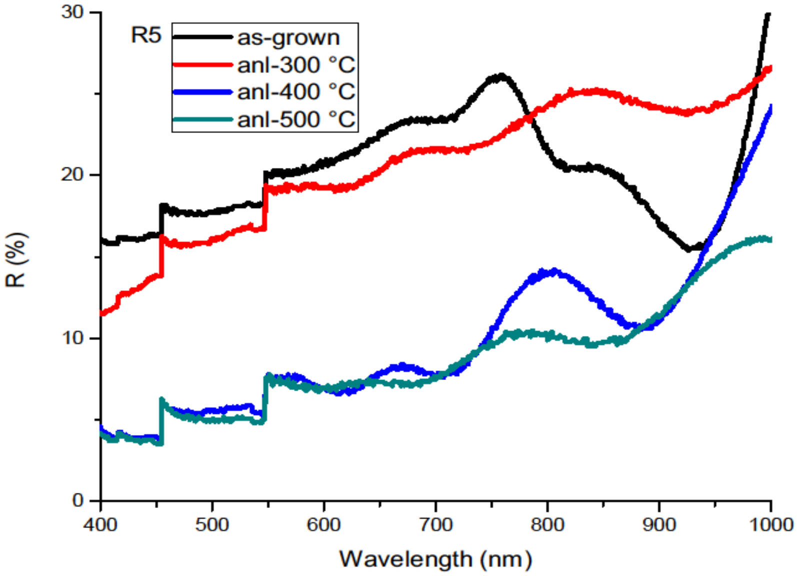

Figure-4.16: The reflection spectra for R2_CAIS, R3_CAIS and R5_CAIS thin films

It can be inferred from the transmittance and reflectance measurements that there is an enhancement in the transparency when CAIS thin films were subjected to annealing between 300-500 °C. The observed variations in transmission and reflection spectroscopy of the materials might depend on the structural transformations and possible re-ordering on the surface of the thin film with annealing process. The poor transmittance could be due to the multiple phases which were emphasized by the XRD analysis. In addition to this, constituent elements, especially Se, re-evaporation from the surface of the thin films; therefore, the modification in the structure of the films may be responsible for the increase in the transmittance with post-annealing process. On the other hand, the CAIS samples in as-grown form show high reflection; however, with annealing the samples, the reflectance of the samples decreases. It is also due to the re-evaporation of the some constituent elements form the surface of the films, and also changes in the structure of the films from metallic behavior.

These reflection and transmission results also used in order to investigate the absorption characteristics of the samples. According to Eq.3.7, optical absorption of the samples was described by an absorption coefficient. The absorption measurement is a strong tool to determine the optical properties of materials. The absorption coefficient of the CAIS samples varies between 2.2×10^4 and 2.08×10^5 (cm^{-1}) with the effect of stoichiometric ratio of the films and thermal annealing. Moreover, plots of $(\alpha h\nu)^2$ versus $h\nu$ are shown in Fig.4.17 where E_g of the samples were calculated from the extrapolated intercept of these graph. The energy gap of the as-grown CAIS films varies between 1.215 and 1.360 eV.

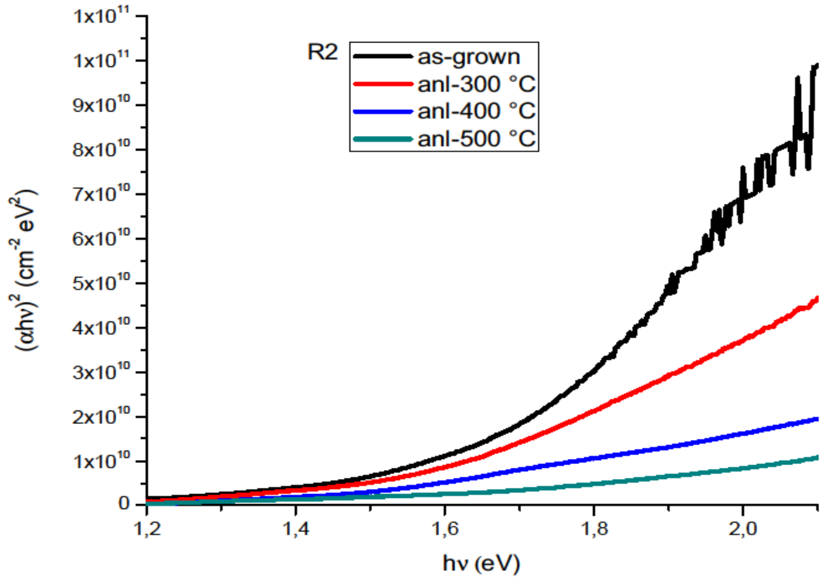
R2
as-grown
anl-300 °C
anl-400 °C
anl-500 °C
1x10^11
1x10^11
9x10^10
8x10^10
7x10^10
6x10^10
5x10^10
4x10^10
3x10^10
2x10^10
1x10^10
0
(αhν)^2 (cm^-2 eV^2)
1,2
1,4
1,6
1,8
2,0
hν (eV)

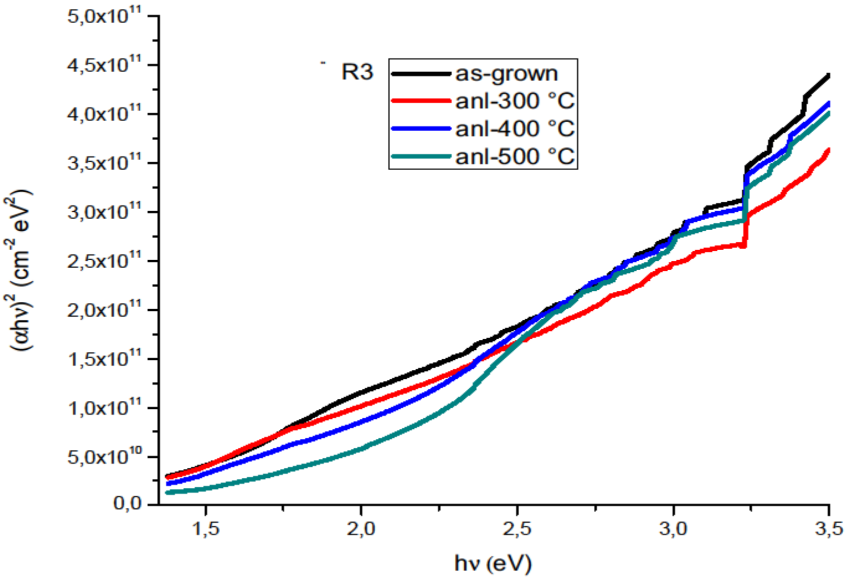
R3
as-grown
anl-300 °C
anl-400 °C
anl-500 °C
5,0x10^11
4,5x10^11
4,0x10^11
3,5x10^11
3,0x10^11
2,5x10^11
2,0x10^11
1,5x10^11
1,0x10^11
5,0x10^10
0,0
(αhν)^2 (cm^-2 eV^2)
1,5
2,0
2,5
3,0
3,5
hν (eV)

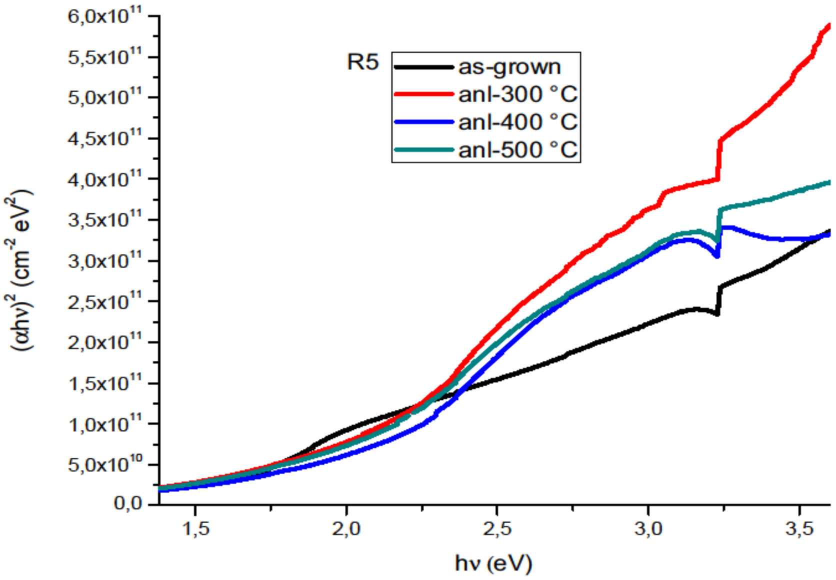

Figure-4.17: The variation of *$(\alpha h\nu)^2$* as a function of hν for as grown, annealed at 400, and 500 °C, R2_CAIS, R3_CAIS and R5_CAIS samples at room temperature

Furthermore, the optical band gaps of CAIS films varying Cu/(Cu+Ag) ratio were derived from transmission and reflection measurements. Energy gap values increased with annealing and were found to be as; 1.265 and 1.315 eV for R2; 1.430 and 1.550 eV for R3; 1.400 and 1.420 eV for R5 with 400 and 500 °C annealing temperatures respectively. It is observed that annealing does not change the energy gap and the compositional fluctuation changes the band gap values in between 1.26 and 1.55 eV.

Having high probability of charge carrier transition across the smaller optical band gap may be the case of the high absorption coefficient and also may explain the changes in the absorption coefficient and decrease in the optical gap. It has been found that the band gap has a tendency towards lower energies in the case of Cu-rich films. That could be due to band gap narrowing between the conduction and defect levels. Intrinsic defects such as selenium interstitials, silver substitutionals, and copper vacancies are thought to be responsible for inducing donor-like levels inside the band gap. Besides, p-d hybidraziation effects, cation-anion replacements, and tetragonal distortions may be the reason for the variations in the band gap values.

An increase in the optical band gap may be the results of the decrease in structural disorder and defect density states with applying thermal annealing. Another possible reason for increasing band gap values of the samples with the increasing annealing temperature could be the saturation of dangling bonds in the structures which are observed in the as-grown films. Besides, the change in the band gap energy following annealing can be explained by the formation of other phases, such as, CuSe, InSe having different band gap values.

4.4.1 Photoconductivity Analysis

The temperature dependent photo-conductivity measurements were carried out in the temperature range of 100-450 K at applied electric field strengths of 0.5 x 10^3 V/m, which were determined according to the resistance of the samples, and under a five different light intensities ranging from 17 to 113 mW/cm^2. 400 °C represents critical annealing temperature where I_{ph} photocurrent reaches its maximum value. Therefore, the photoconductivity variation for each of the CAIS thin films annealed at 400 °C with the inverse temperature was plotted in Fig.4.18 – 4.20.

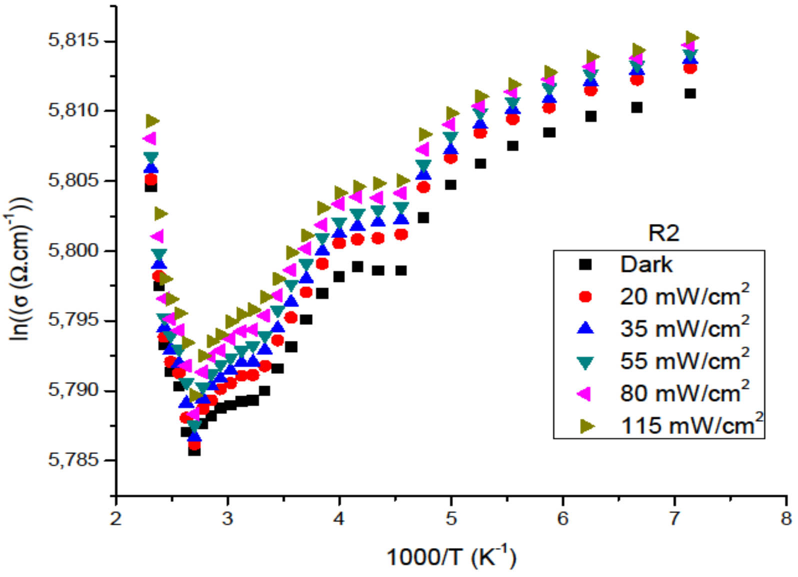

Figure-4.18: The variation of photo-conductivity as a function of reciprocal temperature for R2_CAIS thin film annealed at 400 °C

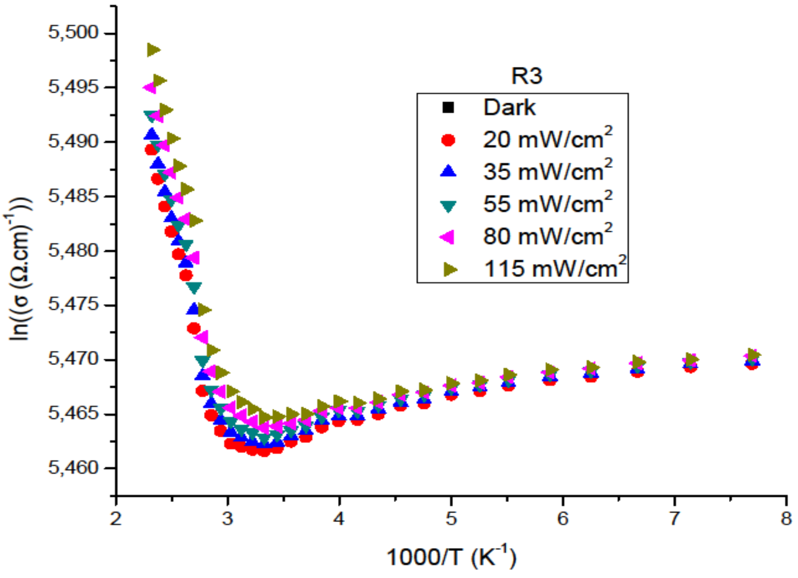

Figure-4.19: The variation of photo-conductivity as a function of reciprocal temperature for R3_CAIS thin film annealed at 400 °C

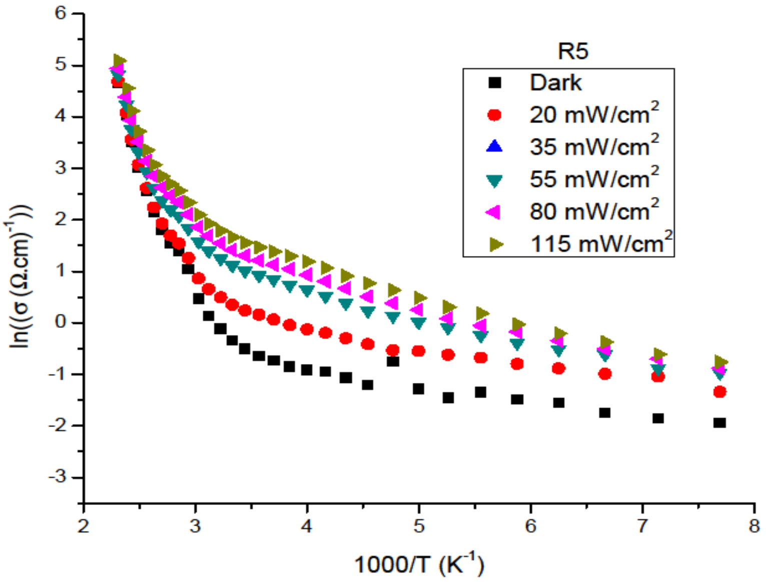

Figure-4.20: The variation of photo-conductivity as a function of reciprocal temperature for R5_CAIS thin film annealed at 400 °C

The photoconductivity values are greater than the dark conductivity values, and it is because of the contribution of the photo-carriers to the conduction. Due to the contribution of the photo-excited carriers to the current conduction, the illuminated conductivity, σ_{Φ} values are higher than those of the dark conductivity, σ_{dark}. When the illumination intensity increases, the conductivity of the samples increases. At low temperature regions between 100 and 300 K there is no significant change in the conductivity with temperature. However, at the temperatures above this range, the variation increases exponentially.

In order to determine the characterization of the recombination centers, the illumination intensity Φ were measured at different temperatures.

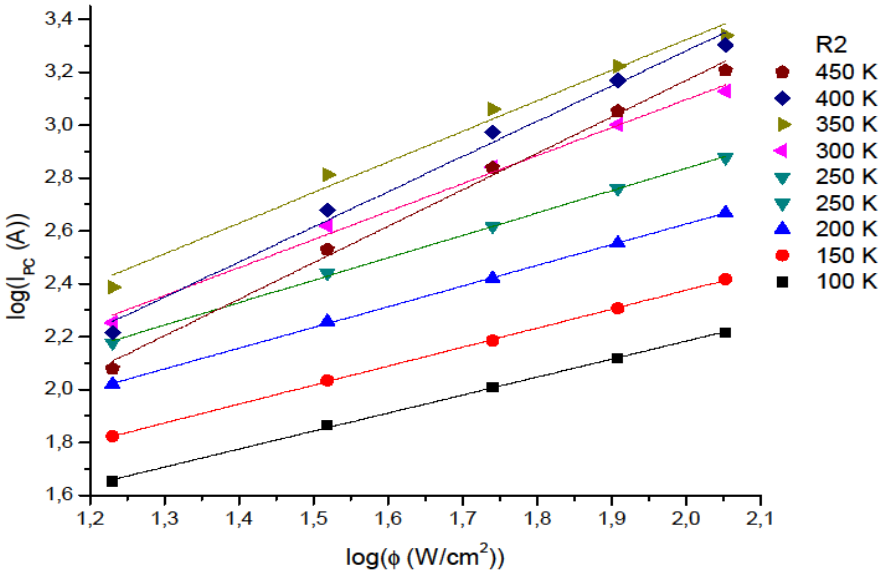
R2
450 K
400 K
350 K
300 K
250 K
250 K
200 K
150 K
100 K
log(I_{PC} (A))
3,4
3,2
3,0
2,8
2,6
2,4
2,2
2,0
1,8
1,6
1,2
1,3
1,4
1,5
1,6
1,7
1,8
1,9
2,0
2,1
log(ϕ (W/cm^2))

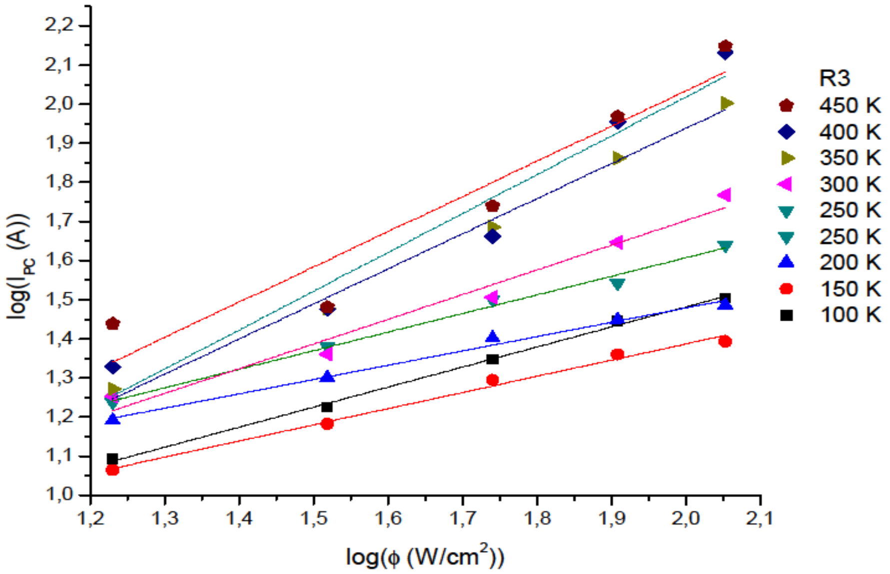
R3
450 K
400 K
350 K
300 K
250 K
250 K
200 K
150 K
100 K
log(I_{PC} (A))
2,2
2,1
2,0
1,9
1,8
1,7
1,6
1,5
1,4
1,3
1,2
1,1
1,0
1,2
1,3
1,4
1,5
1,6
1,7
1,8
1,9
2,0
2,1
log(ϕ (W/cm^2))

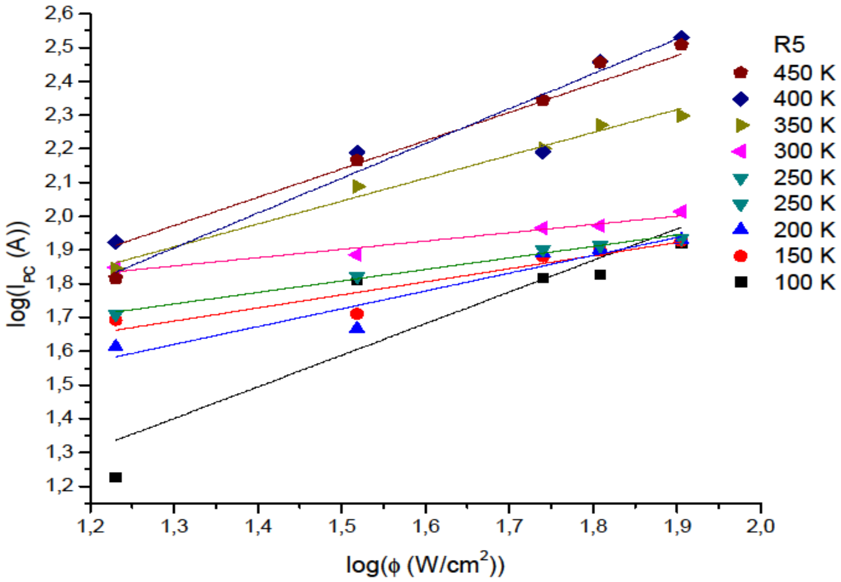

Figure-4.21: Variation of $I_{pc} - \Phi$ at several temperatures for R2_CAIS, R3_CAIS and R5_CAIS samples annealed at 400 °C

Fig.4.21. indicates the plot of $ln(I_{pc})$ (A) versus $ln(\Phi)$ (mW/cm^2) at different ambient temperatures. The relation between the photocurrent and the illumination intensity is of $I_{pc}\ \alpha\ \Phi^n$ type [8] where the exponent, n, is a distinctive indicator of the non-equilibrium carriers. Photocurrent, I_{pc}, increases with increasing illumination intensity. Based on the two-center recombination model; linear dependence on photoconductivity indicates monomolecular, and if n = 0.5, it gives bimolecular recombination. When it is found as greater than 1, the photoconductivity behavior shows supralinear case and it is related to an increase in lifetime with photo-excitation intensity [73].

The result of these analyses indicates that there is a linear characteristic for both samples and also we obtained n values in the Cu/(Cu+Ag) different ratios in the range of 0.8 - 1.3 for the R2, R3, and R5. Increasing exponent n values with increasing temperature confirm the longer life-time for free carriers and stronger recombination process at the film surface. Dominantly, this gives the supralinear characteristic which can be explained by the two-center recombination model having two donor levels dominant at both low and high temperature regions.

The spectral distribution of photoconductivity is a useful and simple tool for obtaining information related to band gap energy of the thin films. Our CAIS materials were found to have high photoresponse over the wavelength range from 600-1100 nm. The main cutoff wavelength, which is around 850 – 880 nm, indicates that the band gap of CAIS material is about 1.409 – 1.458 eV. There is also second cut-off region at approximately 1060 nm, which corresponds to 1.180 eV. These values are consistent with the result of the transmission and reflectance measurement.

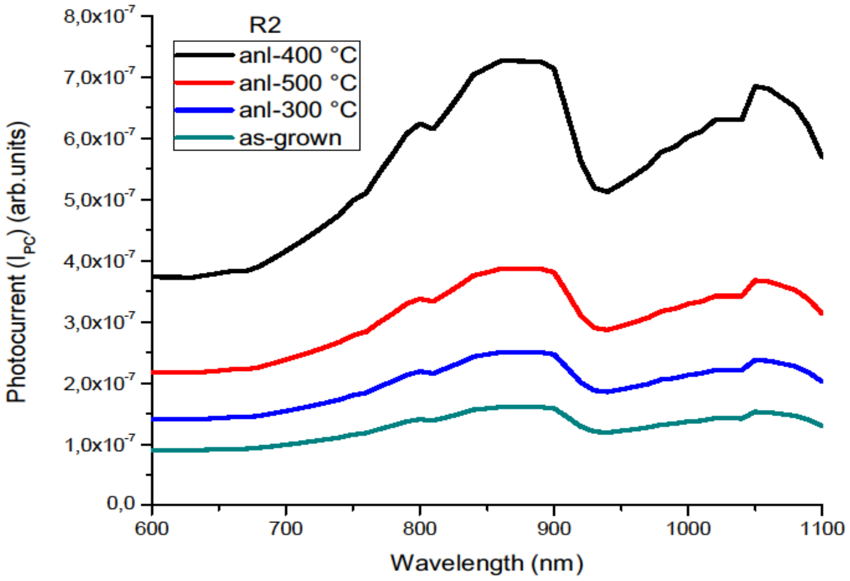

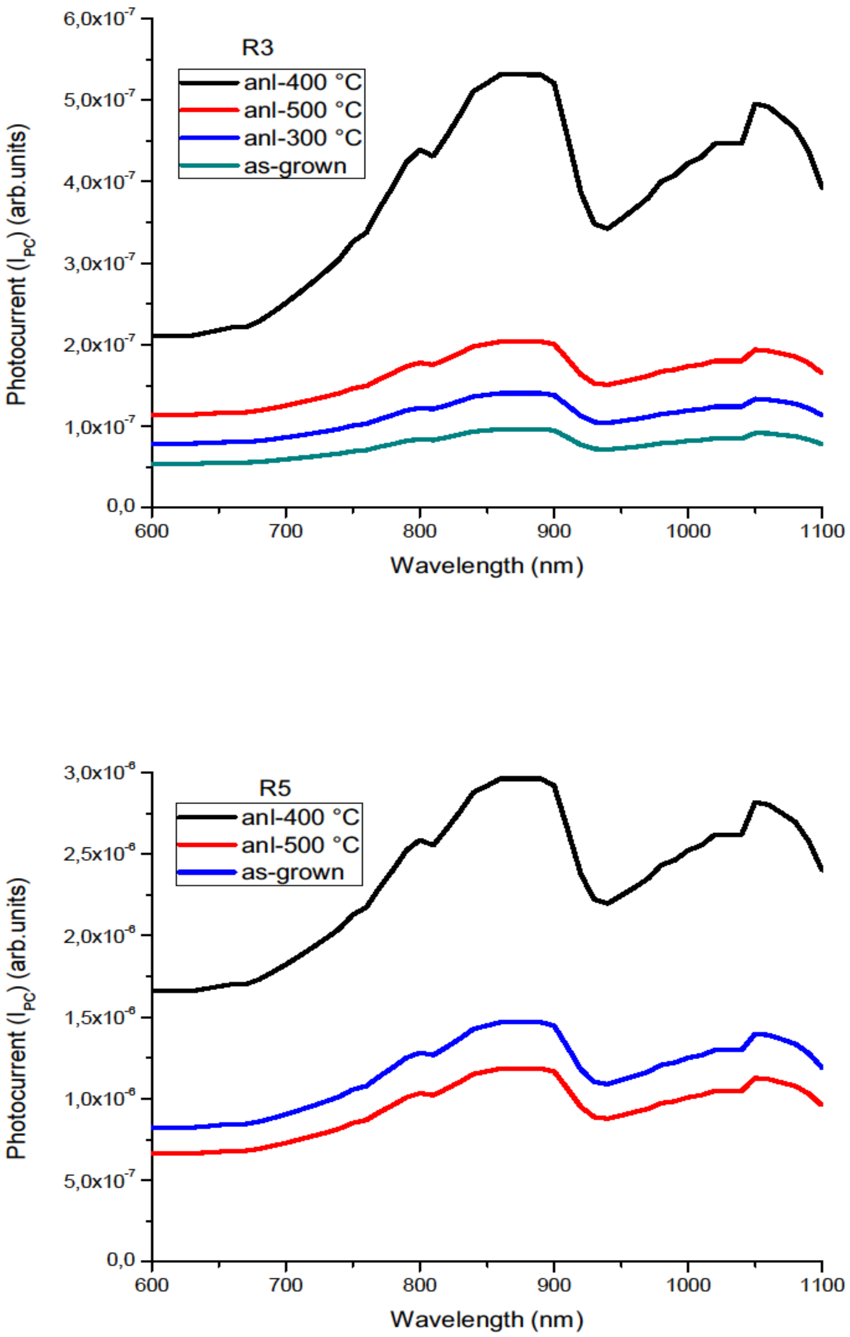

Figure-4.22: The normalized photoresponse plot of the R2_CAIS, R3_CAIS and R5_CAIS thin films

CHAPTER 5

CONCLUSION

In this study, the quaternary system $Cu_{1-x}Ag_xInSe_2$ (CAIS) was analyzed in order to investigate the effects of Ag contribution and exchange with Cu in $CuInSe_2$, and also the change in Cu/(Cu+Ag) atomic ratios in CAIS thin films. To do this, CAIS single crystal was grown by using 3-zone vertical Bridgman-Stockbarger crystal growth technique and CAIS thin films having different Cu and Ag elemental contributions were deposited by using e-beam evaporation technique. In addition, post-thermal annealing was carried out mostly at two different temperature, 400 °C, 500 °C for 30 minutes under the nitrogen environment to deduce the effects of annealing on the structural, electrical and optical properties of the deposited thin films, and therefore all of the characterization of the thin films were done between as-grown and these two annealing temperatures.

In the structural analysis, atomic ratios of the elements in the composition of both grown crystal and deposited thin films and also post-annealing conditions on the structural, morphological and compositional properties of thin films were studied. As a consequence of the structural analysis of the single crystal, it was obtained that the CAIS crystal was in the atomic composition closer to Cu:Ag:In:Se = 0.5:0.5:1.0:2.0. However, the as-grown thin films were formed at different Cu/(Cu+Ag) ratios; 0.10, 0.18 and 0.76 in the three thin film decompositions, R2, R3 and R5 respectively. This order in the thin films was not change with the thermal annealing although there were little differences in the elemental ratios. The visual appearance of the thin films were observed as smooth and having clusters of small grains varying between 50-2000 nm on their outer surfaces. As a result of XRD measurements, the peak positions of the CAIS single crystal and thin films were consistent with the XRD profile of $Cu_{0.5}Ag_{0.5}InSe_2$ thin film reported in the literature. The XRD measurements showed that the deposited thin films were in the (112) phase orientation with tetragonal crystalline structure having reported lattice parameters $a = 0.5937$ nm and $c = 1.1633$ nm. Moreover, some extra diffraction peaks, CIS, AIS, CuSe and Se, were detected in the XRD pattern of the thin films. As the annealing temperature was increased, the diffraction peak intensities of the XRD profiles become to be distinct and more intense indicating that polycrystalline structure of the films are improved. It was found that the peak intensities in preferred orientation dominated with increasing annealing temperature and as a result of this, the annealing process were found to improve crystallinity. In addition to this, the average microcrystalline grain size d was calculated from the XRD pattern, and it was found that the grain size was increased with increase in annealing temperature and Cu/(Cu+Ag) ratio. This indicates that the increase in grain size confirms improvement in crystallinity following to the annealing process, and the annealing temperature point 400 °C is the optimum temperature of the post-thermal annealing process for these CAIS thin films.

The temperature dependent conductivity in CAIS thin films was analyzed between the temperature ranges 100-400 K. In all of the CAIS samples, the conductivity measurements showed Arrhenius behavior and they increases exponentially with increasing temperature. However, there is almost no change in the conductivity with the temperature at low temperature region (100-250 K) and there is a sharp increase of the conductivity at the high temperature region (300-400 K). As a result of temperature dependent conductivity measurements, the room temperature conductivity values for the CAIS thin films were determined to around 25 – 3000 ($\Omega^{-1}.\mathrm{cm}^{-1}$) depending on the annealing temperature and Cu/(Cu+Ag) atomic ratios in the composition of the samples. There is an increasing trend for the values of the conductivity CAIS samples with annealing and Cu/(Cu+Ag) ratios. With annealing temperatures and Cu/(Cu+Ag) ratio and also Cu content of the film, the conductivity of the samples increases. The increment in the conductivity of the films can be explained by structural transformation from amorphous to polycrystalline structure via annealing. The atomic ratio of Cu element is excessive in the R5 samples than the others, so the more contribution of Cu in the structure may cause the increase in the conductivity values. The increase in the activation energies of the samples were obtained from the slope of the conductivity-temperature relation as 81, 78 and 91 meV for the as-grown thin films depending on the Cu and Ag content. The increase of activation energy from 81 to 190 meV with the annealing temperature is the indication of the improvement in the crystallinity in the samples, annealing decreases the effects of defects and clears out some traps exist in the band gap region introduced during the deposition in the structure of the films as observed in the XRD analysis. The conductivity type of each thin films was determined by both the hot-probe technique and Hall effect measurement, and the conductivity studies on all CAIS thin films gave the same result as to be n-type. The temperature dependent Hall effect measurements were carried out in order to determine the carrier concentrations and Hall mobilities of the thin films in the temperature range of 100-400 K. The carrier concentration found at different temperatures varies between 1×10^{19} - 2×10^{21} cm^{-3} and a mobility of around 5 – 580 (cm^2 / (V.s)). It is apparent that the carrier concentrations and mobility of the samples showed an exponential behavior at the high temperature region (300-450 K) which is the same characteristics with the conductivity behaviors. In other words, it is also increase exponentially with the increase in the ambient temperature. As in the case of the conductivity analyses, with increasing annealing temperature and Cu/(Cu+Ag) ratio, the electron concentration and also mobility of the samples increases. Furthermore, the analysis of the temperature dependence of the mobility of these samples pointed that the ionized scattering is dominant mechanism.

The starting optical characterizations of the films were transmission, reflection and absorption analysis. It can be observed from these initial optical measurements that there is an increase in the transparency of the CAIS thin films with the annealing process. The structural modifications and re-ordering on the surface of the thin film may be the reasons for these variations in transmittance and reflectance values. The band gap analysis of the samples indicated that the band gap has a tendency towards lower energies in the case of Cu-rich films. In addition, the energy gap of the as-grown CAIS films was found between 1.215 and 1.360 eV. It is observed that annealing does not change the energy gap and the compositional change the band gap values in between 1.26 and 1.55 eV.

The results of the photoconductivity measurements showed that the photoconductivity values were greater than the dark conductivity values and when the illumination intensity increases, the conductivity of the samples increases. The samples were not high photo-sensitive. Besides, the photoconductivity behavior was found to be appropriate to supralinear case in the two-center recombination model. As a consequence of the spectral distribution of photoconductivity, the energy gap was found in the range of 1.180 – 1.409 eV which is consistent with the result of the transmission and reflectance measurement.

In general, annealing temperature and Cu-Ag content in the composition of the samples strongly affects the structural, electrical and optical properties of the CAIS polycrystalline thin films. These conditions were found to be the remedial effects for the structural, electrical and optical properties of the CAIS thin films. As it was found before, the most appropriate post-thermal annealing temperature for CAIS thin films is 400 °C in order to observe the semiconductor characteristics of the deposited thin films. Moreover, the more contribution of Cu in the structure yields the increase in the conductivity, mobility and electron concentration values.

REFERENCES

[1] Eckertova, L., *Physics of Thin Films*, Czechoslovakia: Plenum Publishing Corporation, Second revised Ed., 1986

[2] Wagner, T., *European White Book on Fundamental Research in Materials Science*, Stuttgart Max Planck Institute, 2000

[3] Heavens, O. S., *Thin Film Physics*, Great Britain: T. & A. Constable Ltd., 1970

[4] Siegel, R. W., Hu, E. H., and Roco, M. C., WTEC Panel Report on R & D Status and Trends in Nanoparticles, Nanostructured Materials, and Nanodevices, Workshop, 1997

[5] Leaver, K. D., and Chapman, B. N., *Thin Films*, London: Wykehan Publications, 1971

[6] Elshabini-Riad, A., and Barlow, F. D., *Thin Film Technology Handbook*, USA: McGraw Hill, 1998

[7**]** Chopra, K. L. and Das, S. R., *Thin Film Solar Cells*, New York: Plenum Press, 1983

[8] Kaleli, M., *Investigation of Electrical and Optical Properties of Ag-In-Se Based Devices*, PhD. Thesis in Physics Department of Middle East Technical University, 2010

[9] Chopra, K. L., Paulson, K. L., and Dutta, V., *Prog. Photovolt.*, vol. 12, pp.69–92, 2004

[10] Asokamani, R., Amirthakumari, R. M., Rita, R., and Ravi, C., *Phys. Stat. Sol. (b)*, vol. 213, p.349, 1999

[11] Shay, J. L., Tell, B., Kasper, H. M., and Schiavone, L. M., *Phys. Rev. B*, vol. 7, no. 10, 1973

[12] Rao, G. V., Chandra, G. H., Hussain, O. M., Uthana, S., and Nadiu, B. S., *Journal of Alloys and Compounds*, vol. 325, pp. 12–17, 2001

[13] Rao, G. V., Chandra, G. H., Reddy, P. S., Hussain, O. M., Reddy, K. T. R., and Uthana, S., *Surface Instrumentation and Vacuum Technology*, vol. 67, pp. 293-298, 2002

[14] Bodnar, I. V., Gremenok, V. F., and Viktorov, I. A., *Journal of Applied Spectroscopy*, vol. 69, No. 3, 2002

[15] Albornoz, J. G., Serna, R., and León, M., *J. Appl. Phys.*, vol. 97, p. 103515, 2005

[16] Lavrentyev, A. A., *Phys. Script*,. vol. T115, pp. 212–214, 2005

[17] McAlpine, N. S., McConville, P., and Haneman, D., *J. Appl. Phys.*, vol. 79, p. 9, 1996

[18] Bodnar, I. V., Viktorov, I. A., and Sergeev-Nekrasov, S. L., *Cryst. Res. Technol.*, vol. 33, pp. 885-990, 1998

[19] Rao, G. V., Chandra, D. H., Reddy, P. S., Hussain, O. M., Reddy, K. T. R., and Uthana, S., *J. Optoelect. and Adv. Mat.*, vol. 4, pp. 387-392, 2002

[20] Rao, G. V., Chandra, G. H., Hussain, O. M., Uthana, S., and Naidu, B. S., *Cryst. Res. Technol.*, vol. 36, pp. 571–576, 2000

[21] Gremenok, V. F., et. al., *Solid State Phenomena*, vols. 67-68, pp. 361-366, 1999

[22] Ashour, A., *Thin Solid Films*, vol. 467, pp. 300– 307, 2004

[23] Mustafa, H., Hunter, D., Pradhan, A. K., Roy, U. N., Cui, Y., and Burger, A., *Thin Solid Films*, vol. 515, pp. 7001–7004, 2007

[24] Sze, S. M., *Physics of Semiconductor Devices*, New York: Wiley - Intersicience, 1969

[25] Rudden, M. N., and Wilson, J., *Elements of Solid State Physics*, England: John Wiley & Sons, Second Ed., 1993

[26] Zeghbroeck, B. V., *"Principles of Semiconductor Devices"*, http://ecee.colorado.edu/~bart/book, Date accessed: 5 August 2010

[27] Streetman, B. G., and Banerjee, S. K., *Solid State Electronic Devices*, USA: Prentice Hall, Sixth Ed., 2010

[28] Kittel, C., *Introduction to Solid State Physics*, USA: John Wiley & Sons, Eight Ed., 2005

[29] Katırcıoğlu, B., *PHYS 440 Semiconductor Physics II*, Lecture Notes, Spring 2010

[30] Mass, T. S., *Photoconductivity in the Elements*, New York: Academic, 1962

[31] Habashi, F., *Chalcopyrite: Its Chemistry and Metallurgy*, USA: McGraw-Hill, 1978

[32] Wearie, D. and Noolandi, *Journal de Physique*, vol. 36, p. C3-27, 1975

[33] Su, D. S., Neumann, W., and Giersig, M., *Thin Solid Films*, vol. 361-362, pp. 218-222, 2000

[34] Berger, L. I., *Semiconductor Materials*, New York: CRC Press, 1997

[35] Jaffe, J. E., and Zunger A., *Phys. Rev. B*, vol. 28, p. 10, 1983

[36] Shay, J. L., and Wernick, J. H., *Ternary Chalcopyrite Semiconductors: Growth, Electronic Properties, and Applications*, Great Britain : Oxford: Pergamon Press, 1975

[37] Pamplin, B. R., *Crystal Growth*, Oxford: Headington Hill Hall, Pergamon Press Ltd., 1975

[38] Karabulut, O., *Structural, Electrical and Optical Characterization of N- and Si-Implanted GaSe Single Crystal Grown by Bridgman Method*, Phd. Thesis in Physics Department of Middle East Technical University, 2003

[39] Brice, J. C., *Crystal Growth Processes*, New York, 1986

[40] Tom, Y., and Fiechter, S., *Journal of Ceramic Processing Research*, vol. 6, pp. 141-145, 2005

[41] Sheinma R., Brandon S. and Lewin D. R., *Optimal Control of Vertical Bridgman Crystal Growth*, http://www.technion.ac.il/~dlewin/publications/VBG_EMCC3.pdf, Date accessed: 8 August 2010

[42] Holland, L., *Vacuum Deposition of Thin Films*, New York: Wiley, 1956

[43] Oxford Vacuum Science, High Vacuum Science and Technology, http://www.oxford-vacuum.com/background/thin_film/sputtering.htm, Date accessed: 1 August 2010

[44] Las Positas College, *Thin Film Deposition Processes*, http://lpc1.clpccd.cc.ca.us/lpc/tswain/chapt14.pdf, Fall 2002, Date accessed: 25 July 2010

[45] Nalwa, S. H., *Handbook of Thin Film Materials*, San Diego: Academic Press, 2002

[46] Seshan, K., *Handbook of Thin Film Deposition: Processes and Technologies*, New York: Noyes, Second Ed., 2002

[47] Katırcıoğlu, B., *PHYS 439 Semiconductor Physics I*, Lecture Notes, Fall 2010

[48] Vossen, J. L. And Kern, W., *Thin Film Processes*, New York: Academic Press, 1978

[49] Ohring, M., *Materials Science of Thin Films: Deposition and Structure*, San Diego: Academic Press, 2002

[50] SreeHarsha, K. S., *Principles of Physical Vapor Deposition of Thin Films*, Amsterdam, Boston, London: Elsevier, 2006

[51] Maissel, L. I. and Glang, R., *Handbook of Thin Film Technology*, New York: McGraw-Hill, 1970

[52] Schiller, S., Heisig, U., and Panzer, S., *Electron Beam Technology*, Berlin: John Wiley & Sons, 1982

[53] Bakish, R., *Introduction to Electron Beam Technology*, New York: John Wiley & Sons, 1962

[54] Schiller, S., Heisig, U., and Panzer, S., *Electron Beam Technology*, New York: Wiley Interscience, 1982

[55] Singh, J., Schriempf, J. T., and Wolfe, D. E., *Electron Beam Physical Vapor Deposition Technology: Present and Future Applications*, The Pennsylvania State University: The Applied Research Laboratory, 2002

[56] Eason, R., *Pulsed Laser Deposition of Thin Film*, USA: John Wiley & Sons Inc., 2006

[57] Ahmed, E., Hill, A. E., Leppavuori, S., Pilkington, R. D., Tomlinson, R. D., Levoska, J., and Kusmartseva, O., *Adv. Materials for Optics and Effect*, vol. 4, p. 423, 1994

[58] Ploog, K., *Epitaxial Growth*, 27th International Conference on the Physics of Semiconductors, 2004

[59] Kemell, M., Ritala, M., and Leskel, M., *Critical Reviews in Solid State and Materials Sciences*, vol. 30, pp. 1-31, 2005

[60] Wasa, K., and Kitabat, M., *Thin Film Materials Technology: Sputtering of Compound Materials*, Heidelberg: William Andrew Pub., 2004

[61] Birkholz, M., Fewster, P. F., and Genzel, C., *Thin film analysis by X-ray scattering*, Germany: Wiley, 2006

[62] Kaelble, E. F., *Handbook of X-Rays*, USA: McGraw-Hill Inc., 1967

[63] Connolly, J. R.,” *Introduction to X-Ray Powder Diffraction”*, http://epswww.unm.edu/xrd/xrdclass/01-XRD-Intro.pdf, 2007

[64] Carleton College Science Education Resource Center, *“X-ray reflection in accordance with Bragg's Law*”, http://serc.carleton.edu/research_education/geochemsheets/BraggsLaw.html, Date accessed: 8 August 2010

[65] Australia Insitute of PhysicsEducation Commite, “*Bragg Diffraction Experiment”*, http://www.vicphysics.org/documents/.../Bragg_Diffraction_Experiment.pdf, Date accessed: 20 July 2010

[66] Cullity, B. D., *“Elements of X-Ray Diffraction”*, USA: Addison-Wesley, Second Edition, 1978

[67] Yılmaz, K. And Karaagaç, H., *Applied Surface Science*, vol. 256, pp. 6454–6458, 2010

[68**]** Egerton, R. F., *Physical Principles of Electron Microscopy: An Introduction to TEM, SEM, and AEM*, New York: Springer, 2005

[69] Swapp, S., “*Scanning Electron Microscopy (SEM)”*, http://serc.carleton.edu/research_education/geochemsheets/techniques/SEM.html, Date accessed: 20 July 2010

[70] Hearle, J. W. S., Sparrow, J. T., and Cross, P. M., *The Use of Scanning Electron Microscope*, New York: Pergamon Press, First Ed., 1972

[71] Hurd, C. M., *The Hall effect in Metals and Alloys*, New York: Plenum Press, 1972

[72] Sze, S. M., *Semiconductor Devices: Physics and Technology*, USA: Bell Telephone Laboratories, 1985

[73] Bube, R. H., *Photoelectronic Properties of Semiconductors*, Cambridge: Cambridge University Press, 1992

[74] Petritz, R. L., *Phys. Rev*., vol. 104, p. 1508, 1956

[75] Bube, R. H., *Photoconductivity of Solids*, New York: Wiley, 1960

[76] Cardetta, V. L., Mancini, A. M., and Rizzo, A., *J. Crystal Growth*, vol. 16, pp. 183-185, 1972

[77] Gilman, J. J., *The Art and Science of Growing Crystals*, London: John Wiley and Sons, Inc., 1963

[78] Karaağaç, H., *Structural, Electrical and Optical Characterization of Ge-implanted GaSe Single Crystal Grown by Bridgman Method*, MSc. Thesis in Physics Department of Middle East Technical University, 2005

[79] Scheel, H. J. And Capper, P., *Crystal Growth Technology: From Fundamentals and Simulation to Large-Scale*, Weinheim, Wiley-VCH, 2008.

[80] MPI-FKF Stuttgart Crystal Growth Service Group, *The Bridgman-Stockbarger Method*, http://www.fkf.mpg.de/crystal/D6-Bridgman_growth.pdf, Date accessed: 20 July 2010

[81] Lim, S. H. N., McKenzie, D. R., and Bilek, M. M. M., *Review of Scientific Instruments*, vol. 80, 075109, 2009

[82] Huş, Ş. M., *Physical Properties of CdSe Thin Films Produced by Thermal Evaporation and E-beam Techniques*, MSc. Thesis in Physics Department of Middle East Technical University, 2006

[83] National Institute of Standards and Technology Electronic and Electrical Engineering Laboratory, *"Hall effect Measurements"*, http://www.nist.gov/eeel/semiconductor/hall.cfm, Date accessed: 2 August 2010

[84] Mattox, D. M., *Handbook of Physical Vapor Deposition (PVD) Processing*, New Jersey: Noyes Publications, 1998.

[85] Digital Instruments/Vecco Metrology, *Dektak 8 Advanced Development Profiler Manual*, Veeco Instruments Inc., 2003-2004

[86] Çolakoğu, T., *The Effects of Post-Annealing Process on The Physical Properties of Silver-Indium-Selenium Ternary Semiconductor Thin Films Deposited by Electron Beam Technique*, PhD. Thesis in Physics Department of Middle East Technical University, 2009

[87] van der Pauw, L.J., *Philips Technical Review*, vol. 20, pp. 220-224, 1958

[88] van der Pauw, L.J., *Philips Res. Repts.*, vol. 13, pp. 1-9, 1958

[89] Deen, M. J. and Pascal, F., *J Mater Sci: Mater Electron*, vol. 17, pp. 549–575, 2006

[90] Schroder, D. K., *Semiconductor Material and Device Characterization*, New York: Jhon Willey and Sons, 1990

[91] Micocci, G., Serra, A., and Tepora, A., *J. Appl. Phys.*, vol. 82, p. 2365, 1997

[92] Milam, J., Lauhon, L., and Allen, J., *"Photoconductivity of Semiconducting CdS Nanowires"*, Nanoscape, http://www.nanoscape.northwestern.edu/Vol2/05Milam.pdf, Date accessed: 7 August 2010

[93] Joseph, C. M., and Menon, C. S., Semiconductor Science Technology, vol. 11, p. 1668, 1996)

[94] Roth, A., *Vacuum Technology*, Amsterdam: North Holland, Second Ed., 1980

[95] Ciszek, T.F., Bacewicz, R, Durrant, J.R., Deb, S.K., and Dunlavy, D., *19th Photovoltaic Specialist's Conference,* , p. 1448, New Orleans, LA, IEEE, New York, 1987

[96] Bernard, J. E. and Zunger, A., *Phys. Rev. B*, vol. 36, p. 3199, 1987

[97] Yılmaz, K. and Karaağaç, H., *Applied Surface Science,* vol. 256, pp. 6454-6458, 2010

[98] Seto, J. Y. W., *J. Appl. Phys. v*ol. 46, p. 5247, 1975

[99] Bacewicz, R., Durrant, J. R., Ciszek, T. F., and Deb, S. K., Proceedings of the 7th International Conference on Ternary and Multinary Compounds, Eds. S. K. Deb and A. Zunger, (Pittsburgh: Materials Research Society Press, 1987) pp. 155-160.

[100] Jaffe, J. E. and Zunger A., *Phys. Rev. B,* vol. 29, p. 1882, 1984

[101] Çolakoğu, T., *The Growth and Characterization of Galium Selenide Thin Films*, MSc. Thesis in Physics Department of Middle East Technical University, 2003

[102] Çolakoğlu, T. and Parlak, M., *Applied Surface Science,* vol. 254, pp. 1569–157, 2008